

OPTIMAL DESIGN AND CONTROL OF COOL THERMAL ENERGY STORAGE AS A  
DISTRIBUTED ENERGY RESOURCE

by  
Karl W. Heine

**Copyright by Karl W. Heine 2021**

All Rights Reserved

A thesis submitted to the Faculty and the Board of Trustees of the Colorado School of Mines in partial fulfillment of the requirements for the degree of Doctor of Philosophy (Mechanical Engineering).

Golden, Colorado

Date: \_\_\_\_\_

Signed: \_\_\_\_\_

Karl W. Heine

Signed: \_\_\_\_\_

Dr. Paulo Cesar Tabares-Velasco  
Thesis Advisor

Signed: \_\_\_\_\_

Dr. Michael Deru  
Thesis Advisor

Golden, Colorado

Date: \_\_\_\_\_

Signed: \_\_\_\_\_

Dr. Jason Porter  
Associate Professor and Interim Department Head  
Department of Mechanical Engineering

## ABSTRACT

The electric grid of the future is envisioned to be a smart grid, where electricity is managed in coordinated manner between suppliers and users. To achieve this, a high level of electric demand flexibility must be integrated into our building infrastructure. In the U.S., 9% of all electricity generated is used to cool buildings, making this end-use an ideal target for active management through cool thermal energy storage (CTES) technologies. Historic uses for CTES are designed around central chilled water plants, but these systems cool less than 25% of U.S. commercial floorspace. Emerging technologies are under development to serve the many smaller distributed cooling systems, such as rooftop units (RTUs), and have the potential to add CTES to an additional 66% of cooled commercial floorspace. However, these unitary thermal storage systems (UTSS) lack the modeling and analysis tools to evaluate them in the future interactive grid context.

The purpose of this research is to develop the modeling and optimization tools necessary to not only examine UTSS within specific building applications, but also within the multi-building, connected community context. To do so, new simulation tools for the U.S. Department of Energy's OpenStudio energy modeling platform are developed, and a novel mixed-integer linear program is devised to optimize the design and dispatch of multiple CTES technologies, both UTSS and central systems. An integrated simulation-optimization workflow is created to allow for rapid customized analysis. Several case studies are presented illustrating the benefits of community-scale optimization and the impacts of storage costs and utility rate structure on CTES design and dispatch. CTES modeling results, demonstrating the energy and flexibility tradeoffs of various implementations are presented. Optimization results are described in terms of minimum cost, optimal design, and optimal dispatch, with analysis on the CTES impacts on the aggregated community electricity use. It is further demonstrated that community-scale optimization yields greater cost savings potential than an individual-building approach and that certain CTES technologies are more appropriate for different demand-response cost signals.

# TABLE OF CONTENTS

ABSTRACT .....	iii
LIST OF FIGURES .....	ix
LIST OF TABLES .....	xv
ACKNOWLEDGEMENTS .....	xviii
CHAPTER 1 INTRODUCTION .....	1
CHAPTER 2 SUMMARY LITERATURE REVIEW .....	6
2.1 Load flexibility metrics .....	6
2.2 Sizing and Control of Cool Thermal Energy Storage .....	6
2.3 Modeling CTES in Building Energy Simulations (BES) .....	8
2.4 Optimizing CTES as a Distributed Energy Resource (DER) .....	8
CHAPTER 3 RESEARCH PLAN .....	9
3.1 Research Tasks .....	10
CHAPTER 4 ENERGY AND COST ASSESSMENT OF PACKAGED ICE ENERGY STORAGE IMPLEMENTATIONS USING OPENSTUDIO MEASURES .....	12
4.1 Abstract .....	12
4.2 Introduction and literature review .....	12
4.3 Methodology .....	15
4.3.1 The OpenStudio measure .....	15
4.3.2 Building models .....	18
4.3.3 DX and UTSS models .....	21
4.3.4 Fan model .....	24
4.3.5 Utility rates and UTSS controls .....	26

4.3.6	UTSS performance metrics .....	28
4.4	Results and discussion .....	30
4.4.1	Annual energy use.....	30
4.4.2	On-peak and off-peak energy use.....	32
4.4.3	Load shift efficiency.....	33
4.4.4	Ice availability .....	35
4.4.5	Cost performance .....	40
4.5	Conclusions and future work .....	41
4.6	Acknowledgements.....	42
CHAPTER 5 MODELING THE LOAD FLEXIBILITY POTENTIALS FOR ICE ENERGY STORAGE.....		43
5.1	Abstract .....	43
5.2	Introduction.....	43
5.3	Methodology .....	45
5.3.1	Measure Description .....	45
5.3.2	Flexibility Metrics and Methods .....	47
5.3.3	Simulated Building Test Cases .....	49
5.4	Results.....	51
5.4.1	Comparing Example Models to Baseline.....	51
5.4.2	Load add and load shed flexibility through post-processing.....	54
5.4.3	Load flexibility testing in-simulation.....	56
5.5	Conclusion .....	60
5.6	Acknowledgement .....	61
CHAPTER 6 DESIGN AND DISPATCH OPTIMIZATION OF PACKAGED ICE STORAGE SYSTEMS WITHIN A CONNECTED COMMUNITY .....		62

6.1	Abstract .....	62
6.2	Nomenclature .....	62
6.3	Introduction and literature review .....	63
6.4	Methodology .....	65
6.4.1	Overview of simulation-optimization workflow .....	65
6.4.2	Notation .....	67
6.4.3	UTSS model .....	69
6.4.4	Distributed storage optimization program .....	72
6.4.4.1	Objective function .....	72
6.4.4.2	Constraints .....	73
6.4.5	Limitations of this approach .....	74
6.5	Case study community .....	76
6.5.1	Building models and location .....	76
6.5.2	UTSS model data .....	78
6.5.3	Annualized life cycle cost estimate .....	79
6.5.4	Solution method and sensitivity analyses .....	80
6.6	Results and discussion .....	82
6.6.1	Minimum annual cost .....	82
6.6.2	System design .....	82
6.6.3	Optimal dispatch .....	83
6.6.4	Sensitivity results .....	87
6.6.4.1	Median UTSS state-of-charge .....	87
6.6.4.2	Optimization timestep .....	88
6.6.4.3	Annualized life-cycle cost estimate .....	89
6.7	Utility of the community optimization approach .....	91

6.8	Conclusions.....	93
6.9	Acknowledgements.....	94
<b>CHAPTER 7 DESIGN AND DISPATCH OF CENTRAL ICE STORAGE SYSTEMS ACROSS MULTIPLE CHILLED WATER PLANTS.....</b>		
7.1	Methodology for central CTES simulation-optimization .....	95
7.2	Chiller performance model .....	98
7.2.1	Getting the chiller performance models from building energy simulation .	100
7.2.2	Charging performance.....	101
7.2.3	Discharging performance .....	102
7.3	CTES performance model.....	104
7.4	Central CTES optimization program .....	105
7.4.1	Central CTES formulation .....	107
7.4.2	Assumptions and limitations of the central CTES program.....	110
7.5	Demonstrating the revised formulation with a two-loop campus .....	110
7.5.1	Description of campus.....	111
7.5.2	Ice thermal storage tanks.....	113
7.5.3	Interruptible service utility rates .....	114
7.6	Central CTES optimization results .....	116
<b>CHAPTER 8 INTEGRATED SIMULATION-OPTIMIZATION WORKFLOW COMBINING DISTRIBUTED AND CENTRAL THERMAL STORAGE SYSTEMS.....</b>		
8.1	Integrated optimization program.....	123
8.1.1	Optimization program notation .....	123
8.1.2	Integrated CTES formulation .....	125
8.1.2.1	Objective function .....	126
8.1.2.2	Constraints.....	126

8.1.2.3	UTSS Parametrization.....	128
8.2	Demonstrating the complete workflow on a mixed case.....	128
8.2.1	Description of buildings and plants.....	129
8.2.2	Utility rates for flexibility .....	130
8.2.3	Thermal storage devices and costs .....	132
8.3	Integrated workflow optimization results .....	132
8.3.1	Minimum cost .....	133
8.3.2	Optimal design .....	134
8.3.3	Optimal dispatch .....	135
CHAPTER 9 CONCLUSIONS AND FUTURE WORK.....		142
9.1	Summary of key conclusions.....	142
9.2	Research contributions.....	143
9.3	Areas for future research.....	144
REFERENCES .....		146
APPENDIX A OPENSTUDIO MEASURES FOR PACKAGED AND CENTRAL ICE THERMAL ENERGY STORAGE SIMULATION IN ENERGYPLUS .....		159
APPENDIX B CODE FOR CTES OPTIMIZATION IN A CONNECTED COMMUNITY ...		160
B.1	Model file: integrated.mod.....	160
B.2	Data file: integrated.dat.....	162
B.3	Run file: integrated.run .....	164
APPENDIX C PERMISSION FROM PUBLISHERS .....		166

## LIST OF FIGURES

- Figure 3-1: The two main methodologies employed by this research project. The upper path is an iterative approach to sizing and controlling cool thermal energy storage (CTES) in buildings via energy simulation. The lower path begins with energy simulation results and then optimizes the CTES design and dispatch to achieve a minimum cost solution. The italics indicate the chapter in which a specific topic is presented. .... 9
- Figure 4-1: Packaged RTU augmented with UTSS. The RTU components are outlined in black dotted line; the UTSS components are outlined in blue dashed line. The EnergyPlus UTSS object contains all the components outlined in red. .... 16
- Figure 4-2: Measure inputs available in the OpenStudio Application..... 17
- Figure 4-3: DOE prototype model for standalone retail buildings ..... 18
- Figure 4-4: (a) DX cooling coil coefficient of performance at select wet-bulb temperatures as a function of ambient dry-bulb temperature. (b) UTSS coefficient of performance during ice tank charging at select states-of-charge as a function of dry-bulb temperature. .... 22
- Figure 4-5: (a) Maximum heat transfer (HX) rate multiplier for UTSS during charging at various states-of-charge as a function of ambient dry-bulb temperature. (b) Maximum heat transfer rate multiplier for UTSS during discharging, which is only a function of ambient wet-bulb temperature..... 24
- Figure 4-6: Part load fraction curve for variable-speed vane-axial fan as a function of flow fraction, used in PVAV models ..... 25
- Figure 4-7: Time-of-use electricity prices with varying on-peak rate multipliers derived from the average electricity price in the United States in 2019 [79]. On-peak hours are from 15:00-20:00 daily and contain ~33% of the baseline buildings daily energy use. .... 27
- Figure 4-8: Relative annual increases in electricity consumption after adding UTSS to each baseline model, divided into facility (i.e., total), cooling, and fan components..... 31

Figure 4-9: Average changes in monthly electricity use and maximum demand during the on-peak and off-peak periods, calculated over the months of June-September.....	32
Figure 4-10: (a) Daily load shift efficiencies for UTSS implemented on retrofit and new-construction PSZAC systems. Wide daily variation is observed, but few days achieve $\eta_{shift} \geq 1$ . (b) Daily load shift efficiencies for the retrofit and new-construction PVAV systems. Significantly more days achieve $\eta_{shift} \geq 1$ compared to the PSZAC designs.....	34
Figure 4-11: (a) Histogram of daily ice availability values for retrofit buildings with either PSZAC or PVAV systems. (b) Histogram of daily ice availability values for new buildings with either PSZAC or PVAV systems.....	36
Figure 4-12: Load duration curves for the retrofit PVAV example for the months of UTSS operation (June 1 - September 30), augmented with the coincident cooling electric power for (a) baseline building total electric (Base) and cooling electric (Base-Cooling) curves without energy storage; and (b) baseline total electric building (Base), total electric for building with UTSS (UTSS) and cooling (UTSS-Cooling).....	39
Figure 4-13: A zoomed-in view of the top 8400 timesteps (700 hours) during UTSS operation of the retrofit PVAV example. (a) shows that in the 6675 timesteps (~556 hours) left of the vertical dashed line, the cooling loads are not reduced by our current UTSS control strategy. However, (b) shows the coincident daily minimum ice availability values for these peak timesteps.....	39
Figure 4-14: Relative annual cost savings for cooling electricity for UTSS implementations as a function of on-peak time-of-use multiplier ( $x_{tou}$ ). Data points are extrapolated into curves to represent the cost savings trends for each model. ....	40
Figure 5-1: Select user inputs for ITS measure .....	46
Figure 5-2: User inputs for demand response tester .....	46
Figure 5-3: September average daily profiles for facility electric demand .....	52
Figure 5-4: Annual load duration curves for facility electric demand.....	54

Figure 5-5: Three-hour load shed event on Sept. 19. Rebound effects observed at end of day and during recharge. ....	57
Figure 5-6: Five-hour load shed event on Sept. 21. Chiller operation is prohibited during DR event and ice is insufficient to meet full load. Rebound effects are immediate and sever; recharge time is also extended. ....	58
Figure 5-7: Five-hour load shed event on Sept. 21 with chiller operation permitted during the DR event. Immediate rebound is less severe, but peak kW <sub>e</sub> reduction during the event is greatly impacted. ....	59
Figure 5-8: Five-hour load add event on Sept. 21. Chiller meets full cooling load during event and ice charge hours are subsequently reduced. ....	60
Figure 6-1: A simulation-optimization workflow to design and dispatch packaged thermal storage systems in a connected community of grid-interactive buildings. Background colors designate element type: blue for models, white for input data sets, orange for simulation and optimization processes, and green for final results. Section numbers indicate where the UTSS and optimization models are presented in this paper.....	65
Figure 6-2: Depiction of a UTSS integrated with an RTU. Components of the UTSS are shown in blue. Note the placement of the UTSS evaporator coil within the RTU airstream [71]. ....	70
Figure 6-3: Aggregated weighted occupancies of each building type, presented to illustrate the temporal coincidence of building occupancy and relative sizes of each building .....	77
Figure 6-4: Aggregated electric power demand over a near-peak summer day from the baseline energy results: (a) total electric power demand; (b) cooling-only electric power demand.....	78
Figure 6-5: Cost comparison of the optimization program solution with baseline community energy bill. The total annual cost is the sum of the energy charges, demand charges, and ALCC for (a) [community aggregate] total electric energy costs and (b) cooling-only electric energy costs.....	82

Figure 6-6: Optimal UTSS placement by RTU, grouped by building. Each gray box depicts the maximum number of UTSS that could be assigned to given RTU, which is equivalent to the parameter  $m_{in}$ . The blue boxes depict the number and location of UTSS given by the optimized solution..... 83

Figure 6-7: Comparison of Baseline and Optimal aggregated electric demand profiles. (a) shows the full-year profile, where optimized maximum values for each demand period  $d$  (one per month) are clearly visible. (b) shows one selected week, illustrating charge and discharge periods, as well as the optimization response to both demand charges and time-of-use energy charges. .... 84

Figure 6-8: Annual load duration curve for the community aggregate power demand..... 85

Figure 6-9: Control signals for each UTSS at their respective RTUs. Positive values are charging signals; negative values are discharging signals. All values are normalized against the appropriate maximum rate of heat transfer at each RTU and timestep ( $Z_{ln} \cdot \bar{q}_{lnt}^x$  or  $Z_{ln} \cdot \bar{q}_{lnt}^y$ ). (a) shows all the UTSS signals for the entire year. (b) shows the dispatch signals for RTUs 3 and 10 for a selected August week..... 86

Figure 6-10: Variance in charging efficiency ( $COP_{tr}^x$ ) as a function of ice tank state-of-charge ( $\tilde{s}_i$ ), normalized against  $\tilde{s}_i = 0.55$ , the value used in our demonstration optimization 88

Figure 6-11: Optimization results as a function of ALCC, bounded by the baseline annual energy bill (Max) in red and the minimum possible energy bill (Min) in green. (a) Total annual cost shown at full scale relative to the energy bill, illustrating a potential 29.7% savings. (b) Zoomed-in results with the total number of UTSS determined by the optimization plotted on the secondary axis..... 90

Figure 6-12: Total number of UTSS determined by the optimization, divided by RTU assignment, as a function of annualized life-cycle cost of the UTSS..... 91

Figure 7-1: Simulation-optimization workflow for ice thermal storage in a connected community with multiple chilled-water loops. To illustrate the workflow capabilities, buildings A, B, and C are shown thermally connected to a district cooling plant; buildings D, E, and F, each have their own chiller(s). The bold numbers serve as references for further discussion the text. .... 96

Figure 7-2: Assumed chiller-storage configuration with return, evaporator-leaving, and supply temperatures indicated .....	99
Figure 7-3: Example chiller power reduction curve with partial and full-storage regions indicated. The black diamond is the point at which the chiller is turned-off, representing the maximum possible reduction in both thermal and electrical loads for a given timestep. ....	103
Figure 7-4: Example linearization of the chiller power reduction curve using two segments for the partial-storage region above the minimum part-load ratio. $\lambda_s^-$ are the segment slopes and $\bar{y}_s$ terms are the applicable ranges.....	103
Figure 7-5: Colorado School of Mines main campus with chiller loops 6 and 7 marked in green and red, respectively [132].....	111
Figure 7-6: Energy use comparison between buildings on chiller loops 6 and 7, with categories for peak non-cooling electricity demand in kW <sub>e</sub> (blue), total annual non-cooling electric energy in MWh <sub>e</sub> (orange), peak thermal cooling load in kW <sub>t</sub> (gray), and total annual thermal cooling load in MWh <sub>t</sub> (yellow).....	113
Figure 7-7: Relative annual savings for optimized scenarios by cost component.....	117
Figure 7-8: Optimal design as a function of utility rate.....	117
Figure 7-9: Base Rate scenario community aggregate electric power demand profiles from March to October, the months of thermal storage operation .....	119
Figure 7-10: ISOC80 scenario community aggregate electric power demand profiles from March to October, the months of thermal storage operation .....	119
Figure 7-11: ISOC160+ scenario community aggregate electric power demand profiles from March to October, the months of thermal storage operation .....	120
Figure 8-1: Integrated simulation-optimization workflow .....	122
Figure 8-2: Selected buildings from the URBANopt example project used to demonstrate the integrated simulation-optimization workflow [109]. The five selected building models are identified in the inset and numbered for identification throughout the remainder of this chapter.....	129

Figure 8-3: Predicted future real-time pricing (RTP) hourly costs of energy over the course of the year for the Cambium Mid-Case 2030 scenario [143] ..... 132

Figure 8-4: Minimum annual cost and relative savings before and after optimization for the E-32, CPP, and Cambium utility rates. The red diamonds represent relative savings between the baseline and optimized cases. .... 133

Figure 8-5: E-32 optimal hourly thermal storage dispatch signals by cooling system over the course of the full year. Positive values are charging signals, negative values are discharging signals. All values are normalized against the maximum rate of charge or discharge at each timestep. .... 136

Figure 8-6: CPP optimal hourly thermal storage dispatch signals by cooling system over the course of the full year. Positive values are charging signals, negative values are discharging signals. All values are normalized against the maximum rate of charge or discharge at each timestep. .... 137

Figure 8-7: Cambium optimal hourly thermal storage dispatch signals by cooling system over the course of the full year. Positive values are charging signals, negative values are discharging signals. All values are normalized against the maximum rate of charge or discharge at each timestep. .... 138

Figure 8-8: Comparison of the community electric power profiles over August 4, during which a critical event occurs coincident with the normal on-peak period ..... 139

Figure 8-9: Hourly cost of electricity on August 4, for the E-32, CPP, and Cambium utility rates..... 140

## LIST OF TABLES

Table 4-1: UTSS object operating modes available in EnergyPlus .....	16
Table 4-2: Envelope characteristics of baseline models .....	19
Table 4-3: Cooling coil capacities by thermal zone, calculated by EnergyPlus, for all baseline models.....	20
Table 4-4: Number of UTSS required by thermal zone for each vintage and HVAC system.....	20
Table 4-5: Design fan pressure rise for retrofit buildings.....	26
Table 4-6: Design fan pressure rise for new construction buildings .....	26
Table 4-7: Annual electricity use for buildings with PSZAC systems. ....	31
Table 4-8: Annual electricity use for buildings with PVAV systems.....	31
Table 4-9: Load shift efficiencies for UTSS implementations .....	34
Table 5-1: Model configurations .....	49
Table 5-2: Model control strategies .....	50
Table 5-3: Annual facility metrics .....	51
Table 5-4: Annual chiller metrics .....	51
Table 5-5: Electric load shifting relative to baseline .....	53
Table 5-6: Summary of annual load shed potentials.....	55
Table 5-7: Summary of load shed during occupied hours .....	55

Table 5-8: Summary of load add potentials .....	56
Table 6-1: Notation for UTSS model and optimization program .....	67
Table 6-2: Summary of connected community building models.....	76
Table 6-3: Baseline building energy results.....	78
Table 6-4: Performance characteristics for the selected UTSS (index $i = 1$ ).....	79
Table 6-5: Cost components used in estimating the annualized life cycle cost.....	80
Table 6-6: Comparison of results using different optimization timesteps.....	89
Table 6-7: Comparison between community and individual building optimization approaches .	92
Table 7-1: Linear approximation errors for the example chiller power reduction curve.....	104
Table 7-2: Notation for the central thermal energy storage optimization program .....	105
Table 7-3: Indexed sets introduced to restrict available operating modes.....	110
Table 7-4: 2019 energy use data for chiller loop 6 .....	112
Table 7-5: 2019 energy use data for chiller loop 7, excluding the Green Center .....	112
Table 7-6: Calculating the cost of generating electricity via Mines’ diesel generators in 2019.	115
Table 7-7: Dates of ISOC service interruption events .....	115
Table 7-8: Annual savings for optimized scenarios by cost component .....	116
Table 8-1: Notation for integrated CTES formulation.....	123
Table 8-2: Summary of annual energy use and cooling systems for selected buildings .....	130

Table 8-3: Summary of energy charges for the three utility rates examined in this scenario.  
All units are in \$/kWh..... 131

Table 8-4: Optimal number and type of CTES devices installed at each building using the  
E-32, CPP, and Cambium utility rates..... 134

## ACKNOWLEDGEMENTS

This work could not have occurred without the support of many generous advisors, mentors, peers, friends, and family, to whom I owe an incredible debt of gratitude.

I first want to thank my advisors, Dr. Paulo Cesar Tabares-Velasco and Dr. Michael Deru for their mentorship and wisdom over the past four years. I hope to emulate their exemplary conduct as researchers and mentors as I progress in my career. I would also like to thank my committee members for their constructive advice: Dr. Tyrone Vincent, Dr. Robert Braun, and Dr. Alexandra Newman. Their challenging questions and feedback were vital to the development of this thesis. I am deeply appreciative of the time and effort they spent evaluating and critiquing my research.

I am further indebted to many individuals at the Colorado School of Mines and the National Renewable Energy Laboratory (NREL) for creating the Mines Energy Fellowship which provided financial support for this work. I want to thank Dr. Michael Deru for working behind the scenes to align my work at NREL closely with my thesis topic, a generous and invaluable service as I pursued this degree.

Over these years, I had the distinct pleasure of working with many individual researchers at NREL. I have learned much from all of them, but am especially indebted to Dr. Ryan Meyer for project leadership and technical advice on thermal storage modeling for commercial buildings, Ben Polly for the opportunity to work on urban building energy modeling and thermal storage projects, and Eric Bonnema for technical instruction on the intricacies of EnergyPlus and OpenStudio.

I thank the current and former members of the AMBER group for their friendship and support. Research may be fascinating, but it is the people with whom we work that gives joy to the process. A special thanks to Dr. Sajith Wijesuriya, Dr. Mohammad Fathollahzadeh, Andrew Speake, Matthew Brandt, and Gabriel Flechas. I also thank the many undergraduate students over the years who put countless hours into creating energy models for various buildings on Mines campus.

Finally, I am incredibly thankful for the love, patience, encouragement, and support of my wife, Stanzie, and my children, Arthur, Martin, and Esther.

*For Stanzie*

## CHAPTER 1

### INTRODUCTION

Across the United States, 36 states have implemented mandates for renewable energy generation over the next several decades, with another eight states implementing renewable goals [1]. With the integration of these new renewable systems comes variability in power generation. California, with its large penetration of solar photovoltaics (PV), has already encountered an excess of mid-day PV generation, a phenomenon which has shifted peak electricity generation costs into morning and evening hours [2, 3]. Vermont, too, has a similar “duck curve” electric demand profile [4]. Other regions of the country, especially the Great Plains states, have large wind potential, which is typically realized during nighttime hours [5]. While each region will uniquely integrate renewables into its energy generation portfolio, all must manage the corresponding variation, thus creating uncertainty for those who make design decisions based on energy cost forecasts.

To plan for future, long-term infrastructure, like buildings, must be designed to be flexible in its energy use. To accomplish this, the U.S. Department of Energy envisions a grid-interactive efficient building (GEB) paradigm. GEB are energy efficient buildings with smart technologies, characterized by the active control of distributed energy resources (DERs) to optimize energy use for grid services, occupant needs and preferences, and cost reductions in a continuous and integrated way [6]. GEBs are differentiated from individual high-performance buildings (such as Net-Zero Energy [7] or Passivhaus [8]) in that they serve as dynamic partners with the grid, providing active electrical load management through load shedding, load shifting, or even load modulation [6].

In the United States, building cooling loads provide a significant challenge and opportunity for the flexible grid future. Approximately 9% of annual electricity generation in the U.S. is used for air-conditioning, and during summer months can drive upwards of 50% of peak electrical demand for a building [9, 10]. These cooling loads provide a challenge because they often do not coincide with times of peak renewable energy generation. Due to the thermal mass of buildings, cooling loads often peak several hours after maximum PV generation, which is

illustrated by the California duck curve mentioned above. However, these loads also provide a flexibility opportunity, as they can be actively controlled through cool thermal energy storage (CTES). CTES systems are used to shift a portion of a building's electricity use out of expensive "on-peak" hours and into lower-cost "off-peak" periods. There are a variety of CTES technologies on the market and under development, but stratified chilled water (sensible storage) and ice (latent storage) are the two dominant mediums. There is a significant body of work covering the models, simulation with building HVAC systems, and optimized design and control for CTES.

Nevertheless, the current body of research does not fully address the needs of a flexible grid. Nearly all the research has focused on integrating CTES with central chiller plants. Only 25% of U.S. commercial floorspace is cooled exclusively using central cooling plants. About 66% of commercial floorspace is cooled using packaged air-conditioning systems that are typically installed on the roof, frequently called rooftop units (RTUs) [10]. The GEB paradigm is not exclusive to large buildings with central plants or to district cooling systems, but must also include this much broader set of smaller buildings that use distributed HVAC equipment. Development of new technologies to provide "packaged" CTES that can be used in distributed manner is underway [11, 12], but has yet to establish an enduring market presence [13]. These packaged CTES are categorized as unitary thermal storage systems (UTSS), and this term is often used to differentiate distributed CTES from the broader category [14]. As these new systems begin to enter the market, two key questions need to be answered:

- How should packaged thermal storage systems be integrated and controlled across a community of GEB to achieve energy flexibility objectives?
- How should these packaged systems coordinate with central CTES technologies in the community context?

Because the value of CTES is dependent on a litany of factors, including local weather, building construction, building operation, utility rates, hardware costs, and overall flexibility objectives, the answers to these questions are best addressed through building energy modeling (BEM) and thermal storage optimization. This research aims to generate a simulation-optimization workflow that can be applied to a wide range CTES technologies, including both

UTSS and central CTES systems. Using this workflow, the above questions may be answered for a broad range of thermal storage scenarios. The goals of this work are to:

1. Create the modeling and simulation tools necessary to evaluate the flexibility potential of multiple CTES technologies working in concert across a connected community. This includes:
  - a. Developing simulation tools for unitary thermal storage systems (packaged CTES) and central CTES using DOE's open-source building energy simulation software.
  - b. Creating optimization formulation(s) to design and dispatch multiple thermal storage systems across a connected community, subject to energy balance and device performance constraints, and using input parameters from building energy simulation.
2. Demonstrate the potential value of CTES (both packaged and centralized) across a connected community to meet flexibility objectives. This is achieved by applying the above tools to example connected communities and evaluating the optimized community performance compared to individual building design approaches, both with and without CTES.

In demonstrating the various developments of the simulation and optimization tools, this research employs ice-based cool thermal energy storage technologies. This restriction is made for several reasons: (1) the only available UTSS on the market are ice-based [15]; (2) charging an ice tank imposes a more significant off-design operating condition for chillers, compared to charging a stratified chilled water tank [16]; and (3) under approximately 7,000 ton-hours of CTES capacity, ice is generally more economical [17], and therefore more appropriate for the majority of buildings for which these analysis tools are intended. Therefore, this thesis focuses exclusively on the ice-based CTES technologies. The remainder of paper is organized into the following chapters:

2. **SUMMARY LITERATURE REVIEW** contains a brief high-level literature review covering load flexibility metrics, available CTES technologies, CTES modeling within building energy simulation, and CTES optimization at the building and community scales.

3. RESEARCH PLAN outlines the main research tasks and presents an overview of the over-arching project methodology.
4. ENERGY AND COST ASSESSMENT OF PACKAGED ICE ENERGY STORAGE IMPLEMENTATIONS USING OPENSTUDIO MEASURES is a journal paper published in *Energy and Buildings* that presents and demonstrates a UTSS modeling tool for the OpenStudio building energy modeling software. This scripting tool, called a “measure,” automates and simplifies the process of adding packaged ice energy storage to building models and controlling them in simulation based on user-inputs. Because the efficacy of CTES is highly dependent on control strategy, this tool allows rapid parametric evaluation of different UTSS capacities and controls within a single building.
5. MODELING THE LOAD FLEXIBILITY POTENTIALS FOR ICE ENERGY STORAGE is a conference paper presented at the 2020 Building Performance Analysis Conference and SimBuild in which a measure for modeling central ice tanks in OpenStudio is presented. Combined with the measure presented in CHAPTER 4, this work helps address CTES questions through an iterative energy simulation approach.
6. DESIGN AND DISPATCH OPTIMIZATION OF PACKAGED ICE STORAGE SYSTEMS WITHIN A CONNECTED COMMUNITY is a journal paper published in *Applied Energy* presenting a mixed-integer optimization program for the design and dispatch of UTSS across a connected community. The paper integrates community-scale building energy simulation and optimization to place, size, and control UTSS at any of the rooftop units (RTUs) within a community of grid-interactive buildings, each containing multiple RTUs. The community-scale optimization is demonstrated to provide greater economic savings compared to optimizing thermal storage at each building individually.
7. DESIGN AND DISPATCH OF CENTRAL ICE STORAGE SYSTEMS ACROSS MULTIPLE CHILLED WATER PLANTS extends the methodology used in CHAPTER 6 to apply to centralized ice storage systems attached to chilled water plants. The unique features presented in this chapter are a method to linearize the chiller efficiency curves at each timestep and a methodology to optimize multiple

chilled water plants simultaneously. This optimization workflow is demonstrated on two chilled water plants located on the Colorado School of Mines campus under interruptible electric utility rate scenarios.

8. **INTEGRATED SIMULATION-OPTIMIZATION WORKFLOW COMBINING DISTRIBUTED AND CENTRAL THERMAL STORAGE SYSTEMS** combines the work of the previous two chapters into an integrated workflow. This allows simultaneous evaluation and comparison of different CTES technologies across a connected community. The optimization formulation is further improved to include explicit electrical flexibility constraints. A five-building case study is evaluated under several utility rates.
9. **CONCLUSIONS AND FUTURE WORK** summarizes the main contributions of this research and proposes areas for further inquiry.

**APPENDIX A. OPENSTUDIO MEASURES FOR PACKAGED AND CENTRAL ICE THERMAL ENERGY STORAGE SIMULATION IN ENERGYPLUS** contains links to the published code for two ice-based CTES simulation tools. These tools allow rapid parametric examination of CTES designs and controls within the U.S. Department of Energy's EnergyPlus simulation software. These files were used to generate the results presented in Chapters 4 and 5.

**APPENDIX B. CODE FOR CTES OPTIMIZATION IN A CONNECTED COMMUNITY** includes the AMPL files required to execute the UTSS optimization program.

## CHAPTER 2

### SUMMARY LITERATURE REVIEW

Optimal design of cool thermal energy storage (CTES) systems in the GEB paradigm requires: (1) well defined flexibility metrics, (2) sizing and control methodologies that are appropriate for the proposed technology in the new environment, and (3) readily accessible modeling tools with which to evaluate system performance. Each is briefly reviewed here. A short literature review on optimization of CTES as a distributed energy resource within a connected community is also provided. Additional, more focused, literature review is provided in each of the chapters containing articles.

#### **2.1 Load flexibility metrics**

GEB requires buildings that can provide some level of demand flexibility. While demand flexibility has been an area of research for several years, it is still lacking industry consensus. From the grid-perspective, load flexibility has been previously described by ramp rate, duration, power, and energy metrics [18]. DOE Buildings Technology Office (BTO) defines four proposed metrics, of which three apply to CTES: energy efficiency [kWh/m<sup>2</sup>], load shifting [kWh/day], and load shedding [kW/event] [6]. Load shifting is the traditional function of ITS today, moving daytime on-peak cooling electricity to nighttime off-peak hours. Energy efficiency gains may simultaneously be achieved relative to a baseline (non-CTES) system. Other studies focused on characterizing building demand flexibility by load categories [19], temporal constraints [20], or preparation and rebound implications [21].

Two key gaps are missing from the above metrics: (1) one glaring absence from the DOE metrics is a load addition metric, needed to characterize how a building with energy storage might assist the grid by absorbing excess renewable generation; and (2) the load shed metric is evaluated on a single event basis, rather than as a building characteristic, making it difficult to use as a design criterion.

#### **2.2 Sizing and Control of Cool Thermal Energy Storage**

Current CTES sizing protocols size chillers and ice tanks based on a design-day cooling load, using simplified equations, followed by an iterative energy analysis to ensure system-

specific mass and energy balances converge. Component sizing is a function of control strategy, which may be full-storage, partial-storage – load limiting, or partial-storage – demand limiting [17]. This sizing method is based on predicted energy use, making it an adequate approach for achieving load shifting objectives.

Research into CTES sizing is less common, generally assuming chiller and ice tank storage capacities based on design-day sizing with no previous work on communities of buildings with distributed cool thermal energy storage. Most CTES research is focused on controls; however, a few recent studies have attempted to produce optimal CTES component sizes for given building loads, weather locations, and cost signals [22-24].

There is a myriad of optimal controller studies associated with cool thermal energy storage, each using a unique cost function and system configuration. Several optimal controllers have been presented for management of ITS operating under variable price signals [25-28]. Some studies improve accuracy by performing the control via co-simulation with a white-box BES [29]. One recent study proposed a control sequence designed to support the increase of renewables on the grid by using cool thermal storage, assessed parametrically considering a 20-year planning horizon [30]. At the campus, district, and community scales, all studies analyze or optimize central chilled water (sensible) systems, rather than ice [31-34], though ice-based systems are used in campus cooling loops [35]. However, there are no studies optimizing distributed CTES, and UTSS have been completely neglected from both sizing and control studies. To date, this review found only two studies [15, 36] that address the potential value of UTSS, despite their emerging presence in the market [11, 37].

The limitation of studies to-date is their custom nature, particularly for the integration of the CTES within the building models; this makes it difficult to apply the results into real-world applications. The exceptions to this are studies that evaluate rule-based controls against optimal controllers to provide comparative insight into high-level control strategies. One, in particular, found that a chiller upstream, storage priority discharge strategy approaches optimal minimum energy use for CTES under partial-storage operation [38].

Two gaps exist with regards to CTES sizing and distribution: (1) no sizing schemes yet account for flexibility requirements, and (2) there is no methodology to simulate and optimize multiple CTES systems distributed across a connected community.

### **2.3 Modeling CTES in Building Energy Simulations (BES)**

Most building energy simulation platforms have CTES models [39-43], but they are not yet available in a format permissive for rapid parametric analysis of various designs and controls in specific applications. Control deficiencies further complicate the evaluation of CTES within building energy simulation (BES). For example, within EnergyPlus, simple control sequences require custom scripting to obtain proper model performance. As a result, industry has avoided using the powerful BES tools for CTES design, instead relying on simplistic sizing equations based on design-day load shifting [17]; this is insufficient for the interactive grid. To facilitate flexibility analyses, improved tools that make CTES models accessible and easily controllable within BES are required.

### **2.4 Optimizing CTES as a Distributed Energy Resource (DER)**

As noted, CTES has been examined as a plant loop resource, whether the chilled water loop serves one building or an entire district; however, a research gap remains for considering the potential value of multiple, coordinated CTES systems meeting different loads across a community. Several distributed energy resource (DER) design and control programs exist, but do not yet consider both central CTES and UTSS. These include Renewable Energy Optimization (REopt) [44], Hybrid Optimization Model for Electric Renewables (HOMER) [45], Distributed Energy Resources-Customer Adoption Model (DER-CAM) [46], and Xendee [47].

A few recent studies show how CTES can be integrated to provide a grid service, such as reducing power generation costs [48] or facilitating renewable penetration and utilization [30, 49]. Yet these also do not address the multiple CTES technologies working in concert across a connected community.

## CHAPTER 3 RESEARCH PLAN

The core of this dissertation focuses on developing and exercising a methodology to optimally design (sizing and location) and dispatch a variety of ice thermal energy storage devices for use in grid-interactive connected community. Figure 3-1 below shows the workflow highlighting the design, verification, and evaluation aspects of the project. Given a set of electrically connected buildings, CTES system designs are produced via both iterative simulation and mathematical optimization.

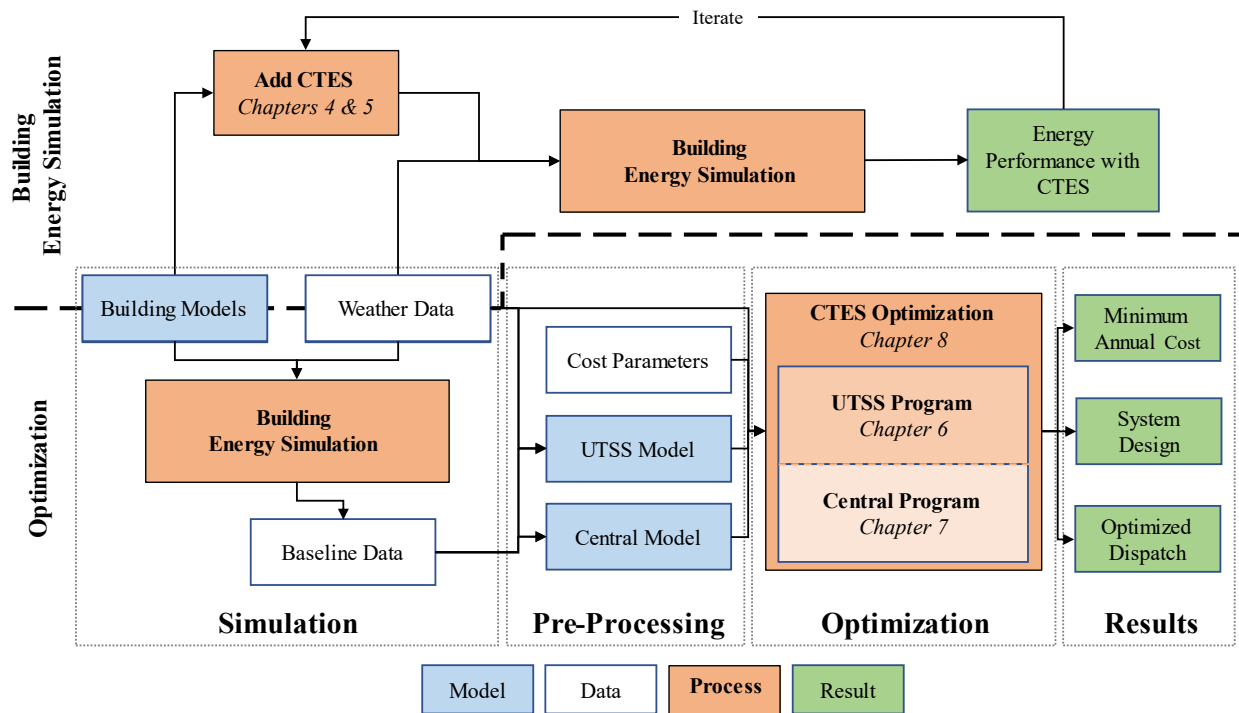


Figure 3-1: The two main methodologies employed by this research project. The upper path is an iterative approach to sizing and controlling cool thermal energy storage (CTES) in buildings via energy simulation. The lower path begins with energy simulation results and then optimizes the CTES design and dispatch to achieve a minimum cost solution. The italics indicate the chapter in which a specific topic is presented.

The upper path, or the Building Energy Simulation path, is a parametric approach to CTES design and requires the ability to simulate various CTES types, configurations, and controls in an efficient manner. To accomplish this, special scripts, called measures, for the

open-source OpenStudio® building energy simulation platform are developed, tested, and published.

The lower path, or the Optimization path, begins with a building set without storage and optimizes the design and dispatch of CTES across the community via mixed-integer linear programming to achieve a minimum annual cost. The cost functions of interest for this project are those associated with incentivizing electrical load shifting via a demand-response signal. The optimization produces an ideal distribution of UTSS or central ice storage tanks, as applicable. It also returns the optimal control schedule for the input cost function. CHAPTER 6, CHAPTER 7, and CHAPTER 8 present the incremental development of the integrated simulation-optimization framework.

### **3.1 Research Tasks**

This research is divided into four key tasks as follows:

1. Perform literature review and define load flexibility metrics: This task consists of performing a literature review of existing and proposed load flexibility metrics for buildings and synthesizing the results into useful inputs for evaluating CTES designs. Contributions from this task are load-add metrics and seasonal or comprehensive add/shed characterizations for buildings with thermal storage. A high-level literature review is included as Chapter 2, with greater detailed literature reviews included in the chapters containing journal papers. Flexibility metrics are presented throughout, but load add and load shed characterizations are explored in detail in CHAPTER 5.
2. Develop cool thermal energy storage (CTES) simulation tools: This task consists of computer programming script development (aka “writing measures”) to allow for rapid simulation of ice thermal energy storage systems using DOE’s OpenStudio and EnergyPlus building energy modeling platforms. Contributions from this task are two ice-storage measures, one for UTSS and one for central CTES, tested, packaged, and published to the Building Component Library maintained by NREL. The UTSS measure is presented in CHAPTER 4; the central CTES measure is demonstrated in CHAPTER 5. The latest versions of each measure are maintained by NREL as part of

the OpenStudio load flexibility measures gem [50], with file locations noted in APPENDIX A0.

3. Develop mixed-integer programs to optimally design and dispatch CTES: This is the primary task of the research and addresses the main research question identified in the proposal – namely, what is the potential value of CTES as a distributed energy resource in a connected community. This task develops a framework that optimally designs and dispatches multiple CTES technologies within a connected community. Due to fundamental differences in the operation of centralized water-side and distributed air-side cool thermal energy storage devices, the optimization will be divided into two formulations: (1) [Distributed] UTSS and (2) Central CTES. The general optimization objective is to obtain a minimum cost CTES design, while meeting building cooling load, hardware performance, and demand flexibility constraints. The contributions of this task are three optimization formulations and their associated pre/post-processing scripts. A journal paper, presenting a simulation-optimization workflow for UTSS within a connected community, is included as Chapter 5. The Central CTES program and its associated pre-processing methods, is presented in CHAPTER 7.
4. Complete and package the simulation-optimization workflow: This task integrates the two distinct UTSS and Central CTES programs into a single simulation-optimization workflow. This permits comparisons between air and water-side thermal storage technologies in specific community contexts. The final optimization formulation and its application are presented in CHAPTER 8. The various scripts required for workflow execution are publicly available online as noted in APPENDIX B.

## CHAPTER 4

### ENERGY AND COST ASSESSMENT OF PACKAGED ICE ENERGY STORAGE IMPLEMENTATIONS USING OPENSTUDIO MEASURES

A paper published in *Energy and Buildings* [51]. Rights managed by Elsevier.

Karl Heine, Paulo Cesar Tabares-Velasco, and Michael Deru

#### **4.1 Abstract**

As renewable portfolio standards enforce the expansion of renewables on the U.S. grid in the coming years, old storage technologies must be re-evaluated for a dynamic, interactive future grid. Ice thermal storage, traditionally for diurnal load shifting on large central chiller plants, is also viable in packaged devices for most buildings that lack central plants. However, modeling of these unitary thermal storage systems (UTSS) has been very limited to-date. To help make packaged thermal storage modeling more accessible, this paper presents a recently developed OpenStudio measure for rapid analysis of UTSS. Using this measure, we assess the UTSS implementation in new and retrofit retail buildings with both packaged single zone air conditioners (PSZAC) and packaged variable air volume (PVAV) systems. Each implementation is evaluated on annual energy use, fan energy use, load shifting efficiency, daily unused ice availability, and potential cost savings under various time-of-use rates. Deficiencies with schedule-based control are highlighted by comparing the daily unused ice and the cooling-electricity load duration curve. Annual energy use increases by 1.2-3.7%, but on-peak electric demand is reduced by 32.2-36.6%.

#### **4.2 Introduction and literature review**

The increased market penetration of distributed renewable energy generation poses several new challenges to the grid, in particular: (1) the intermittent nature of wind and solar power sources can lead to large, rapid variations in the electrical demand from the power grid throughout the day; (2) regions with large solar generation suffer from large end-of-day ramp requirements as residential loads increase coincidentally with sunset. As the majority of states in the U.S. implement Renewable Energy Portfolio Standards (RPS) in the coming decades [1],

electricity generation costs will become more variable, and storage requirements will greatly increase to accommodate the variable generation. This storage may be installed at the utility-level or it may be distributed across the grid, as envisioned by the Department of Energy's grid-interactive efficient building program [6]. While batteries remain the most versatile electricity storage platform, thermal energy storage (TES) can also play a role in grid flexibility, as batteries have higher capital and embodied energy costs making them prohibitive for ubiquitous behind-the-meter storage applications [52, 53].

Cool thermal energy storage (CTES) is a proven technology for providing flexibility through diurnal load shifting. When properly sized and controlled, chillers with ice-based CTES systems can provide both energy-use and energy-cost savings relative to systems without storage [17]. The potential energy and cost impacts of controlling building cooling loads with CTES under traditional utility rates are well documented [25-29], and cost savings can be significant when under time-of-use electricity rates [16, 26, 54]. While CTES applications extend beyond space cooling to include commercial refrigeration processes [55, 56], turbine inlet cooling [57, 58], and industrial applications [17], it remains primarily a technology for temporally shifting the electricity use required for cooling buildings. This shifting may be provided by either sensible or latent mediums. Sensible CTES are predominately stratified chilled water tanks connected to district cooling systems. Tank sizes vary substantially, ranging from ~200,000 gallons to over 15 million gallons. When serving individual buildings or smaller chiller plants, latent storage via ice is more frequently used due to space and economic constraints [17]. Though water and ice dominate, other storage phase-change materials (PCMs) are both currently available on the market and under active research [59-64].

CTES has been traditionally employed at central chiller plants, yet only 25% of U.S. commercial building floorspace is cooled exclusively by central chillers or district systems [10]. Packaged thermal storage units, called unitary thermal storage systems (UTSS), differ from a central "tank farm" and are designed to bring thermal storage to the smaller buildings that do not use central plants. An estimated 66% of U.S. commercial floorspace is cooled using equipment compatible with UTSS [10]. UTSS are fairly new implantation of CTES technology, with ice-based devices entering the market in 2010 [65]. These were successfully used as public utility assets in California to help address their existing duck-curve [37], but struggled to achieve

success in the consumer market [13]. Other, packaged thermal storage designs using new PCMs are currently under development [11, 54, 66]. Nevertheless, UTSS of any variety have not yet successfully penetrated the air conditioning market.

One of the challenges facing UTSS is a lack of technical analysis on possible implementations under the grid-interactive efficient building (GEB) paradigm. As with any type of energy storage, the efficacy of UTSS depends not only on the design of the storage medium, but also on how it is implemented within the building. Building type, climate, installed cooling equipment, type of air distribution system, occupancy, thermal loads, electric utility rate, control strategy, and owner energy goals all impact how effective a particular storage technology may be [15, 17]. To make such case-specific evaluations, rapid, flexible modeling tools for UTSS are needed. However, very little has been published on the modeling and application of UTSS at the building level. Because UTSS contain their own internal charging equipment and are incorporated into the air-side of an HVAC system, they require different component models than an ice-tank object which is charged by an external chiller and integrates with a chilled-water loop. To date, the available experimentally-derived performance curves for modeling UTSS are extremely limited.

The most comprehensive work on UTSS to-date is a study that developed an EnergyPlus model object for the ice-based UTSS [36]. This UTSS object, with a set of ice-based performance curves, is integrated into EnergyPlus distributions as a single-speed cooling coil, called “Coil:Cooling:DX:SingleSpeed:ThermalStorage” [40]. However, this object is not readily accessible through any of the graphical user interfaces that employ EnergyPlus as their underlying simulation engine, including DOE’s OpenStudio [67], making it effectively invisible to modelers. The alternative is to use an external UTSS model via co-simulation tools such as the Building Controls Virtual Test Bed [68] or a Functional Mockup Interface [69], but no studies have been published on UTSS using this method. The general inaccessibility of the existing models has limited the performance analysis which has been conducted on UTSS to date.

This study addresses these simulation gaps with the following two objectives: (1) present an improved method of rapidly modeling packaged thermal storage units and (2) assess the energy and cost impacts of adding ice storage to buildings with both centralized and decentralized air conditioning distribution systems. The novel contributions of this study include:

(1) development of new OpenStudio measure for parametric analysis of UTSS design and controls, (2) inclusion of fan pressure rise requirements in modeling the UTSS, (3) detailed energy use and efficiency analysis of realistic UTSS implementations in both packaged variable air volume (PVAV) and packaged single zone air conditioner (PSZAC) systems, and (4) a UTSS economic analysis using five time-of-use energy cost multipliers.

### **4.3 Methodology**

To achieve this chapter's two objectives, the methodology is divided into four subsections. First, an overview of the OpenStudio measure developed for this project is presented. Second, we describe four example buildings used as a demonstration case and their pertinent subcomponent models. Third, we create a set of example utility rates and define a thermal storage control sequence that mitigates cooling electricity use during on-peak hours. Finally, we define the metrics used in assessing the UTSS performance in each building.

#### **4.3.1 The OpenStudio measure**

This study develops a simulation tool for packaged ice storage systems (aka UTSS) using the EnergyPlus building energy modeling platform. The simulation tool is an OpenStudio measure that makes the EnergyPlus packaged ice storage object easily accessible to users within the OpenStudio Application and Parametric Analysis Tool. The measure is published under the name "Add Packaged Ice Storage" and is included with the OpenStudio Load Flexibility Measures gem [70]. The packaged thermal storage component is the Coil:Cooling:SingleSpeed:DX:ThermalStorage, hereafter denoted as the UTSS object. It is a compound object that includes a direct-expansion (DX) cooling coil, a separate UTSS refrigerant coil, the ice storage tank, and all associated performance curves and parameters. The coil can be placed into any EnergyPlus CoilSystem:Cooling or AirLoop:HVAC container object for placement in an air loop. Six operating modes, listed in Table 4-1 on the following page, are available within EnergyPlus and are actuated through an integer schedule value.

Table 4-1: UTSS object operating modes available in EnergyPlus

Mode	Description	DX Availability	UTSS Operation
0	System Off	Off	Off
1	Cooling Only	Available	Off
2	Cooling and Charge	Available	Charging
3	Cooling and Discharge	Available	Discharging
4	Charge Only	Off	Charging
5	Discharge Only	Off	Discharging

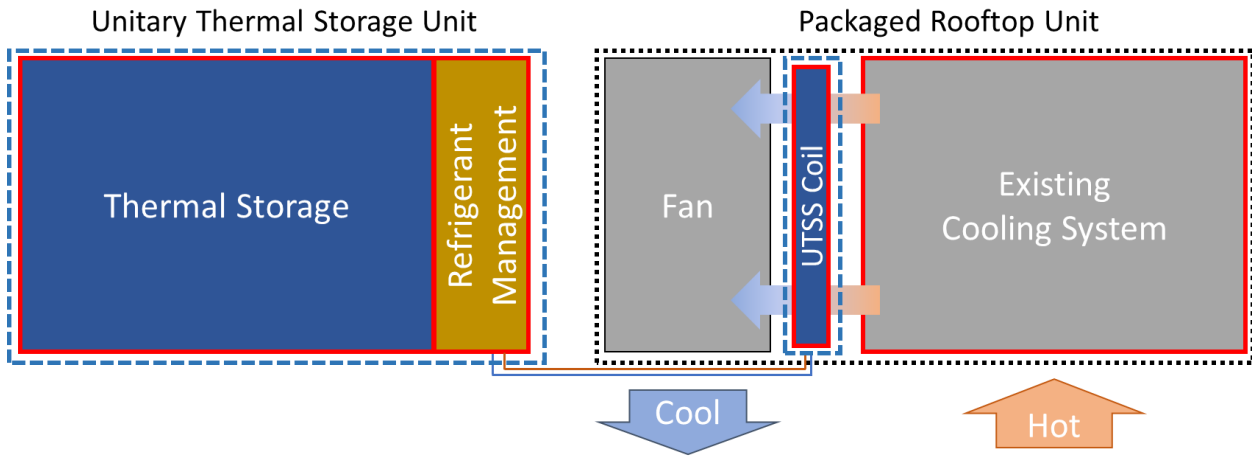


Figure 4-1: Packaged RTU augmented with UTSS. The RTU components are outlined in black dotted line; the UTSS components are outlined in blue dashed line. The EnergyPlus UTSS object contains all the components outlined in red.

Using the ice-based performance data publicly available in EnergyPlus 9.3 example file “RetailPackagedTESCoil.idf,” operating modes 0, 1, 4, and 5 are accessible within the measure. Operating modes 2 and 3 require performance curves generated from the specific partial-storage operating point of the combined DX and UTSS. No example open-source curves are currently available for these operating modes, and development of such curves exceeds the scope of this project. Figure 4-1 shows the schematic of a packaged rooftop unit (RTU) with an integrated UTSS, and highlights in red the physical components that are included within the UTSS object. The UTSS contains a thermal storage tank filled with water/ice and a collection of submerged heat exchange coils. The latent energy storage in the ice serves as a nearly uniform temperature

reservoir for heat rejection from a refrigerant that is used to both charge and discharge the ice tank. During ice charging mode, the refrigerant is circulated between the UTSS-internal compressor and the storage tank in a vapor compression cycle using the ice as the evaporator. During ice discharge mode, the refrigerant is pumped between the storage tank and a cooling coil placed into the RTU airstream to provide zone cooling.

Inputs	
<p>Select Coils to Replace:</p> <p><input checked="" type="checkbox"/> Coil Cooling DX Single Speed 1</p> <p>Input the ice storage capacity [ton-hours] To specify by coil, in alphabetical order, enter values for each separated by comma.</p> <p>AutoSize</p> <p>Enter a sizing multiplier to manually adjust the autosize results for ice tank capacities</p> <p>1.0</p> <p>Select ice storage control method</p> <p>EMSCControlled</p> <p>Select the operating mode schedule for the new TES coils Use the fields below to set a simple daily ice charge/discharge schedule. Or, select from pre-defined options.</p> <p>Simple User Sched</p>	<p><input checked="" type="checkbox"/> Run TES on the weekends Select if building is occupied on weekends</p> <p>Select season during which the ice cooling may be used Use MM/DD-MM/DD format</p> <p>01/01-12/31</p> <p>Input start time for ice charge (hr:min) Use 24 hour format</p> <p>22:00</p> <p>Input end time for ice charge (hr:min) Use 24 hour format</p> <p>07:00</p> <p>Input start time for ice discharge (hr:min) Use 24hour format. If 'AutoSize' is selected for ice capacity, these Inputs set an Ice capacity sizing factor. Otherwise, these only affect discharging schedule.</p> <p>12:00</p> <p>Input target end time for ice discharge (hr:min) Use 24 hour format</p> <p>18:00</p>

Figure 4-2: Measure inputs available in the OpenStudio Application

Several measure arguments for UTSS design and control are accessible to users via the OpenStudio Application graphical user interface or through a command-line workflow. Figure 4-2 shows the user input screen for an example building with a single DX unit. Users may autosize or specify total UTSS capacity to be placed at each RTU, as well as specify a capacity multiplier for parametric analysis. UTSS control may be performed using built-in or user-defined schedules, or with an Energy Management System script – should more complex controls be required. UTSS operation may be controlled directly from the measure arguments through operating season, permitted daily charging window, and permitted daily discharging window. This allows users to easily compare the building energy and thermal comfort impacts of different UTSS control schedules. Based on the user selections, the measure will inspect the EnergyPlus building model, add UTSS objects to the specified RTUs, create and apply control sequences, and generate UTSS-related output variables for simulation analysis. Further information on the

measure and the latest code revision are publicly available as part of the OpenStudio load flexibility measures gem [70, 71].

### 4.3.2 Building models

To evaluate the potential benefits of UTSS, this study uses the new OpenStudio measure using two vintages of DOE prototype stand-alone retail buildings with two different cooling system configurations, for a total of four baseline buildings. Each of these baseline buildings is modified by adding UTSS, thus eight buildings are evaluated. The intent of this analysis is to assess the relative impacts of adding ice storage to centralized and decentralized conditioned-air distribution systems in both retrofit and new construction applications.

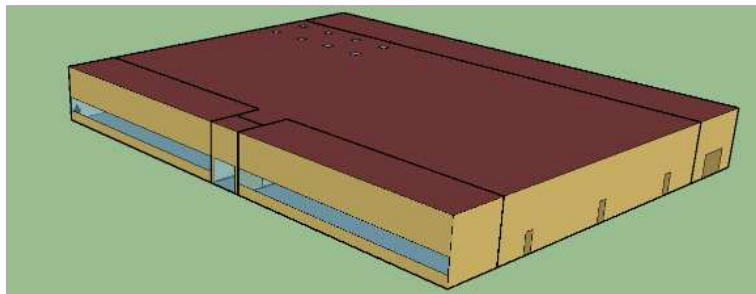


Figure 4-3: DOE prototype model for standalone retail buildings

The two analyzed stand-alone retail buildings are the Pre-2004 and 90.1-2013 vintages for a warm-dry climate zone (3B), both created using the OpenStudio standards gem [72]. The older vintage represents a retrofit opportunity; the 2013 vintage represents more-efficient new construction. All simulations are conducted using TMY3 weather data from El Paso, TX [73]. Both buildings, illustrated in Figure 4-3, have a floor area of 24,695 ft<sup>2</sup> (2,294 m<sup>2</sup>), an aspect ratio of 1.28, and a street-side window-to-wall ratio of 0.254. The hours of operation are 8am-9pm Monday through Saturday, and 10am-7pm on Sunday. The maximum occupancy of both buildings is 330 and plug loads are identical; however, the retrofit building experiences higher infiltration and much greater lighting power density. Table 4-2 highlights the envelope and lighting differences between the vintages.

Table 4-2: Envelope characteristics of baseline models

Parameter	Retrofit Building	New Construction
Exterior Mass Walls	R-3.45 h-ft <sup>2</sup> -°F/Btu (U-1.647 W/m <sup>2</sup> -K)	R-8.13 h-ft <sup>2</sup> -°F/Btu (U-0.698 W/m <sup>2</sup> -K)
Built-up Roofs	R-20.83 h-ft <sup>2</sup> -°F/Btu (U-0.273 W/m <sup>2</sup> -K)	R-25.64 h-ft <sup>2</sup> -°F/Btu (U-0.221 W/m <sup>2</sup> -K)
Glazing	Single-Pane SHGC-0.25	Double-Pane SHGC-0.25
Maximum Infiltration	0.82 ACH	0.68 ACH
Lighting Power Density	3.0 W/ft <sup>2</sup> (32.3 W/m <sup>2</sup> )	1.3 W/ft <sup>2</sup> (14.6 W/m <sup>2</sup> )

To ensure all systems have equivalent comparisons, we modified the original cooling HVAC systems on the DOE prototypes to use single-speed compressors, each with a rated COP of 3.23. This value was taken from the original 2013 DOE prototype model and applies only to the compressor, not the full air-handling unit. Two baseline HVAC systems are used in both building vintages: a single packaged variable air volume (PVAV) system or four packaged single zone air conditioners (PSZAC). The former represents a centralized conditioned-air distribution design; the latter is a distributed design. Both are used in mid-sized commercial applications and, in this case, serve four conditioned zones to maintain a cooling setpoint temperature of 23.9°C (75°F) during operating hours. Table 4-3 shows the cooling coil capacities by serviced zone for each of the two HVAC designs applied to the two building vintages. Each system is sized using a summer design day based on the 0.4% dry-bulb  $\geq$  mean wet-bulb conditions for El Paso International Airport in Texas [74]. Using these conditions for equipment sizing produces almost no difference in the total cooling capacities required for the retrofit and new construction examples for each HVAC system type. From this we conclude that the cooling loads for our selected building type are dominated by occupancy, infiltration, and internal loads, rather than envelope gains.

Table 4-3: Cooling coil capacities by thermal zone, calculated by EnergyPlus, for all baseline models

Thermal Zone	PSZAC Capacities [kW <sub>t</sub> (tons)]		PVAV Capacities [kW <sub>t</sub> (tons)]	
	Retrofit	New	Retrofit	New
Core Retail	110 (31.2)	114 (32.4)	171 (48.6)	173 (49.2)
Front Retail	17 (4.8)	13 (3.7)		
Point-of-Sale	20 (5.7)	16 (4.5)		
Back Space	26 (7.4)	26 (7.4)		

From the four baseline buildings, we create another four models with ice storage, using our OpenStudio measure to add 40 ton-hour (0.51 GJ) ice storage units to meet a five-hour cooling load at design-day conditions. Because we assume UTSS comes in discrete sizes, multiple devices are required for larger zones. Ice storage units are added to every PVAV or PSZAC system within the baseline models for a whole-building comparison.

Table 4-4: Number of UTSS required by thermal zone for each vintage and HVAC system

Thermal Zone	PSZAC [No. UTSS]		PVAV [No. UTSS]	
	Retrofit	New	Retrofit	New
Core Retail	4	4	6	5
Front Retail	1	1		
Point-of-Sale	1	1		
Back Space	1	1		

After preliminarily sizing the UTSS units on a continuous range using the design day conditions, we re-evaluate the sizing applying the discrete size requirements. In several instances, this resulted in drastic over-sizing of the ice storage equipment and large fractions of unused ice during simulation. We progressively decreased the number of UTSS until we reached the minimum number of ice storage tanks to fully meet the desired cooling requirements without

daily exhaustion of the ice supply. This approach ensures sufficient ice capacity with minimal excess, but other sizing approaches or different ice storage devices may produce preferable results. Table 4-4 lists the number of UTSS required to meet the 5-hour cooling load shift requirement.

Even though the PVAV sizing for both the Retrofit and New buildings is nearly identical, the New building requires fewer UTSS than the Retrofit. This is due to the difference in sizing approaches between the primary HVAC equipment and the UTSS. Because the PVAV systems are sized on a continuous scale against a peak load, but the number of fixed-size UTSS is determined by evaluating routine daily loads, the required number of UTSS is one fewer for the newer, more-efficient building.

### 4.3.3 DX and UTSS models

The energy efficiency of the DX coil, used for all four baseline buildings, is determined by the rated coil coefficient of performance ( $COP_{Coil,Rated}$ ) and the energy input ratio as a function of temperature ( $EIR_{Coil}$ ) curve. Equations (4-1) and (4-2) define this efficiency at each timestep as the  $COP_{Coil}$  [40]. Equation (4-2) is a function of dry-bulb ( $T_{db}$ ) and wet-bulb ( $T_{wb}$ ) temperatures in °C, which are obtained from the weather file.  $COP_{Coil,Rated}$  is 3.23 for all baseline DX coils.

$$COP_{Coil} = \frac{COP_{Coil,Rated}}{EIR_{Coil}} \quad (4-1)$$

$$EIR_{Coil} = 0.2829 + 0.0238T_{wb} - 0.0008T_{wb}^2 + 0.1346T_{db} + 0.0003T_{db} - 0.0005T_{wb}T_{db} \quad (4-2)$$

The energy efficiency of the UTSS is a function of operating mode. During the charging-only mode, device COP is characterized as by functions of  $T_{db}$  and ice tank state-of-charge  $SOC$ , given in equations (4-3) and (4-4) 3 and 4 [40]. The coefficients for the UTSS performance curves were derived by Kung, et al. from experimental and field data [36].

$$COP_{Charge} = \frac{COP_{Charge,Rated}}{EIR_{Charge}} \quad (4-3)$$

$$EIR_{Charge} = 0.6134 + 0.4652SOC - 1.4639SOC^2 - 0.0069T_{db} + 0.0008T_{db}^2 + 0.01395SOC \cdot T_{db} \quad (4-4)$$

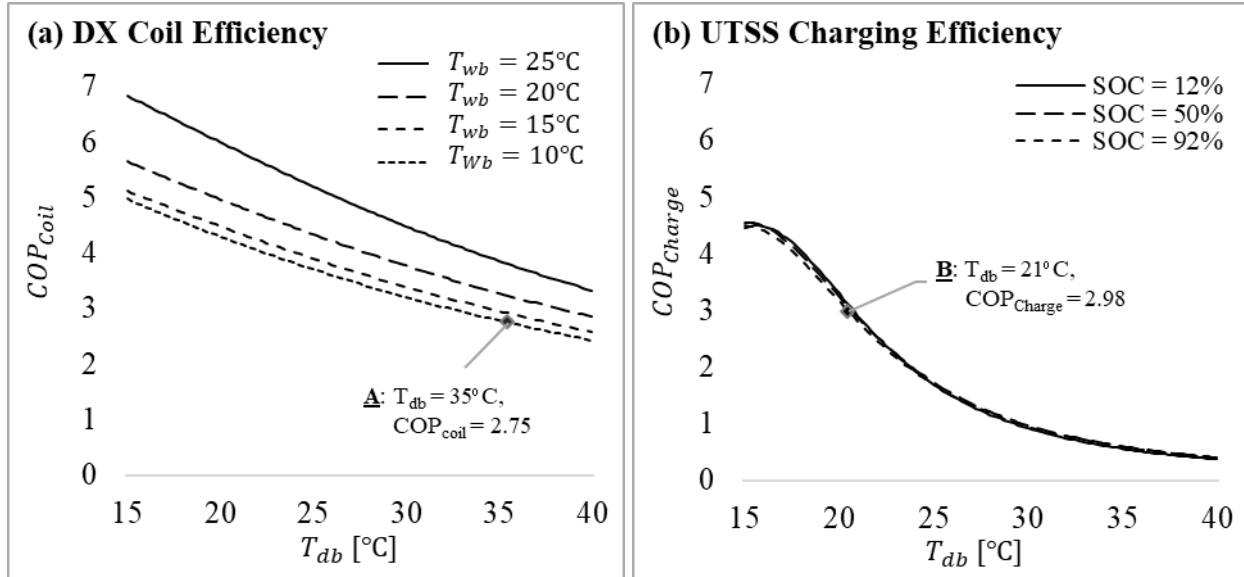


Figure 4-4: (a) DX cooling coil coefficient of performance at select wet-bulb temperatures as a function of ambient dry-bulb temperature. (b) UTSS coefficient of performance during ice tank charging at select states-of-charge as a function of dry-bulb temperature.

Figure 4-4 shows the calculated coefficients of performance over ambient temperatures ranging from 15-40 °C for (a) the baseline DX coil and (b) the UTSS during the charging-only operating mode. The side-by-side comparison helps identify the conditions during which it is advantageous, from an efficiency standpoint, to charge and discharge the thermal storage. For example, if nighttime charging occurs at 21°C (point **B**) and daytime discharging occurs at 35°C (point **A**), the  $COP_{Charge}$  is 2.98 while  $COP_{Coil}$  would have been only 2.75. In this case, whole system energy use would decrease through UTSS operation. However, these situations can only occur in dry climates with high diurnal temperature swings. Other system effects such as the fan power increase and thermal energy losses from the tank further negate the potential for net energy savings. From Figure 4-4(b) we also observe that the charging efficiency of the UTSS is not significantly dependent on the ice tank state-of-charge, but is primarily determined by  $T_{db}$ .

Though  $SOC$  does not significantly impact the charging efficiency of the UTSS, it heavily impacts the rate at which the UTSS is charged. Equations (4-5) to (4-7) give the maximum rate of heat transfer when making ice ( $\dot{Q}_{Charge}$ ) where  $\dot{Q}_{UTSS,Rated}$  is the rated charging capacity of the UTSS compressor and  $CAP_{Charge}$  is the non-dimensional heat transfer multiplier as a function of  $SOC$  and  $T_{db}$ . Equation (4-6) applies when  $SOC$  is greater than or equal to 15%; equation (4-7) applies when  $SOC$  is less than 15%. Both are derived from tabulated data in the EnergyPlus example file [40].

$$\dot{Q}_{Charge} = \dot{Q}_{Charge,Rated} \cdot CAP_{Charge} \quad (4-5)$$

$$CAP_{Charge} = 1.293 - 0.127SOC + 0.0186SOC^2 - 0.0083T_{db} - 0.0001T_{db}^2 + 0.0013SOC \cdot T_{db} \quad \forall \quad SOC \geq 0.15 \quad (4-6)$$

$$CAP_{Charge} = 1.415 - 1.7705SOC + 4.8638SOC^2 - 0.0069T_{db} - 0.0001T_{db}^2 + 0.0046SOC \cdot T_{db} \quad \forall \quad SOC < 0.15 \quad (4-7)$$

The maximum UTSS heat transfer rate during discharge ( $\dot{Q}_{Discharge}$ ) is modeled as a function of the  $T_{wb}$  of the coil inlet air, independent of  $SOC$ , where  $\dot{Q}_{Discharge,Rated}$  is the rated discharging capacity of the UTSS coil and  $CAP_{Discharge}$  is the non-dimensional heat transfer rate multiplier as a function  $T_{wb}$ . Equations (4-8) and (4-9) define the maximum cooling rate that the UTSS can provide during discharge [40]:

$$\dot{Q}_{Discharge} = \dot{Q}_{Discharge,Rated} \cdot CAP_{Discharge} \quad (4-8)$$

$$CAP_{Discharge} = -0.5615 + 0.1340T_{wb} - 0.0028T_{wb}^2 \quad (4-9)$$

During discharge, only the refrigerant circulation pump consumes electricity for the system, resulting in exceptional efficiency in that operating mode. The available example model uses a constant  $COP_{Discharge}$  of 63.9 [40]. Figure 4-5, on the following page, shows the heat transfer rate multipliers for both UTSS charging and discharging as functions of  $T_{db}$  and  $T_{wb}$ , respectively. In Figure 4-5(a) the significant effect of ice tank state-of-charge is apparent, with a ~14% decrease in maximum charging rate at any given temperature as  $SOC$  increases from 5%

to 92%. Figure 4-5(b) shows the strong dependence of ice discharging rate on ambient wet-bulb temperature, especially at  $T_{wb}$  less than 15°C.

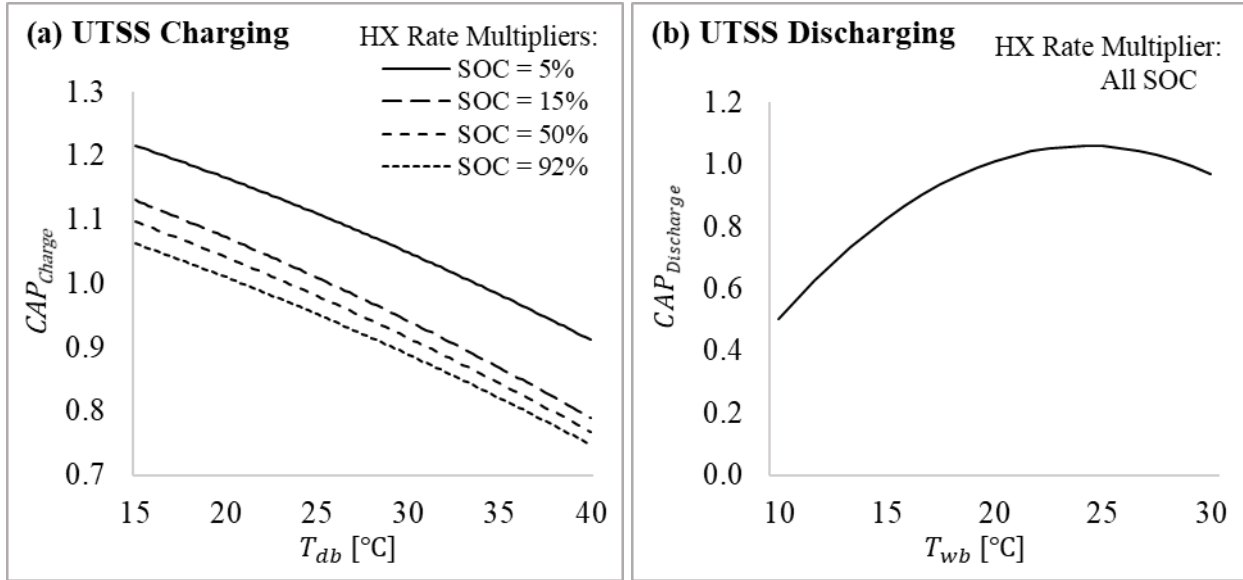


Figure 4-5: (a) Maximum heat transfer (HX) rate multiplier for UTSS during charging at various states-of-charge as a function of ambient dry-bulb temperature. (b) Maximum heat transfer rate multiplier for UTSS during discharging, which is only a function of ambient wet-bulb temperature.

Storage losses from the tank to ambient (i.e., heat gains) are calculated using a heat transfer coefficient of 7.913 W/K [40]. We multiply this by the number of UTSS units at each cooling coil within our building models to obtain the total thermal losses at each timestep.

#### 4.3.4 Fan model

Fan energy increases with the addition of another coil into the airstream. While the pressure rise across the fan increases by only 0.1 in H<sub>2</sub>O, or 23.9 Pa, for each UTSS, the penalty impacts the entire lifetime of the system regardless of storage operation; annual energy-use due to these additional heat exchange coils in the airstream should not be neglected. For our baseline buildings with the PVAV, we use an axial fan performance curve taken from the OpenStudio standards spreadsheet [72], where part-load fraction ( $PLF_{fan}$ ) is calculated as a function of the airflow fraction relative to the rated mass flow rate ( $FF$ ) according to equation (4-10). Equation

(4-11) converts  $PLF_{fan}$  into fan power ( $\dot{W}_{fan}$ ) using the design mass flow rate ( $\dot{m}_{design}$ ), fan pressure rise ( $\Delta P$ ), fan motor efficiency ( $\eta_{motor}$ ), and the air density at the fan inlet ( $\rho_{air}$ ).

$$PLF_{fan} = 0.212 - 0.5693FF + 1.3452FF^2 \quad (4-10)$$

$$\dot{W}_{fan} = \frac{PLF_{fan} \cdot \dot{m}_{design} \cdot \Delta P}{\eta_{motor} \cdot \rho_{air}} \quad (4-11)$$

As all other coefficients in Equation 11 are constants or near constants, the variable speed fan power is essentially a function only of flow fraction ( $FF$ ). Figure 4-6 shows this performance curve over its full operating range; the minimum flow fraction for the fan is 0.15.

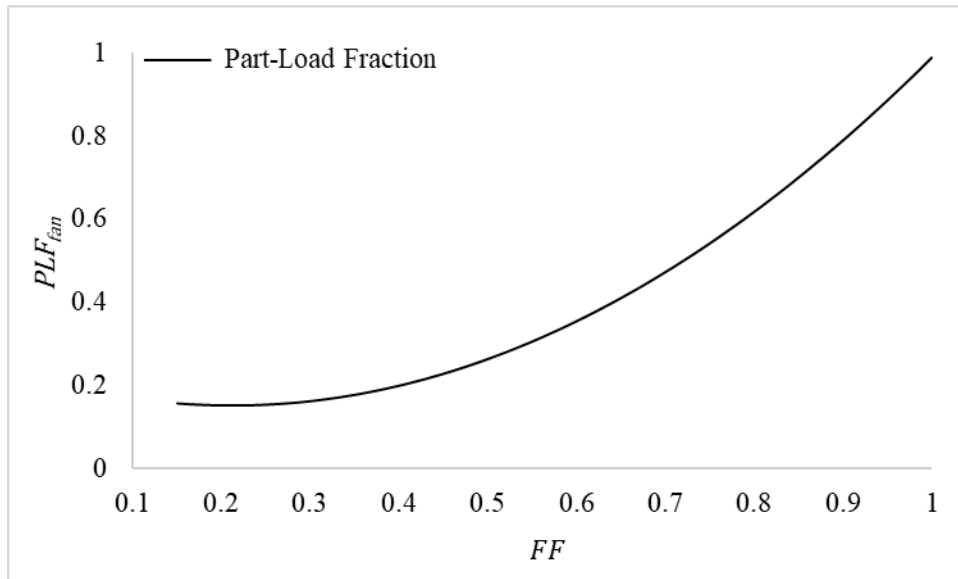


Figure 4-6: Part load fraction curve for variable-speed vane-axial fan as a function of flow fraction, used in PVAV models

The decentralized air distribution models have constant speed fans at each PSZAC unit with all specifications taken from the 2013 vintage prototype. Table 4-5 and Table 4-6 show the different fan pressure requirements for the baseline and UTSS models for each HVAC type by thermal zone. Each increase of 0.1 in  $H_2O$  (23.9 Pa) indicates the addition of one UTSS to the cooling system associated with that thermal zone. Thus, small zones with PSZAC only see an increase of 0.1, while the large PVAV systems incur up to 0.6 in  $H_2O$  (150 Pa) increases.

Table 4-5: Design fan pressure rise for retrofit buildings

Thermal Zone	PSZAC [Pa (in H <sub>2</sub> O)]		PVAV [Pa (in H <sub>2</sub> O)]	
	Baseline	UTSS	Baseline	UTSS
Core Retail	1110 (4.5)	1211 (4.9)	1390 (5.6)	1540 (6.2)
Front Retail	623 (2.5)	648 (2.6)		
Point-of-Sale	623 (2.5)	648 (2.6)		
Back Space	623 (2.5)	648 (2.6)		

Table 4-6: Design fan pressure rise for new construction buildings

Thermal Zone	PSZAC [Pa (in H <sub>2</sub> O)]		PVAV [Pa (in H <sub>2</sub> O)]	
	Baseline	UTSS	Baseline	UTSS
Core Retail	1019 (4.1)	1119 (4.5)	1390 (5.6)	1514 (6.1)
Front Retail	623 (2.5)	648 (2.6)		
Point-of-Sale	623 (2.5)	648 (2.6)		
Back Space	623 (2.5)	648 (2.6)		

#### 4.3.5 Utility rates and UTSS controls

Thermal storage is typically employed to avoid high time-of-use (TOU) energy or demand charges, so UTSS controls are inherently coupled with the local utility rate structure. The maximum reduction in cooling electricity use during on-peak rates is achieved through a full-storage control, in which no mechanical cooling is permitted during a specified time-window and all cooling is provided by the UTSS. Ice charging is performed during overnight hours when  $COP_{Charge}$  is highest. This demonstration study focuses on demonstrating the capabilities of the model and UTSS potential; therefore, we use rule-based controls designed to capitalize on potential electricity bill savings. UTSS optimization is done at the subsequent study found in [75].

The full-storage control mode that discharges between 15:00-20:00 every day from June 1 to September 30, for a total of 121 days of UTSS operation. The afternoon to early-evening discharge window is selected because it coincides with high cooling loads and the end-of-day

decrease in solar generation when high power generation ramp rates would be required. This general rate structure is currently used in several places across the U.S. with high renewable energy penetration [76-78] and provides a starting point for generic UTSS cost analysis. Ice charging is performed between 23:00 and 07:00 daily.

Since electricity rates vary significantly across the U.S., we derive five example rates using average electricity price data for commercial customers [79] as functions of TOU multipliers between the off and on-peak electricity prices. In December 2019, the average cost of electricity for commercial customers in the U.S. was 10.57 ¢/kWh. Based on the fraction of a building’s total electricity use that occurs during on-peak hours, which is ~33% in our baseline buildings, we can calculate both the off-peak and on-peak electricity prices required to achieve that same average cost over the course of a year. The goal is to develop a set of utility rates that vary in their on-peak TOU multiplier ( $x_{tou}$ ), but result in approximately the same total electricity bill at the end of the year. In this analysis, we explore five  $x_{tou}$  values ranging from 1.5 to 3.5. The resulting utility rates are shown in Figure 4-7 on the following page.

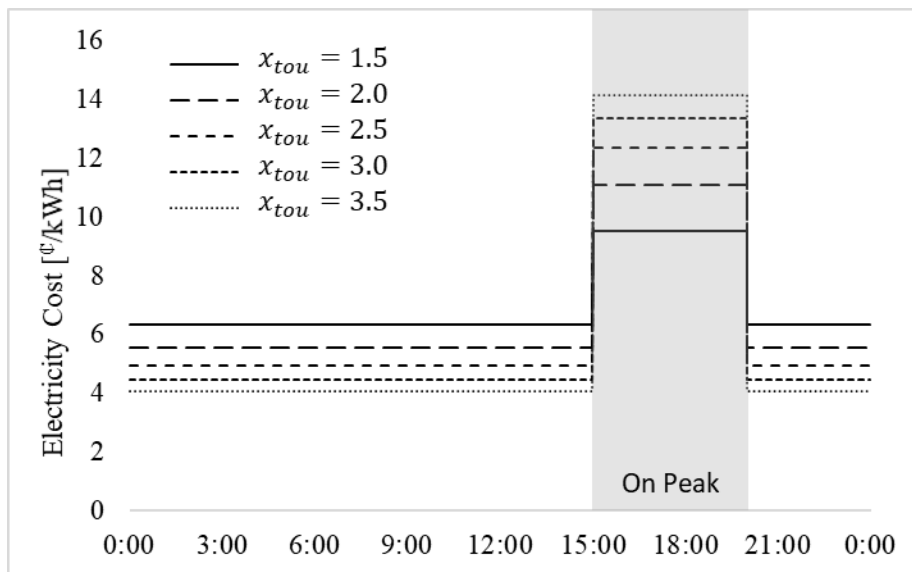


Figure 4-7: Time-of-use electricity prices with varying on-peak rate multipliers derived from the average electricity price in the United States in 2019 [79]. On-peak hours are from 15:00-20:00 daily and contain ~33% of the baseline buildings daily energy use.

One of the major economic drivers of current thermal storage implementations is demand charge reduction. We choose not to include an explicit demand charge in our economic analysis

for several reasons. First, the demand savings potential of thermal storage is already documented in literature with various case studies [22, 80, 81]. Second, a future grid dominated by variable electricity generation incentivizes a direct connection between production cost and the price charged to the consumer. This is best manifest in real-time-pricing assessed on a kWh basis. And third, for general analyses, without specific utility rate information, the demand charge may be subsumed into the TOU energy costs.

#### 4.3.6 UTSS performance metrics

Comparison and analysis of UTSS requires a variety of annual, seasonal, and daily energy and cost metrics. We use the metrics below to evaluate system performance with additional discussion on load shift efficiency and ice availability provided.

- Annual electricity use divided into total, cooling-only, and fan-only categories;
- Facility electricity and demand divided into on- and off-peak categories;
- Daily thermal storage load shifting efficiency;
- Daily thermal storage unused ice availability; and,
- Relative change in annual electricity costs as a function of  $x_{tou}$ .

While there are other definitions of load shift efficiency ( $\eta_{shift}$ ), such as that proposed by Le Dréau and Heiselberg [82], we define  $\eta_{shift}$  as the ratio of electric energy use avoided by discharging the UTSS to the electric energy increased by charging the UTSS. This metric captures the impacts of  $COP_{Coil}$  and  $COP_{Charge}$  variation as well as thermal losses, but must be calculated relative to a baseline model and is a function of the control strategy for the tank, as defined in equation (4-12):

$$\eta_{shift} = \frac{E_{shed}}{E_{add}} \quad (4-12)$$

where,  $\eta_{shift}$  is the load shift efficiency of the UTSS, calculated on the whole building level over any complete discharge-recharge cycle;  $E_{shed}$  is the total electrical energy use avoided by discharging the UTSS on a given day relative to the baseline; and  $E_{add}$  is the total electrical energy required to subsequently recharge the UTSS. Unlike a thermal energy round-trip

efficiency, it is possible to achieve  $\eta_{shift}$  values greater than 1 if nighttime charging conditions are relatively superior to daytime DX cooling conditions. We choose this metric over ice tank round trip efficiency because it provides a whole-building metric for the daily efficacy of using thermal storage.

Because our UTSS sizing is calculated from a design day and our discharge window is fixed according to the utility rate on-peak window, a substantial amount of ice may go unused each day. This unused ice could be a building or grid-level resource, especially in a GEB environment, outside the fixed on-peak window. We quantify this unused thermal storage as ice availability ( $S_{avail}$ ), a non-dimensional total cooling capacity available at the end of each discharge period. It represents the unused ice in all the storage tanks within the building across all the cooling coils. For the PVAV systems, this value is equal to the state-of-charge of the UTSS at the end of each daily discharge period. For the PSZAC systems, this value is the capacity-weighted average of all the UTSS states-of-charge within the building. The ice availability is generally expressed by:

$$S_{avail} = \sum_i \frac{\bar{Q}_i}{\bar{Q}_{Total}} SOC_i \quad (4-13)$$

where,  $\bar{Q}_i$  is the nominal thermal storage capacity of an individual UTSS coil  $i$ ;  $\bar{Q}_{Total}$  is the sum of the nominal thermal storage capacities of all UTSS within a building; and  $SOC_i$  is the state of charge of UTSS device  $i$ . This metric can be calculated at any timestep, but for this analysis, we calculate it at the end of each daily discharge period (i.e., 20:00).

The ice availability metric is useful for evaluating potential control strategies when used in conjunction with a building power load duration curve. These curves present the building power demand at each timestep sorted from highest to lowest. Each y-axis value represents the number of non-consecutive timesteps within the year during which the facility power demand exceeds the corresponding x-axis value. A load duration curve combined with coincident cooling power and  $S_{avail}$  can show the additional load flexibility potential of any simulated UTSS design and control strategy.

## 4.4 Results and discussion

### 4.4.1 Annual energy use

Table 4-7 and Table 4-8, on the following page, summarize the annual facility, cooling, and fan energy use of the baseline and UTSS models. They highlight the relative electricity tradeoffs of adding UTSS to each of our four baseline cases. Table 4-7 shows the results for the PSZAC designs, while Table 4-8 shows the same for the PVAV designs. Annual unmet occupied cooling hours were consistent between associated baseline and UTSS models, with slightly fewer unmet hours accrued in three of the four UTSS examples.

In all cases, total energy use increases with the addition of the packaged ice storage devices. In the PSZAC models, both retrofit and new, the electricity used by the cooling coils increases by an average of 5.25 MWh over the course of the year; the electricity used by the fans increases by an average of 6.35 MWh. For the PVAV buildings, the addition of the UTSS incurs an average cooling electricity increase of 2.1 MWh and a fan electricity increase of 3.2 MWh. The smaller increases in energy use found in the PVAV UTSS designs can be attributed to each system's ability to meet smaller cooling loads with less aggregate compressor operation. Instead of running four smaller PSZAC units intermittently, the PVAV can run its single, larger compressor less frequently. It is important to note that each UTSS coil only operates for one third of the year, June through September; whereas the fans face an additional pressure rise every time the HVAC is operating.

Where Tables 7 and 8 present absolute energy use numbers, Figure 4-8, on the following page, shows the relative annual changes in electric energy use, broken into facility (total), cooling, and fan subcategories, after adding UTSS. We see that for PSZAC designs, the relative increases in cooling and fan electricity are similar after adding thermal storage; however, for the PVAV systems, the relative impact on fan energy use is more than double that on cooling energy use.

Table 4-7: Annual electricity use for buildings with PSZAC systems.

Model	Facility Electricity [MWh]	Cooling Electricity [MWh]	Fan Electricity [MWh]
Retrofit Base	528.3	65.9	87.8
Retrofit UTSS	539.8	71.1	94.2
New Base	313.5	58.4	79.8
New UTSS	325.1	63.7	86.1

Table 4-8: Annual electricity use for buildings with PVAV systems.

Model	Facility Electricity [MWh]	Cooling Electricity [MWh]	Fan Electricity [MWh]
Retrofit Base	485.1	66.4	34.9
Retrofit UTSS	490.8	68.7	38.3
New Base	271.7	62.5	27.2
New UTSS	276.6	64.4	30.1

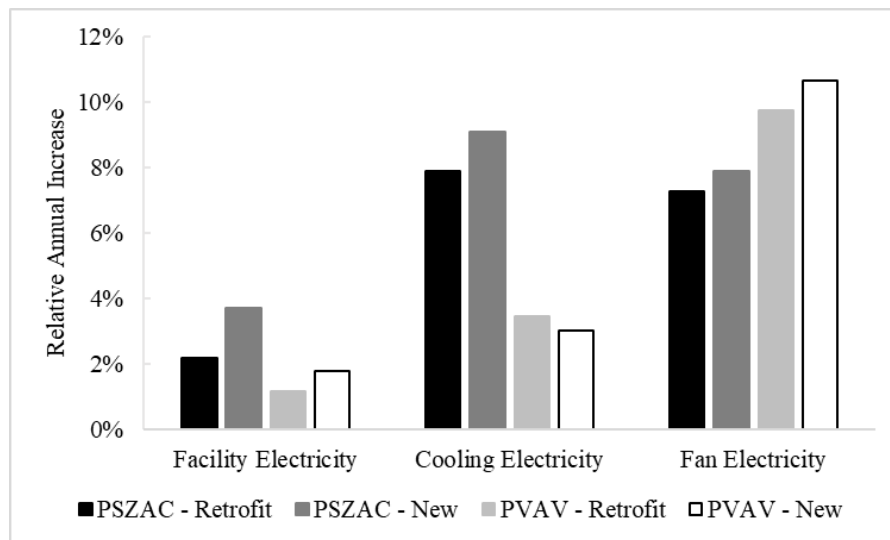


Figure 4-8: Relative annual increases in electricity consumption after adding UTSS to each baseline model, divided into facility (i.e., total), cooling, and fan components

Table 4-7, Table 4-8, and Figure 4-8 show two trends. First, it is essential to capture the effects of the added UTSS cooling coils within the airstream, as the impact on fan energy use is non-trivial. In this case, the absolute increases in fan energy use when using the UTSS exceed the increases associated with the cooling coils. The PSZAC buildings incur a higher absolute penalty because they use four constant speed fans compared to the single variable speed fan found in each of the PVAV buildings. Second, the relative impact on total facility energy use when using UTSS is less for our centralized conditioned-air distribution systems than for the distributed cooling designs. This is primarily attributable to the fewer total number of UTSS required for the PVAV systems, which provides a better match between thermal storage requirements and installed capacity at the whole-building level. This improved capacity-to-load alignment helps minimize both the cooling and fan electricity usage in the PVAV designs.

#### 4.4.2 On-peak and off-peak energy use

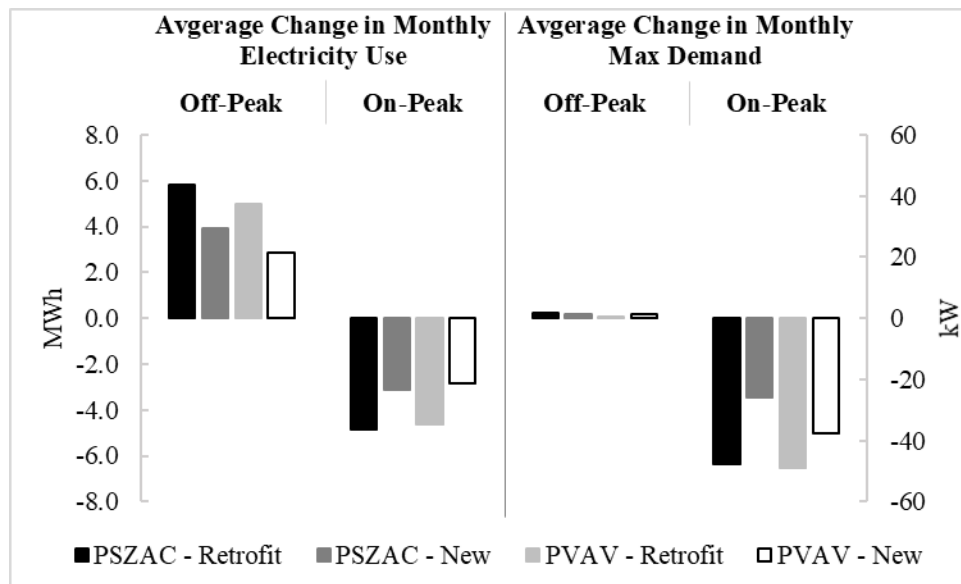


Figure 4-9: Average changes in monthly electricity use and maximum demand during the on-peak and off-peak periods, calculated over the months of June-September

Figure 4-9 shows the changes in both annual electricity use (left) and maximum demand (right) during on-peak and off-peak periods after adding the UTSS to each baseline. The positive values indicate increases in energy use or maximum demand, while negative values indicate reductions. UTSS is effective at shifting electricity use, with an average monthly reduction in on-

peak electricity use ranging between 2.9 and 4.8 MWh. Comparing the loads added during off-peak hours to those shed during on-peak hours, the PVAV systems perform more efficiently than their PSZAC counterparts, as seen by the smaller differentials between the electricity added and the electricity shed. In the best case, the new construction with PVAV, the UTSS is nearly electricity-use neutral during its June to September operating season, relative to the no-storage baseline.

The value of the UTSS is more apparent when comparing changes in maximum demand. During on-peak ice discharge, the average monthly maximum demand is reduced by between 25.9 kW and 49.1 kW. This translates into a maximum demand reduction of 32.2% to 36.6% during that window. However, during the off-peak period, only very slight increases in maximum demand are incurred. The 0.2% to 1.8% increases are attributable to the increased fan power required after adding the UTSS coils to the airstream. For our implementations, the PVAV and PSZAC systems with UTSS achieve approximately the same demand reductions relative to their baseline buildings. We conclude that for on-peak maximum demand reduction, UTSS performs equally well for both PSZAC and PVAV systems.

#### **4.4.3 Load shift efficiency**

Figure 4-10, on the following page, shows the daily values of  $\eta_{shift}$  for both the (a) PSZAC and (b) PVAV systems. The load shift efficiency,  $\eta_{shift}$ , is calculated on whole-building level for each diurnal discharge-recharge cycle, thus capturing coil, fan, and ancillary system impacts. Any value greater than 1 indicates a net energy savings for that day compared to the corresponding baseline building. Electric load shift efficiency is a function of ambient conditions during charge and discharge, and is therefore highly variable over the course of the cooling season.

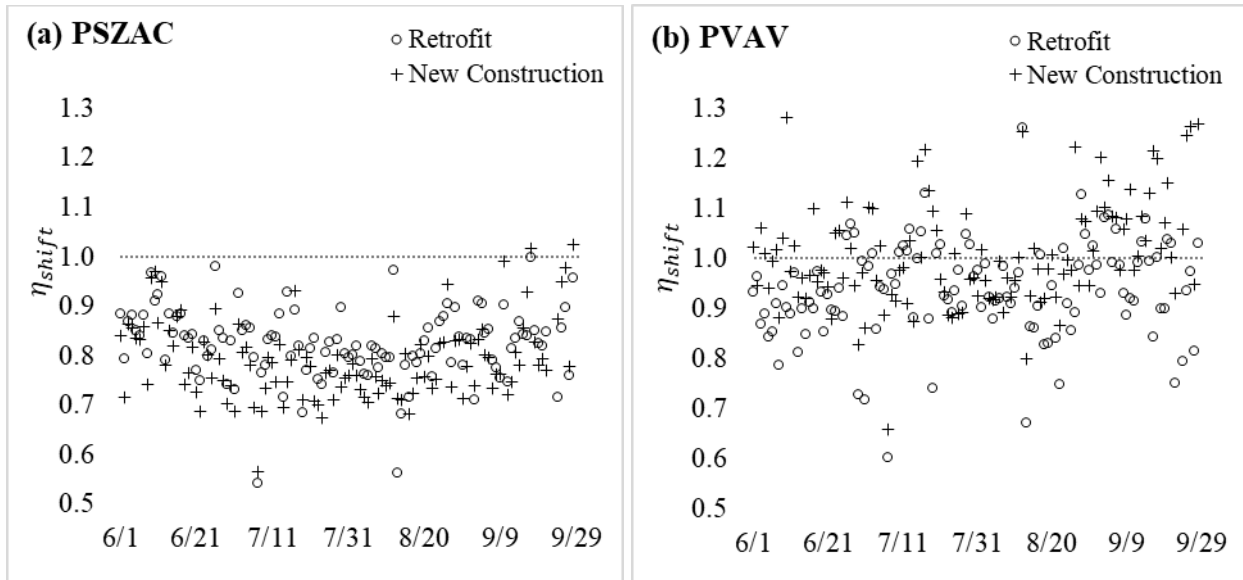


Figure 4-10: (a) Daily load shift efficiencies for UTSS implemented on retrofit and new-construction PSZAC systems. Wide daily variation is observed, but few days achieve  $\eta_{shift} \geq 1$ . (b) Daily load shift efficiencies for the retrofit and new-construction PVAV systems. Significantly more days achieve  $\eta_{shift} \geq 1$  compared to the PSZAC designs.

For the PSZAC systems, the daily load shift efficiencies are nearly always less than 1. Over the course of the four summer months, the retrofit building achieves  $\eta_{shift} \geq 1$  only once and the new construction only achieves it twice. Conversely, for the PVAV systems,  $\eta_{shift}$  is greater than 1 nearly 25% of the time for the retrofit building and 47% of the time for the new construction. This daily performance is summarized in Table 4-9.

Table 4-9: Load shift efficiencies for UTSS implementations

Model	Average $\eta_{shift}$	Number of Days $\eta_{shift} \geq 1$	Number of Days $\eta_{shift} < 1$
PSZAC - Retrofit	0.82	1	120
PSZAC - New	0.79	2	119
PVAV - Retrofit	0.94	30	91
PVAV - New	1.01	57	64

Little difference is observed between the retrofit and new construction buildings. For the PSZAC, the retrofit achieves a 3% higher average load shift efficiency over the course of the summer. For the PVAV buildings, the new construction out-performs the retrofit  $\eta_{shift}$  in both average and total number of days exceeding 1. The greater contrast is between HVAC system types. Like the annual energy use results, the centralized air conditioning systems with UTSS achieve higher daily load shifting efficiencies compared to decentralized units.

The envelope impact on HVAC and UTSS is reflected on  $\eta_{shift}$  values primarily through their different storage capacity requirements (Table 4-4), which in turn affect their respective fan energy usages. In the case of the PSZAC systems, both the retrofit and new construction require the same total number of UTSS units, and the average load shift efficiency slightly decreases. Conversely, the new construction with PVAV requires one fewer UTSS unit compared to the retrofit, which results in an improved average  $\eta_{shift}$ .

Finally, because the PVAV systems experience substantially more days with  $\eta_{shift} \geq 1$ , there is a possible opportunity to achieve a net energy-use reduction using predictive or optimal controllers. Such opportunity is not present with the distributed storage implementation as the cumulative energy penalties exceed the potential energy savings at the UTSS coil. This reinforces the preliminary conclusion that the centralized UTSS implementations are likely more energy efficient than the distributed designs.

#### **4.4.4 Ice availability**

One result of implementing UTSS under a full-storage control based solely on a utility rate structure, as we have done in this study, is that the thermal storage may be under-utilized for much of the year. This unused thermal storage is a potential asset, even if used outside the on-peak window, if there is a grid benefit or an off-peak demand charge to incentivize its utilization within the building.

Figure 4-11, on the following page, shows two histograms of the daily ice availability,  $S_{avail}$ , grouped by building vintage and sorted into bins with width of 5% storage capacity. The

grouping by vintage maintains an equitable comparison as the cooling loads are a function of building model, not of baseline HVAC system.

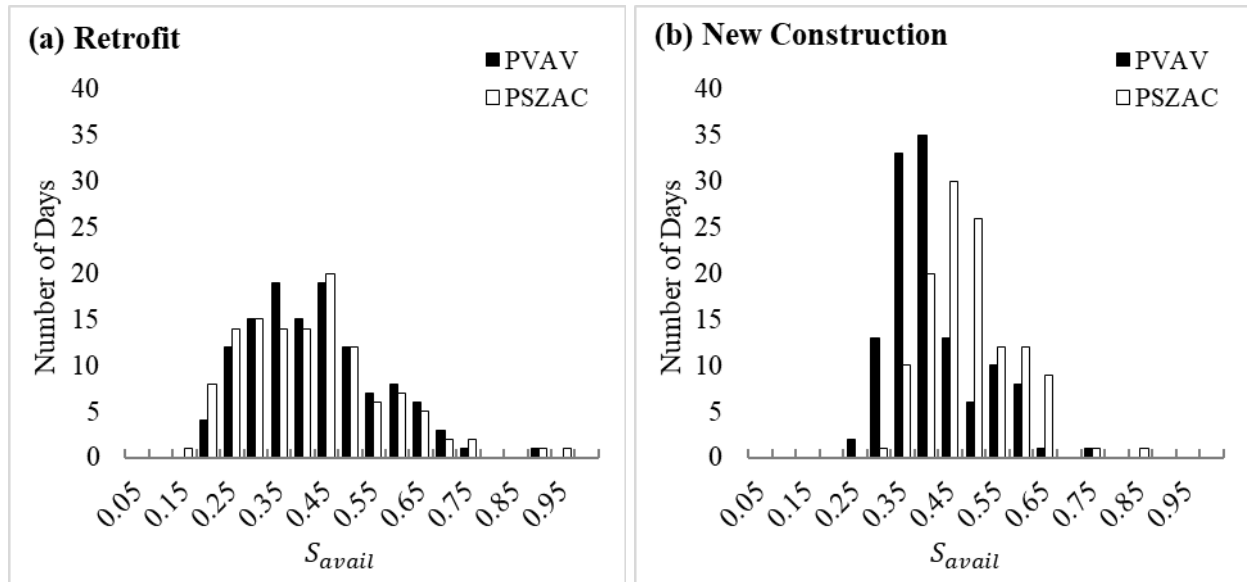


Figure 4-11: (a) Histogram of daily ice availability values for retrofit buildings with either PSZAC or PVAV systems. (b) Histogram of daily ice availability values for new buildings with either PSZAC or PVAV systems.

Several observations can be made from Figure 4-11:

1. Due to the design-day sizing, the thermal storage systems never fall below 15% state-of-charge. This potential oversizing may be acceptable if the  $S_{avail}$  can be used as a grid service or for some economic advantage during the off-peak hours.
2. The retrofit buildings have a wider distribution of  $S_{avail}$  compared to the new construction buildings. The standard deviation of the mean for the PVAV and PSZAC retrofit buildings is 13.6% and 14.8%, respectively. For new construction, standard deviation is 9.2% for both HVAC designs. This is due to the tighter new construction envelopes which results in a more consistent daily cooling load.
3. Recalling the total number of UTSS for each building (Table 4-4) we confirm that the centralized, PVAV systems more efficiently employ their available thermal storage.

In Figure 4-11(a), the nearly identical distributions of daily ice availability imply similar system performance. However, the PVAV achieves this with six total UTSS units, compared to

the seven units required in the PSZAC design. In Figure 4-11(b), the PVAV and PSZAC distributions do split, but the former requires only five UTSS units compared to the seven in the latter. Thus, similar ice utilization by a PVAV system can be obtained with less installed capacity compared to the PSZAC systems.

In all cases, the UTSS systems were sized against design-day conditions. Therefore, for most of the cooling season, a large fraction of the ice is unused each day. Under a static utility rate structure (and thus control), this may be considered a drawback as a large portion of the purchased capacity goes routinely unused. However, under the dynamic control envisioned for the interactive grid of the future, this unused capacity becomes an asset for both the building owner and the grid operator and should be quantified with proposed UTSS implementations.

Another method of visually inspecting the performance of a distributed energy resource is the load duration curve. By augmenting each facility power load duration curve with the coincident mechanical cooling electric power, potential load shift opportunities are highlighted. Figure 4-12 and Figure 4-13 (on page 39) presents the seasonal load duration curves for the baseline (no storage) and UTSS (with storage) retrofit PVAV model for the period of June 1 to September 30. As all buildings produce similar plots and the same lessons, only a single illustrative case is presented here.

Figure 4-12(a) shows the baseline facility (Base) power load duration curve during the 35,136 five-minute timesteps (2,928 hours) of the summer months. The coincident cooling electric power (Base-Cooling) is also plotted, showing the potential electrical loads which could be mitigated through cool thermal storage. At the periods of peak power demand, cooling is responsible for 35% of the electrical load. Figure 4-12(b) shows the baseline facility (Base) power load duration curve, the facility power after adding the UTSS thermal storage (UTSS), and the coincident cooling electric power (UTSS-Cooling). This allows for comparing cooling energy use with and without storage as a function of how significant it is in relation to the total energy use of the building. When building electricity use is high and cooling electricity is responsible for a significant portion of it, there is potential benefit from load shifting via thermal storage.

Our UTSS implementation provides some minor leveling in the middle section of the total power load duration curve, as shown in Figure 4-12(b), achieved at the expense of increasing the variation in cooling energy use, observed by comparing the cooling curves in Figure 4-12(a) and Figure 4-12(b). This change is due to both the variation in timing of cooling electricity use and the variation in COP of the UTSS ice-making compressor. However, the left-most region, when building demand is highest, cooling demand remains unmitigated as our dispatch strategy was coordinated with the TOU rate, and not explicitly targeting peak power (due to no demand charges).

To evaluate the potential of the current UTSS design and control strategy to be modified to address this peak demand region, we further examine the UTSS load duration curves while plotting the coincident ice availability in Figure 4-13.

Figure 4-13(a) zooms to the peak 8,400 timesteps (700 hours) and adds the coincident values for the daily minimum ice availability using a shared x-axis (Figure 4-13(b)). Minimum  $S_{avail}$  values exceed 30% for the entire peak region. Thus, we know that up to 54 kW in cooling power can be targeted for reduction at the times when building demand is maximum; and that the UTSS has approximately 30-40% capacity available each day to be used for this reduction. By adding UTSS coincident cooling power and  $S_{avail}$  to the load duration curves additional energy flexibility potential becomes apparent. Even without neglecting to avoid the on-peak TOU electricity prices, the thermal storage has great potential for building demand reduction. However, to access this energy shifting potential, a smarter control scheme is required—an area of potential future research beyond the scope of this study.

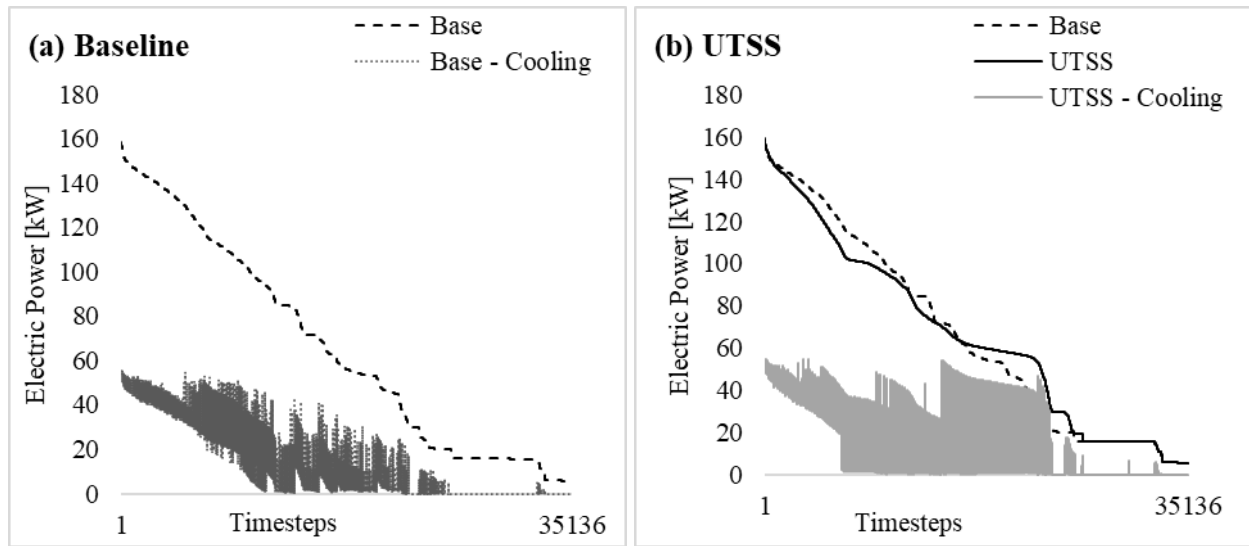


Figure 4-12: Load duration curves for the retrofit PVAV example for the months of UTSS operation (June 1 - September 30), augmented with the coincident cooling electric power for (a) baseline building total electric (Base) and cooling electric (Base-Cooling) curves without energy storage; and (b) baseline total electric building (Base), total electric for building with UTSS (UTSS) and cooling (UTSS-Cooling).

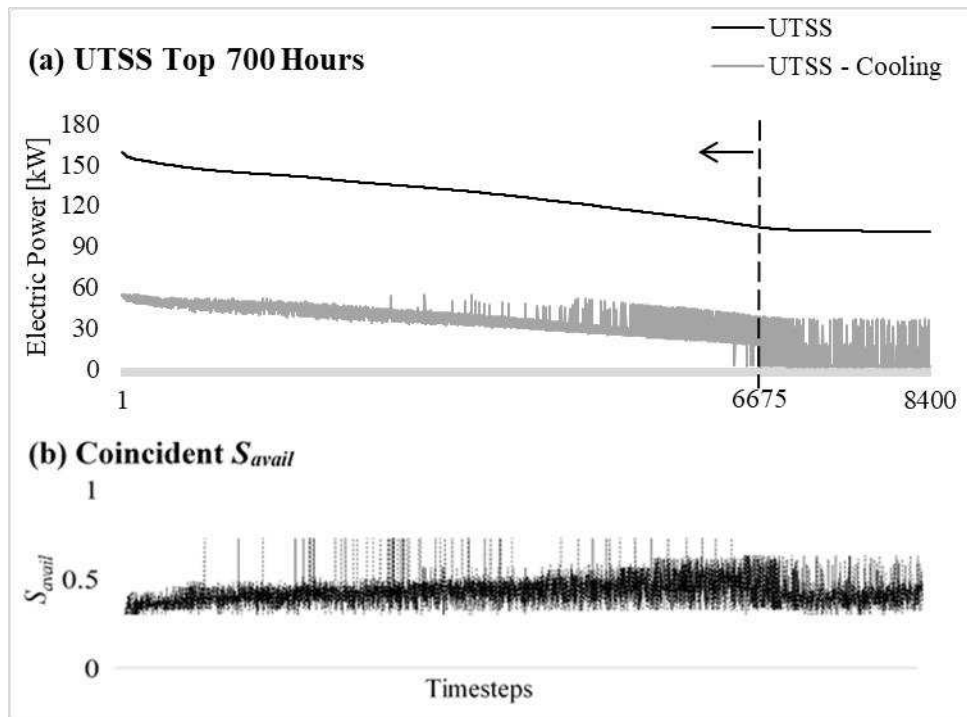


Figure 4-13: A zoomed-in view of the top 8400 timesteps (700 hours) during UTSS operation of the retrofit PVAV example. (a) shows that in the 6675 timesteps (~556 hours) left of the vertical dashed line, the cooling loads are not reduced by our current UTSS control strategy. However, (b) shows the coincident daily minimum ice availability values for these peak timesteps.

#### 4.4.5 Cost performance

The potential energy bill savings for any given UTSS installation is a function of not only the utility rates but also the fraction of the total bill that is associated with cooling equipment. In our buildings, the maximum total annual energy bill savings (when  $x_{tou} = 3.5$ ) range between 4.5% and 6.5%. However, when we examine the cost savings associated with only the cooling load, these relative values increase as a function of the magnitude of the shifted load. Figure 4-14 shows cost savings for cooling-only electricity use compared to baseline buildings for the five analyzed electric rate multipliers ( $x_{tou}$ ). Using these five data points, we extrapolate a trendline for each building vintage and HVAC system. For the retrofit models, savings range from 7.6% to 38.6%. For the new construction, the potential is somewhat reduced due to the improved building efficiency, but savings still range from 3.5% to 29.1%.

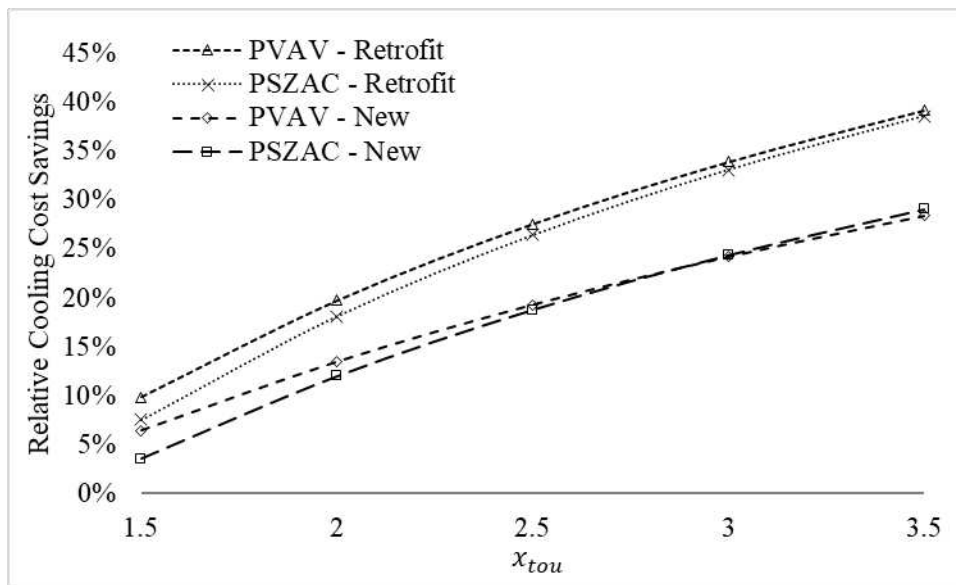


Figure 4-14: Relative annual cost savings for cooling electricity for UTSS implementations as a function of on-peak time-of-use multiplier ( $x_{tou}$ ). Data points are extrapolated into curves to represent the cost savings trends for each model.

Though the PVAV and PSZAC trendlines are very similar for both retrofit and new buildings, this performance is achieved with less installed storage capacity in the PVAV cases. In both the Retrofit and New cases, the UTSS with PVAV produce higher relative savings at lower time-of-use multipliers than their PSZAC counterparts. However, as  $x_{tou}$  increases, the observed

difference in relative cooling cost savings due to HVAC system type decreases. In the new construction case, the savings curves for PVAV and PSZAC cross at  $x_{tou} \approx 3$ . This is due to the increased impact of cooling on the total electric bill as the TOU rates increase, especially when more cooling devices and fans are present in the building.

While there appears to be little difference in cost savings performance between PVAV and PSZAC systems for each respective building vintage, we recall that this savings performance is achieved with fewer total number of UTSS in each PVAV case compared to the PSZAC. Therefore, in relative cost terms, the centralized UTSS implementations out-perform their decentralized counterparts.

Due to limited market penetration for this technology and uncertain cost data, capital costs for the UTSS are not included in this analysis. As such, a broader life cycle analysis is not performed. However, the annual electricity bill savings information presented in Figure 4-14 may be used by building owners to develop their own unique procurement criteria should they consider packaged thermal storage options.

#### **4.5 Conclusions and future work**

In this chapter we develop and employ an OpenStudio measure that facilitates the rapid, parametric analysis of packaged ice thermal storage devices, known as unitary thermal storage systems. The measure allows modelers to add package ice thermal storage to existing DX cooling coils and evaluate the performance of different UTSS designs and controls. The UTSS model used by the measure accounts for COP variation with ambient and zone conditions and tracks thermal losses. Using the measure, we analyze four UTSS implementations with centralized PVAV systems and decentralized PSZAC systems for two vintages of a stand-alone retail building in El Paso, TX and five different time-of-use rates, specifically accounting for the increased fan pressure rise requirements when using thermal storage. We employed energy-use, load shift efficiency, unused ice availability and relative cost savings metrics to compare UTSS performance. We construct cooling-only cost savings curves for each building type and HVAC system, allowing us to visualize the savings potential of each thermal storage implementation over a wide range of on-peak energy prices.

Based on the limited analysis, preliminary results suggest that PVAV systems are more conducive to the addition of UTSS because of (1) less storage capacity was required to achieve the same cooling load shift with the PVAV and (2) a smaller increase in fan energy use due to the variable speed fans used in the PVAV. If these two characteristics can be maintained, we suggest that this conclusion is generalizable to any PVAV to PSZAC UTSS comparison. However, the primary goal of this work is to enable fast modeling and analysis of thermal storage using open-source tools. Despite its recent attention, there is still significant work remaining in analyzing the performance and assessing the role of thermal storage in the future grid. The publicly available performance data for thermal storage devices and technologies remains limited, presenting an opportunity for experimental work creating performance maps. Additionally, UTSS has yet to successfully penetrate the market as a distributed energy resource (DER), inviting inquiry into the techno-economic barriers to adoption. Finally, for an interactive grid implementation, UTSS must operate harmoniously with other DERs, which presents myriad opportunity for design and control optimization studies. We hope that this work, and particularly the increased accessibility of open source UTSS modeling made possible through the OpenStudio measure, support the future of thermal energy storage analysis and, perhaps, implementation.

#### **4.6 Acknowledgements**

This work was funded by the Alliance Partner University Program No. UGA-0-41025-152, between the National Renewable Energy Laboratory and Colorado School of Mines, both in Golden, Colorado.

## CHAPTER 5

### MODELING THE LOAD FLEXIBILITY POTENTIALS FOR ICE ENERGY STORAGE

A paper presented at the 2020 Building Performance Analysis Conference and SimBuild [83]. Rights managed by ASHRAE.

Karl Heine, Paulo Cesar Tabares-Velasco, Ryan Meyer, and Michael Deru

#### 5.1 Abstract

With the increasing interest in grid-interactive efficient buildings, energy storage technologies are being re-evaluated for their role in the future grid. Ice thermal energy storage (ITS) has a large potential to provide load flexibility to a grid dominated by variable generation assets, but it requires careful design, analysis, and control to be effective. Evaluation is possible using building energy simulations but is not often done because of the complexity and added effort required to include ice storage in building simulation models. The objectives of this study are two-fold: (1) automate the addition of ice energy storage to building models through OpenStudio measure scripting and (2) evaluate the load flexibility potential of example ITS design and control strategies. This paper presents a new OpenStudio measure that provides the ability to easily and accurately model a variety of potential design options and common control schemes. After applying this measure, we then bound the ability of the building to increase or decrease its predicted future electric load over 30-minute to 6-hour windows using chiller and ice storage performance constraints at each simulation timestep. Finally, we evaluate the ITS performance against in-simulation demand response events.

#### 5.2 Introduction

Considering the increase in uncertainty and electricity generation variability on the grid due to the growth of renewable assets and distributed energy resources (DERs), buildings are an emerging asset for dynamic demand response and grid services. One of the largest electrical end-uses within buildings is space conditioning, accounting for 9% of the total U.S. electricity production, and up to 50% of a building's total electricity demand during summer [84]. This vast amount of energy use is theoretically controllable via thermal energy storage. Ice has traditionally been used to shift on-peak daytime cooling loads to off-peak nighttime hours,

capable of providing significant energy cost savings [38]. And, if properly sized and controlled, it can also provide a reduction in total facility energy use [16]. In a grid dominated by renewables, however, this strategy may be insufficient – the dynamic flexibility of a given system’s design and control sequence should also be assessed. Some recent work on the value ice thermal storage (ITS) for flexibility and promoting penetration of renewables has begun exploring this topic [30, 33].

The U.S. Department of Energy Buildings Technology Office (BTO) characterizes building demand flexibility as: (1) energy efficiency, (2) load shifting, (3) load shedding, and (4) load modulation [6]. ITS can readily address the first three characterizations; however, it is not well suited for load modulation due to the short timesteps required (seconds and sub-seconds).

The traditional design approach to ice systems is based on load shifting evaluated over a design-day. Chillers may then be downsized, thereby decreasing capital cost and improving device efficiency during part-load operation [17]. These factors then impact the building’s overall efficiency, with potential to reduce energy use intensity (EUI).

Ice storage also provides a load shedding ability within a building. The ice available within the storage tank at each point in time can be converted into a temporary reduction in building electrical demand (load shed). Conversely, a partially discharged ice tank and/or a chiller operating with a demand limiter provides an opportunity for a temporarily increase in building demand while saving the stored ice for later (load add). This may be a useful service in the event of excess renewables that might otherwise be curtailed. Thus, ice storage system designs and controls should be evaluated for their ability to provide both load shed and load add in a grid-interactive manner.

To perform load flexibility assessments, detailed whole- building energy modeling (BEM) that incorporates an accurate ice energy storage model with proper controls is required. While most BEM software can simulate ice storage systems, implementation is a time-consuming, custom endeavor [17]. This limits parametric analysis potential and more widespread consideration. Furthermore, controlling the ice storage models may require scripting within the HVAC iteration loops in order to achieve performance similar to real-world applications. These challenges have limited the analysis of ITS within BEM to date.

Thus, the objective of this chapter is to present a method to automate the implementation of ITS within BEM and allow users to quickly define and evaluate a wide variety of possible control schemes, even permitting the testing of a system during a simulated demand response event. This allows rapid parametric analysis of possible ice storage system designs and high-level control strategies. We demonstrate the measure on a single building model, exploring several configuration and control options. We then examine the impact of each design option on building energy efficiency, electrical load shifting, and ability to provide temporary load shedding or addition in response to a grid event.

## **5.3 Methodology**

### **5.3.1 Measure Description**

EnergyPlus is the BEM engine used for this project, including the ThermalStorage:Ice:Detailed object, accessed through the OpenStudio Software Development Kit. The measure can be implemented directly within the graphical user interface, from the command line, or as part of a scripted workflow. The measure may be applied to any OpenStudio model that includes a chilled water loop. The configuration options available in the measure include the ice tank position relative to chiller, the ice tank capacity in ton-hours, and a chiller capacity multiplier. The high-level control strategies available within the measure are those defined by the ASHRAE Design Guide for Cool Thermal Energy Storage:

- Full Storage, where the ITS meets the entire cooling load during discharge; and,
- Partial Storage, where cooling loads are met by simultaneous operation of both the chiller and ITS.

Within partial storage, there are many additional control considerations, such as load-leveling, demand-limiting, and chiller or storage-priorities. All of these may be implemented through user inputs within the measure, thus allowing comparative analysis. Due to the nature of EnergyPlus, demand limits [ $\text{kW}_e$ ] on the chiller are implemented as capacity limits [ $\text{kW}_t$ ] within simulation. Figure 5-1 shows a selection of the measure's user inputs related to ITS configuration and controls.

Inputs

Select Energy Storage Objective:

Full Storage

Select Upstream Device:  
Partial storage only. See documentation for control implementation.

Chiller

Enter Thermal Energy Storage Capacity for Ice Tank [ton-hours]:

3200

Select Thaw Process Indicator for Ice Storage:

InsideMelt

Select Loop:  
This is the cooling loop on which the ice tank will be added.

Chilled Water Loop

Select Chiller:  
The ice tank will be placed in series with this chiller.

90.1-2010 AirCooled WithCondenser Chiller 0.456tons 1.3kW/ton

Enter Chiller Sizing Factor:

1

Enter Chiller Max Capacity Limit During Ice Discharge:  
Enter as a fraction of chiller capacity (0.0 - 1.0).

1

Figure 5-1: Select user inputs for ITS measure

All controls, except for the chiller capacity limiter, are provided through component operating schedules, which are created by the measure for the user. Custom schedules generated by the user may also be applied. The chiller capacity limiter is controlled by a simple Energy Management System (EMS) script inside the HVAC iteration loop.

Test Demand Reponse Event?

Select if a Load Add or Load Shed Event

Shed

Enter date of demand response event:  
Use MM/DD format.

9/19

Enter start time of demand response event:  
Use 24hr format.

11:30

Enter duration of demand response event [hr]:

3

Allow chiller to back-up ice during DR event?  
Unselection may result in unmet cooling hours

Figure 5-2: User inputs for demand response tester

One additional feature of the measure is an optional supervisory control EMS script that can be used to test partial-storage designs against user-defined demand response (DR) events. The DR tester overrides the routine ITS controls for a user-specified event time and duration to

either maximize (load add) or minimize (load shed) energy use associated with space cooling. The in- simulation tester is valuable for exploring the rebound effects associated with using ITS for dynamic load flexibility. Figure 5-2 shows the user inputs for the DR tester.

### 5.3.2 Flexibility Metrics and Methods

We evaluate the ITS models against a variety of energy metrics associated with the BTO's characterizations of load flexibility mentioned above. Cost metrics are not discussed here as they are functions of not only design and control, but also local utility rates and programs. Cost considerations may be evaluated by applying the appropriate tariffs and demand response incentives. This measure provides a tool to help evaluate ITS within any price structure.

Load shifting is evaluated relative to a baseline system without ITS. It involves both the ice discharge and subsequent recharge periods. The peak power reduction [ $\text{kW}_e$ ] during discharge and the total electric energy shifted [ $\text{kWh}$ ], evaluated over at least one complete charge-discharge cycle are useful. We consider the four metrics below to characterize the load shifting potential of our example ITS models:

- Average Daily Shifted Load [ $\text{kWh}$ ], defined as the average reduction in facility electricity use during ice discharge, relative to the baseline;
- Average Fraction of Daily Load Shifted [-], defined as the average of the daily shifted loads divided by the average daily total electric load in the baseline;
- Annual Total Shifted Load [ $\text{MWh}$ ], which is the sum of the reductions in daily facility electric load during ice discharge, relative to the baseline; and,
- Maximum Annual Peak Demand, which is the single point of maximum facility electric demand (15-minute average) over the course of the year.

Monthly values for peak demand are of interest for utility rate calculations; but for brevity, we here present only the annual peaks which, in our demonstration cases, equate to late summer peak demand.

Energy efficiency is evaluated at the building level with EUI, and at the chiller level through three metrics evaluated over the ITS operating season to capture charge and discharge performance:

- Chiller Average COP;
- Chiller Total Electricity Use; and,
- Chiller Total Runtime Hours.

Load shed and load add potentials are assessed through both post-processing of simulation results and through the in-simulation DR tester. They are quantified in terms of peak power [kWe], energy [kWh], and potential duration of flexibility [hours] at each simulation timestep. We perform the calculations for DR events ranging from 30-minutes to 6 hours.

For the load shed events, we assume that ITS controls switch their routine partial-storage control to full storage for the duration of the event, thus allowing the chiller to turn off. If the ITS state of charge (SOC) is insufficient to meet the full load (either energy or cooling rate) over the required duration, we indicate a 0 flexibility potential. We do this to identify the limits of a particular ITS control strategy for early-design consideration. For load add events, we assume that the chiller will meet the full cooling load. Any ice that would have been discharged during the DR event is saved for later use.

We aggregate these calculations, performed at each timestep for each DR window (30-min to 6-hours), into average potential power change [kWe], average potential energy change [kWh], and the availability of the response type. This availability is defined as the percent of timesteps over which the complete shed or add responses could be successfully executed. For example, at a given timestep, a system may be able to switch to full storage and meet the future cooling loads (determine from baseline model) the next hour, but not for any longer duration. In this case, 30-minute and 1-hour responses are considered available at the given timestep, where 2+ hour responses are not. Availabilities are presented as percentages of annual timesteps and of only the occupied timesteps.

These add and shed potentials derived from post- processing provide information on the flexibility that the building may provide to the grid only during the DR window; they do not capture any rebound effects. In the case of the load shed events, negative rebound impacts may occur immediately following the DR event or several hours later during ice tank recharge. The in- simulation DR tester allows us to use BEM to capture those rebound effects. These are best explored through visual examination of the timestep energy output data.

### 5.3.3 Simulated Building Test Cases

To demonstrate the capabilities of this measure and our load flexibility analysis, we use the DOE Prototype Secondary School, vintage 90.1-2010 for climate zone 2A, with the Houston, TX TMY3 weather file, simulated at 15-minute timesteps. We select this building model and location because (1) the building cooling is provided through a primary-secondary chilled water loop supplied by a single air-cooled chiller, (2) the facility in this location requires space cooling for the entire year, and (3) space cooling constitutes a large percentage of the total facility electric load. In order to facilitate study repeatability, no changes are applied to the model beyond our ITS measure. The peak cooling period for this model occurs during September when high occupancy is coincident with hot and humid weather conditions.

To showcase the potential of the measure five different ITS configuration and control cases are modeled and presented here. Cases with a “P” title are partial storage configurations.

Table 5-1: Model configurations

Case	Chiller Capacity [Tons (kWth)]	Ice Capacity [Ton-hr (GJ)]	Upstream Device -
Base	578 (2,033)	N/A	N/A
Full	578 (2,033)	3,200 (40.5)	Ice
P1	405 (1,424)	2,000 (25.3)	Ice
P2	405 (1,424)	2,000 (25.3)	Chiller
P3	347 (1,220)	2,000 (25.3)	Chiller

Table 5-1 lists the five cases and their basic configuration options. Using percentage multipliers, the chillers in P1- P3 are downsized from the original baseline. Chiller capacities in Table 1 are the result of a 70% multiplier in models P1 and P2, and a 60% multiplier in P3. These multipliers are selected based on the ASHRAE Design Guide for Cool Thermal Storage sizing equations and recommendations in order to demonstrate the performance of systems with downsized chillers [17].

Table 5-2: Model control strategies

Case	Strategy	Priority	Limiter
Base	N/A	N/A	N/A
Full	Full Storage	N/A	N/A
P1	Partial Storage	Chiller	57%
P2	Partial Storage	Ice	65%
P3	Partial Storage	Ice	68%

Table 5-2 defines the high-level control strategies applied in each model. For model P1, the limiter imposed on the chiller during ice discharge is a function of a fixed temperature difference across the downstream chiller evaporator. This is applied using temperature setpoint schedules, rather than the EMS limiter script used in P2 and P3.

The cooling season for these buildings encompasses the entire year. The full storage system charges from 2100- 0800 daily, and discharges from 0900-1800 on weekdays. The partial storage systems charge from 2300-0800 every day, and discharge from 0800-2100 on weekdays. The chilled water loop temperature setpoint is 44°F (6.7°C) with a design loop temperature difference of 10°F (5.6°C). The working fluid is 25% ethylene glycol. To charge the ice tank during the overnight hours, the primary loop is isolated from the building cooling coils and the chiller cools the working fluid to 25°F (-3.9°C). This results in a reduced chiller capacity equal to approximately 65% of the nominal capacity during ice charging.

These models are selected to concisely demonstrate the variety of configuration and control options made available through the OpenStudio measure. To demonstrate the flexibility analysis described above, we select one model for further examination. Case P2 (partial storage, chiller-upstream, storage-priority, with a 65% chiller capacity limiter imposed during ice discharge) is selected because it produces an approximately equivalent EUI to the baseline model, and has nearly identical total chiller electric energy use over the course of the year.

## 5.4 Results

### 5.4.1 Comparing Example Models to Baseline

All five cases are evaluated in terms of energy efficiency and load shifting over the entire cooling season; and all five meet zone temperature requirements for full the year. The minimum annual ice tank SOC is checked to ensure thermal storage capacity is sufficient for all cases. These are shown for measure demonstration purposes; conclusions on the superiority of a configuration or control strategy should not be drawn from the data below. Such conclusions will depend on the building type, climate, and energy objectives.

Table 5-3: Annual facility metrics

Case	EUI [kBtu/ft <sup>2</sup> ]	Peak Demand [kW <sub>e</sub> ]	Minimum SOC
Base	49.5	989	N/A
Full	50.1	797	12.3%
P1	49.3	795	14.3%
P2	49.6	801	11.4%
P3	48.8	764	1.5%

Table 5-4: Annual chiller metrics

Case	Chiller Energy Use [MWh]	Average COP [kW <sub>t</sub> /kW <sub>e</sub> ]	Chiller Runtime [hours]
Base	963	2.55	5,945
Full	980	2.71	4,346
P1	942	2.76	6,286
P2	963	2.68	5,794
P3	918	2.79	6,029

Table 5-3 summarizes the energy results for the analyzed cases. In terms of energy efficiency, all ITS are within +1.2% to -2.0% of the baseline EUI. However, all ITS reduce the facility peak electricity demand during the ITS operating season. The peak values shown in Table 3 are the maximum facility demand over the year; average monthly reductions range from

14-27%. All analyzed ITS have similar or lower unmet cooling hours compared to baseline. Annual minimum ice tank SOC values range from 1.5% (essentially empty) to 14.3%.

Table 5-4, on the previous page, lists each chiller’s annual electric energy use, average COP, and runtime. Examining the chiller performance between cases highlights the tradeoffs in energy use, runtime, and efficiency associated with ITS designs. All ITS models improved the average chiller COP, shown as an annual average, but most incur either increased runtime hours (P1 and P3) or increased energy consumption (Full). P2 produced nearly identical total chiller energy use, but had 150 fewer runtime hours over the year – when the ice-priority discharge was sufficient to temporarily provide full storage. This occurred occasionally in the winter and shoulder seasons.

It is noteworthy that case P2 has the same annual chiller electric energy use, but produces a higher EUI compared to the baseline. This is due to increased energy use associated with pumping the working fluid at lower temperatures.

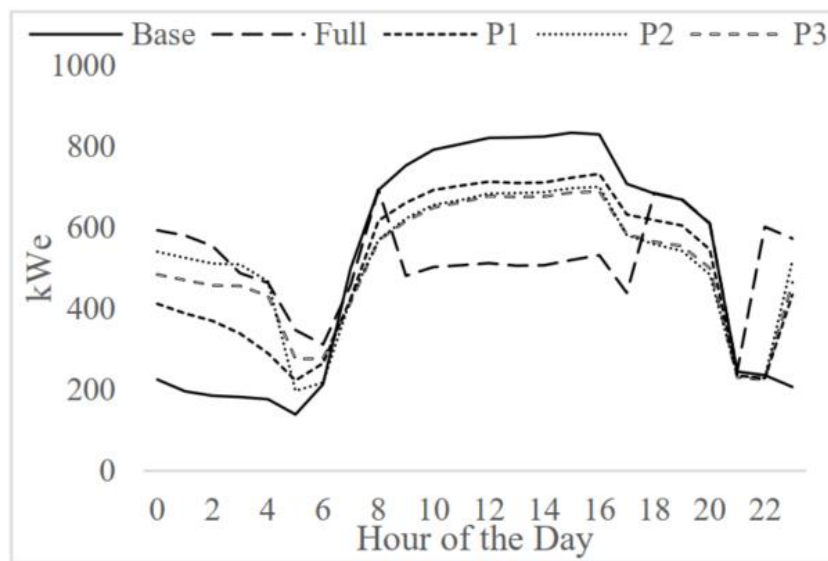


Figure 5-3: September average daily profiles for facility electric demand

To better illustrate the variation in model performance, Figure 5-3 shows average weekday facility electric demand profiles for the month of September. Full storage ITS provides greater facility peak demand reduction relative to the partial storage models, but for a shorter duration (9 vs. 13 hours), with a higher storage capacity requirement (3,200 vs. 2,000 ton-hours),

and without the economic benefits of downsizing the chiller. P1 and P2 both have the same size chiller, but the impact of the discharge priority and chiller limiter is observed throughout the day. Cases P2 and P3 have the same configuration and very similar controls strategies during discharge. However, the larger chiller in P2 recharges the ice tank more quickly each night and at a higher power requirement.

Table 5-5 summarizes the load shifting achieved by each ITS model. Load shifting occurs over up to 260 days out of the year (no weekends) and constitutes annual averages between 8.6% and 24.2% of the total facility electric load each day. P1 is significantly lower than the other ITS models due to the static chiller-priority control applied. This results in less average daily ice utilization compared to the ice-priority control, despite the lower fractional capacity limiter placed on the chiller.

Table 5-5: Electric load shifting relative to baseline

Case	Avg. Daily Shift [kWh]	Rel. Daily Shift [%]	Annual Total [MWh]
Full	1,990	24.2%	323
P1	735	8.6%	189
P2	1,617	20.3%	308
P3	1,573	19.7%	342

The annual total shifted load cannot be directly converted into energy bill savings without local utility rates, but does illustrate the magnitude of the flexibility in energy consumption provided by a given ITS design. Its value is most easily visualized using a load duration curve, where a flatter profile means a more uniform energy demand by the facility over the year. Figure 5-4 shows the load duration curves for all five analyzed cases. All ITS are flatter than the baseline to varying degrees, illustrating the impact of control selections within the energy simulation.

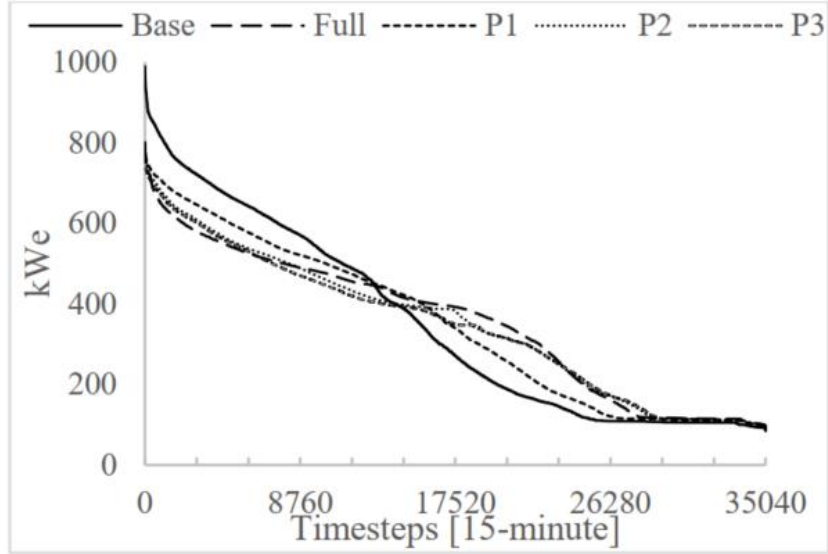


Figure 5-4: Annual load duration curves for facility electric demand

#### 5.4.2 Load add and load shed flexibility through post-processing

Case P2 is used for further flexibility analysis through both post-processing and the in-simulation DR tester. The post-processing method bounds the energy use of the facility at each timestep by modifying the ITS controls for a maximum shed or add response, but it does not account for any rebound effects after termination of the DR event.

Table 5-6, on the following page, summarizes the load shed potentials of P2, aggregated over the entire year. The average shed values represent the average reduction in facility peak demand that can be achieved over the duration of the DR event, relative to normal operation. The average energy shed represents the average reduction in facility energy use relative to normal ITS operation. This shed potential is available for a certain percentage of the year, when cooling loads are present and the ITS SOC is sufficient to meet them. The “Shed Availability” column tabulates the percentage of timesteps in the year at which a full- storage demand response control is feasible for the entire event duration specified. These results assume no-notice demand response signals, where no preparatory changes in ITS operation are made prior to the event.

Table 5-6: Summary of annual load shed potentials

Duration of DR Event [hours]	Average Peak Demand Shed [kW <sub>e</sub> ]	Average Energy Shed [kWh]	Shed Availability
0.5	128	63	57%
1	123	120	48%
2	115	208	33%
3	108	267	26%
4	100	321	22%
5	98	386	20%
6	103	466	18%

Table 5-7 presents the same analysis, but limited only to facility occupied hours (8am-8pm on weekdays). In this example, the P2 configuration and control provides a shed flexibility potential of 127 kW<sub>e</sub> for 30-minute events over 63% of all occupied hours. However, for 6-hour DR events, only 90 kW<sub>e</sub> reduction in peak demand can be provided over 15% of occupied hours.

Table 5-7: Summary of load shed during occupied hours

Duration of DR Event [hours]	Average Peak Demand Shed [kW <sub>e</sub> ]	Average Energy Shed [kWh]	Shed Availability
0.5	127	63	68%
1	126	122	61%
2	115	209	43%
3	106	270	31%
4	100	310	22%
5	93	314	17%
6	90	322	15%

Table 5-8 displays the results of an analysis for load add events. The availability is restricted to hours with cooling load and the chiller operating at a restricted capacity. By eliminating the chiller restriction and stopping ice discharge, facility power demand is increased; the ice tank SOC is preserved for later use. Changes in peak demand are not displayed, as they are less pertinent during a load add event. Only average energy use increases are presented with

their associated annual and occupied-hour availabilities. During occupied hours, it is nearly always possible to absorb additional energy as the chiller is operating under partial storage. During the late evening and early morning hours, cooling loads are small and are already being met by the chiller. This explains why the availabilities of the load add potentials during occupied hours are much higher than the full-year potentials.

Table 5-8: Summary of load add potentials

Duration of DR Event [hours]	Annual		Occupied	
	Avg. Add [kWh]	Add Availability	Avg. Add [kWh]	Add Availability
0.5	65	39%	66	94%
1	126	41%	130	98%
2	234	44%	257	100%
3	329	47%	376	100%
4	413	50%	486	100%
5	487	53%	586	100%
6	553	56%	675	100%

This post-processing assessment presents a method to characterize the load add or load shed flexibility of a given ITS configuration and control strategy, for consideration in the early design stage. If regional utility programs heavily incentivize periodic load shed events, similar analysis can help system designers size ITS to ensure sufficient capacity will likely be available. If excess renewables frequently result in curtailed PV-generation, the analysis can quantify the potential service that a given ITS design might provide to help maximize renewable utilization. Through the development of this measure, such analysis may now be readily repeated on a wide variety of potential ITS designs using the OpenStudio platform.

### 5.4.3 Load flexibility testing in-simulation

As previously noted, post-processing does not capture the rebound effects of changing ITS control strategies in response to a DR event. We select two days during a peak-cooling week using case P2 to test and illustrate the broader effects of using the ice for dynamic load add/shed flexibility. A three-hour load shed event is simulated on September 19th, beginning at 11:30 a.m.

A five-hour event is simulated for both load add and load shed on September 21st, beginning at noon.

Figure 5-5 shows the impacts of the three-hour shed event on September 19th from 11:30 to 14:30. Facility peak demand during the event is reduced by 239 kWe, from 787 kWe to 548 kWe. The total additional energy shifted out of the window is 688 kWh. There is no change to peak demand outside the DR event window. The ice is sufficient to supply full storage during the DR event. However, due to the additional depletion mid-day, the ice runs out before the end of the day, thus requiring additional chiller cooling over the last few hours of occupation. The required ITS recharge time is extended relative to the routine operation profile.

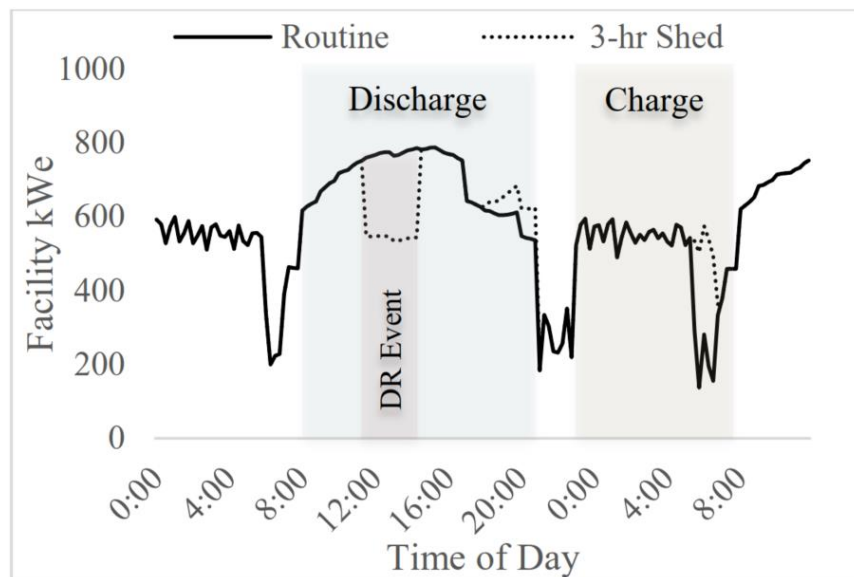


Figure 5-5: Three-hour load shed event on Sept. 19. Rebound effects observed at end of day and during recharge.

Figure 5-6 through Figure 5-8 show the potential impacts of a longer DR event. This day is selected because it is one of the highest cooling loads throughout the year, thus the chiller and ITS are already operating near their design limits under routine operation. The five-hour load shed is selected to explore the impacts when the ice runs out prior to the end of the DR event.

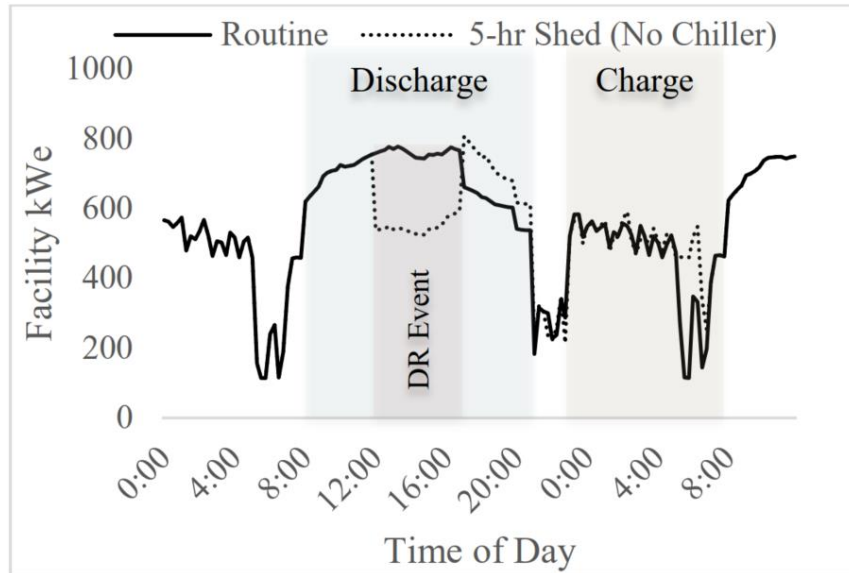


Figure 5-6: Five-hour load shed event on Sept. 21. Chiller operation is prohibited during DR event and ice is insufficient to meet full load. Rebound effects are immediate and severe; recharge time is also extended.

In Figure 5-6, the chiller is forced off for the entire event, regardless of the ITS performance. As the ice runs out, at approximately 16:00, an hour before the end of the DR event, facility electric energy increases despite the chiller being forced off. This is due to the variable speed pumps and fans ramping-up to try to meet zone temperature setpoints. During the event, peak demand is reduced from 771 kW to 593 kW. The additional energy shift totals 1,068 kWh. Immediately following the DR event, at 17:00, the chiller power spikes to provide maximum cooling as it attempts to recover. The spike exceeds the peak demand of the facility during routine operation, increasing the daily peak from 771 kW to 807 kW. As the ice is depleted, the building cannot return to partial storage control following the event; all loads for the remainder of the day must be met by the chiller. Recharge time is increased commensurate with the increased ice discharge.

Figure 5-7 repeats the DR test previously described, but allows for staged chiller operation during the DR event. As the ice approaches a low state-of-charge, the chiller is permitted to operate up to 50% capacity. Once the ice fully runs out this chiller limit is relaxed to the routine operation chiller limiter, which is 65% in model P2. This is not meant to simulate a smart controller, but rather to allow chiller operation to begin meeting cooling loads without a

large, immediate power spike in the simulation. As the ice runs out early, a large increase in facility demand is observed as the chiller turns on at its limited capacity. Peak facility demand during the DR event is now only reduced by 50 kW<sub>e</sub>, from 771 kW<sub>e</sub> to 721 kW<sub>e</sub>. The total electricity use avoided during the event is 901 kWh. Rebound is immediate, but does not cause an increase in facility peak demand for the day. Recharge time is extended as expected.

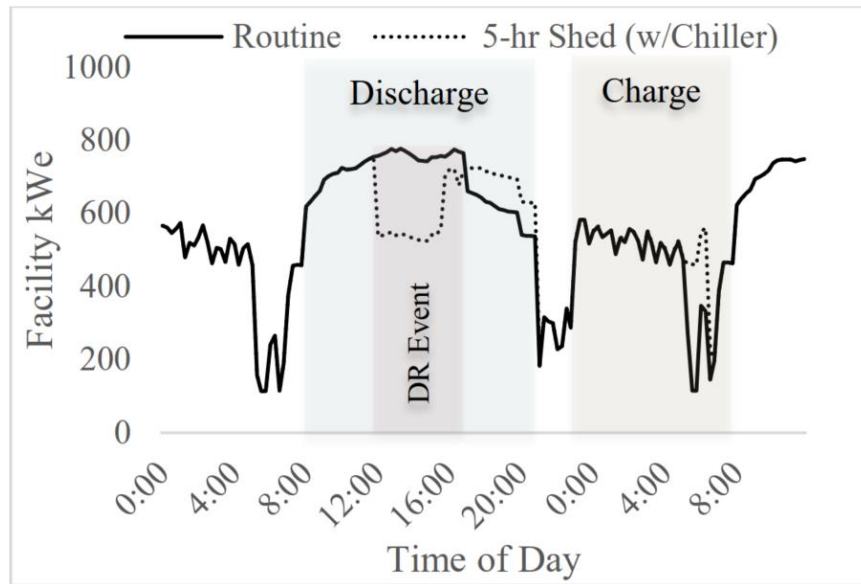


Figure 5-7: Five-hour load shed event on Sept. 21 with chiller operation permitted during the DR event. Immediate rebound is less severe, but peak kW<sub>e</sub> reduction during the event is greatly impacted.

Figure 5-8 shows the performance of ITS under a load add event scheduled for September 21st, beginning at noon. By maximizing chiller usage, and minimizing ice discharge, the facility can temporarily increase its power demand by an average of 106 kW<sub>e</sub> for those five hours. This value is a function of the building cooling load and chiller capacity, as a downsized chiller may not be able to meet the full load. This would require ice discharge during the add event, but at a reduced rate. Conversely, if the chiller is sufficiently large or the load relatively small, the chiller may be able to go into an ice-make operation during the add event, providing an even greater energy storage service to the grid.

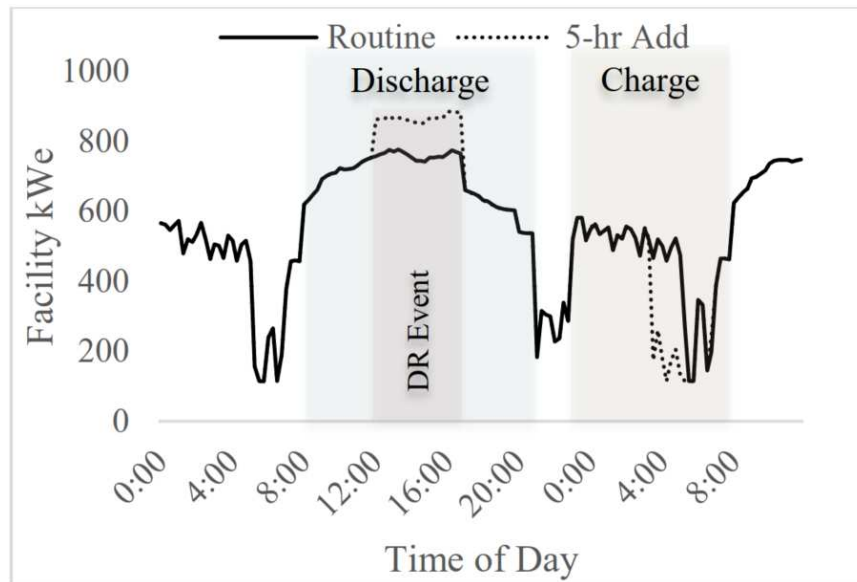


Figure 5-8: Five-hour load add event on Sept. 21. Chiller meets full cooling load during event and ice charge hours are subsequently reduced.

The results depicted in Figure 5-5 through Figure 5-8 provide the information to bound on the building’s flexibility over a given DR event window. The potential increases or decreases in power or energy usage both during and after the DR event provide the necessary information to building operators (or smart controllers) to evaluate possible responses to potential grid signals. Such analysis, previously a tedious, custom endeavor, is now easily performed on any building with a chilled water loop through the use of the OpenStudio measure developed in this project.

## 5.5 Conclusion

This chapter presents a new OpenStudio measure that easily models ITS systems for buildings with central chilled water loops. The measure allows users to explore various hardware configurations and high-level control strategies, and evaluate their performance through detailed building energy simulation. Furthermore, a built-in DR testing feature allows users to examine the potential impacts, including rebound, of using ITS for flexible demand response.

Four ITS models are generated using the measure and compared to the baseline. With no increase in unmet hours, facility EUI’s fall between +1.2% and -2.0% of baseline. Average daily

shifted loads range from 7.4% to 13.3% of total facility electricity use. Total electric energy shifted by these example ITS ranged from 189 to 342 MWh over the course of the year.

One partial-storage model is selected for further flexibility evaluation. In addition to the load shifting previously quantified, this ITS provides average demand shed potentials ranging from 127 kWe for 30-minute events to 90 kWe for 6-hour events during occupied hours. With routine ITS operation, these potentials are available between 68% and 15%, respectively, of the building's occupied hours. Future work will increase the fidelity of chiller limiting controls within the measure and to extend the flexibility analysis to a wider range of ITS designs.

## **5.6 Acknowledgement**

This work was authored in part by the National Renewable Energy Laboratory, operated by Alliance for Sustainable Energy, LLC, for the U.S. Department of Energy (DOE) under Contract No. DE-AC36-08GO28308. Funding provided by U.S. Department of Energy Office of Energy Efficiency and Renewable Energy Building Technologies Office. The views expressed in the article do not necessarily represent the views of the DOE or the U.S. Government. The U.S. Government retains and the publisher, by accepting the article for publication, acknowledges that the U.S. Government retains a nonexclusive, paid-up, irrevocable, worldwide license to publish or reproduce the published form of this work, or allow others to do so, for U.S. Government purposes.

CHAPTER 6  
DESIGN AND DISPATCH OPTIMIZATION OF PACKAGED ICE STORAGE SYSTEMS  
WITHIN A CONNECTED COMMUNITY

A paper published by *Applied Energy* [85]. Rights managed by Elsevier.

Karl Heine, Paulo Cesar Tabares-Velasco, and Michael Deru

## 6.1 Abstract

The traditional implementation of cool thermal energy storage (CTES) must be reimagined within the context of a dynamic grid and smart buildings operating as connected communities. As most buildings do not operate central chillers or connect to district cooling loops, this necessitates a broader use of packaged CTES. Our objective is to begin answering the question of how such packaged CTES should be implemented within a connected community. We do so by presenting a simulation-optimization workflow employing building energy modeling software and a mixed-integer linear program to design and dispatch a packaged CTES technology to achieve minimum total annual cost. We demonstrate this methodology on a seven-building case study using current utility rates and find that total annual cooling energy costs can be reduced by 17.8% compared to baseline, after accounting for the cost of storage. We perform three parametric sensitivity studies to evaluate modeling assumptions and obtain the prioritization of storage procurement as a function of annualized life-cycle cost of storage. We find that a community optimization approach provides significantly different results than individual building optimizations and provides greater savings compared to baseline.

## 6.2 Nomenclature

BEM	Building energy modeling
COP	Coefficient of performance
CTES	Cool thermal energy storage
GEB	Grid-interactive efficient buildings
MILP	Mixed-integer linear program
PSZAC	Packaged single zone air conditioner
PVAV	Packaged variable-air-volume

RTU	Rooftop unit
SOC	State-of-charge
TOU	Time-of-use
UTSS	Unitary thermal storage system

### 6.3 Introduction and literature review

The growth of renewable assets within energy generation portfolios across the U.S. is changing the paradigm that buildings are simple energy users [86]. Instead, the future grid requires interactive buildings with smart controls, that can coordinate with other buildings for the mutual benefit of the building occupants, facility owners, and utility providers. These grid-interactive efficient buildings (GEB) can provide electric load flexibility as a service to the grid [6]. One of the primary methods of providing this flexibility is through load shifting, in which a portion of the building’s electricity use is temporally moved into off-peak hours or hours with excess renewable energy generation through the use of energy storage [87]. Considering the significant energy use by cooling equipment, especially during summer mid- to late-afternoon hours during which cooling drives electric peak demand, substantial electrical load shifting can often be performed using cool thermal energy storage (CTES) [23, 24, 88, 89]. Furthermore, coordination between multiple buildings with diverse electricity profiles can provide greater value to the grid compared to controlling individual building loads in isolation [90]. A broad research question is implied: how *should* CTES be installed and operated in a GEB community to best support the dynamic generation of the future grid? This paper presents a tool to help answer that question using the specific technology of packaged ice storage.

Centralized CTES, attached to main chiller plants, is a proven method for load shifting to obtain energy bill savings [16, 17, 91]. Under common commercial utility rates, centralized CTES consistently provides substantial electric demand reduction, and sometimes total energy use reduction [92]. Building energy simulation and parametric analyses have shown total plant operating cost reductions of 9-18.6%, and demand reduction during on-peak hours of 25-78% throughout the year [80, 93, 94]. Optimizations of ice storage using non-linear, linear, and mixed-integer programming [27, 95-97], neural networks and genetic algorithms [29, 98, 99], and multi-objective approaches [25] have shown the potential to greatly reduce cooling energy costs – up to 25-30% in hot climates with high on-peak electric rates. These studies were

performed on a mix of individual commercial buildings and district cooling loops. Chilled water storage is often economically preferable to ice at very large scales; however, ice thermal storage has been effectively implemented in district cooling systems [35, 100]. In the context of a dynamic grid, recent studies show how CTES in general, and ice thermal storage specifically, provide a grid service, such as reducing power generation costs [48] or facilitating renewable penetration and utilization [30, 49]. However, only 25% of commercial floorspace in the U.S. is cooled via central plants, while an estimated 66% of commercial floorspace is cooled by packaged rooftop units (RTU) [84]. It is this latter market category which offers the most aggregated potential for cooling load flexibility, but has not been well assessed in literature.

To address this growing need for thermal storage in distributed applications, recent research has focused on the development of unitary thermal storage systems (UTSS). These are self-contained cool thermal storage devices that can be readily integrated into a building's existing packaged cooling equipment, specifically RTUs [14]. While some technologies using various phase-change materials are under development [64, 101], only one ice-based system was commercially available in recent years [37, 102]. This system serves as the basis for a packaged ice storage model within the EnergyPlus building energy modeling (BEM) software [36, 40]. The charge and discharge performance for this packaged unit are described in [103]. We employ this UTSS performance regression model in this study, with additional discussion in §6.4.3.

Modeling and optimization of cooling systems as distributed energy resources (DERs) at the community scale is an area of active research and technological development. Several studies have shown that approaching energy flexibility at the community scale can provide greater potential than through an individual building approach [104-107]. New tools are available for assessing and optimizing thermal storage within the community context, both open-source [108, 109] and proprietary [47, 110]. However, none of these tools yet have the capability of modeling or optimizing ice-based UTSS at individual RTUs. Thus, the question of how beneficial such a technology might be to the GEB future remains unanswered.

The objective of this study is to address this research gap by developing a new workflow that optimizes the location and operation of unitary thermal storage systems (UTSS) as distributed energy resources (DERs) within a connected community. The contributions of this paper are: (1) a simulation-optimization workflow for evaluating unitary thermal storage systems

(UTSS) as DERs; (2) a mixed-integer linear program (MILP) to procure and dispatch UTSS within a connected community; (3) a demonstration of the efficacy of this workflow and assessment of MILP sensitivity to three UTSS model parameters using a seven-building case study; and (4) an application of the MILP to show that community optimization of UTSS outperforms the aggregation of individual building optimizations.

## 6.4 Methodology

### 6.4.1 Overview of simulation-optimization workflow

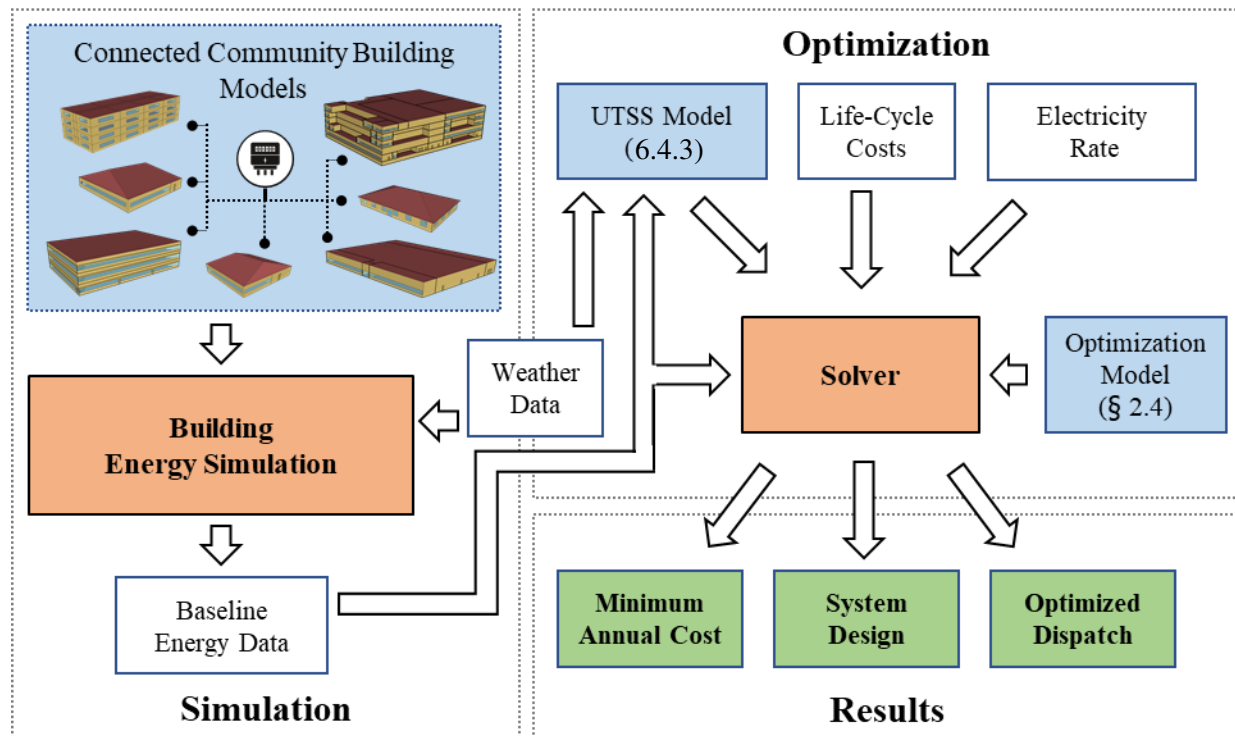


Figure 6-1: A simulation-optimization workflow to design and dispatch packaged thermal storage systems in a connected community of grid-interactive buildings. Background colors designate element type: blue for models, white for input data sets, orange for simulation and optimization processes, and green for final results. Section numbers indicate where the UTSS and optimization models are presented in this paper.

We present a simulation-optimization workflow that employs BEM and MILP optimization to design and dispatch packaged ice energy storage within a connected community. The workflow is modular and scalable, capable of simultaneously evaluating multiple thermal storage systems at scales ranging from a single building with one air conditioner to many

buildings, each containing several RTUs. The workflow is intended to provide early-design insight into the optimal placement and control of distributed cool thermal storage under the GEB paradigm. Figure 6-1 (page 65) depicts the workflow, illustrating the required building energy, ice storage, and mathematical optimization models (blue), input data sets (white), simulation and optimization processes (orange), and final output results (green). There are three distinct phases of the workflow described below:

- The Simulation phase requires building energy models and weather data. The results of the BEM are the baseline energy use for all buildings and specific data at each RTU cooling system for every simulation timestep. These data become inputs for both the packaged ice storage model and the optimization program.
- The Optimization phase of the workflow requires the pre-processed parameters from the baseline energy data, the packaged ice storage model results, life-cycle cost data, and the electric utility rate. The packaged ice storage model is a stand-alone Python script that uses baseline building energy data and weather data to calculate charging and discharging capacities and efficiencies for the packaged ice storage system at each timestep and potential installation site within the community. This model and its assumptions are described in §6.4.3. The life-cycle cost estimate for the packaged ice storage must be scaled to the optimization time horizon. To capture the seasonality of energy use, we examine a 12-month window and calculate the cost of storage using an annualized life-cycle cost (ALCC). The ALCC includes initial capital and installation costs, government and utility incentives, annual device maintenance, and end-of-life costs, annualized over the expected lifespan of the device. Electricity rate information is the final input required for the optimization. Any combination of variable time-of-use energy and/or demand charges may be used, though complex tiered electricity rates may require constraint reformulation.
- The Results phase post-processes the optimization outputs for (1) minimum annual cost, (2) distributed packaged storage system design, and (3) the optimized dispatch, into user-friendly visualizations. In assessing these results, we determine the load shift efficiency ( $\eta_{shift}$ ) of the optimized system, calculated relative to the total baseline energy use for the community. It is equal to the ratio of the electric load reduction from ice discharging

(Load Shed) and the electric load increase from ice charging (Load Add), given by equation (6-1) (see Table 6-1 for notation). Because this metric is highly sensitive to operating conditions and dispatch strategy, it is useful for comparing thermal storage design and control options.

$$\eta_{shift} = \frac{\text{Load Shed}}{\text{Load Add}} = \frac{\sum_{\{t|P_t < \bar{p}_t\}} P_t}{\sum_{\{t|P_t \geq \bar{p}_t\}} P_t} \quad (6-1)$$

### 6.4.2 Notation

To keep the mathematical expressions required by the UTSS model and the optimization formulation as short as possible, single-character symbols are preferred, except where such might cause confusion. Table 6-1 defines all notation used in both the packaged ice storage model and the optimization program formulation. For brevity, we use the UTSS acronym to refer to packaged ice storage systems for the remainder of this paper. Generally, parameters are designated with lower-case symbols and optimization variables are uppercase, except for temperature ( $T$ ), heat transfer coefficient ( $UA$ ), and coefficient of performance ( $COP$ ). Superscripts provide descriptors and subscripts are reserved for indexing. Sets are also capitalized but are differentiated from variables with script font.

Table 6-1: Notation for UTSS model and optimization program

<i>Sets</i>	
$i \in \mathcal{I}$	Set of available UTSS types
$d \in \mathcal{D}$	Set of utility demand periods in the optimization horizon
$n \in \mathcal{N}$	Set of RTUs within the community
$t \in \mathcal{T}$	Set of all timesteps within the optimization period
$t \in \mathcal{T}_d^p$	Indexed set of timesteps within each utility demand period $d$
$t \in \mathcal{T}_n^l$	Indexed set of timesteps during which cooling load exists at RTU $n$

Table 6-1 continued

<i>Building Simulation Parameters</i>	
$COP_{nt}^N$	Coefficient of performance for RTU $n$ at time $t$ [ $\text{kW}_t/\text{kW}_e$ ]
$l_{nt}$	Thermal cooling load served by RTU $n$ at time $t$ [ $\text{kW}_t$ ]
$\tilde{p}_t$	Aggregated average power for the community at time $t$ [ $\text{kW}_e$ ]
$T_t^d$	Ambient dry-bulb temperature at time $t$ [ $^\circ\text{C}$ ]
$T_{nt}^w$	Wet-bulb temperature at the inlet to RTU $n$ at time $t$ [ $^\circ\text{C}$ ]
<i>UTSS Parameters</i>	
$\epsilon_{int}$	Discharge effectiveness of UTSS type $i$ at RTU $n$ and time $t$ [-]
$\tilde{\epsilon}_i$	Nominal discharge effectiveness of UTSS type $i$ [-]
$\eta_{it}^S$	Thermal storage tank efficiency for UTSS type $i$ at time $t$ [-]
$COP_i^{X,nom}$	Nominal Coefficient of performance for charging of UTSS $i$ [ $\text{kW}_t/\text{kW}_e$ ]
$COP_{it}^X$	Coefficient of performance of charging for UTSS type $i$ at time $t$ [ $\text{kW}_t/\text{kW}_e$ ]
$COP_i^{Y,nom}$	Nominal Coefficient of performance for discharging of UTSS $i$ [ $\text{kW}_t/\text{kW}_e$ ]
$COP_{it}^Y$	Coefficient of performance for discharging UTSS type $i$ at time $t$ [ $\text{kW}_t/\text{kW}_e$ ]
$\bar{q}_i$	Maximum thermal storage capacity of UTSS type $i$ [ $\text{kWh}_t$ ]
$\dot{q}_i^{X,nom}$	Nominal rate of charging of UTSS type $i$ at time $t$ [ $\text{kW}_t$ ]
$\dot{q}_{it}^X$	Maximum rate of charging of UTSS type $i$ at time $t$ [ $\text{kW}_t$ ]
$\dot{q}_i^{Y,nom}$	Nominal rate of discharging of UTSS type $i$ at time $t$ [ $\text{kW}_t$ ]
$\dot{q}_{it}^Y$	Maximum rate of discharging of UTSS type $i$ at time $t$ [ $\text{kW}_t$ ]
$\tilde{s}_i$	Constant for approximate median state-of-charge for UTSS type $i$ [-]
$T_i^{fz}$	Freezing temperature of the thermal storage medium in UTSS type $i$ [ $^\circ\text{C}$ ]
$UA_i$	Net tank heat transfer coefficient times surface area for UTSS type $i$ [ $\text{kW}_t/^\circ\text{C}$ ]

Table 6-1 continued

<i>Cost Parameters</i>	
$c_t^e$	Cost of electric energy at time $t$ [ $\$/\text{kWh}_e$ ]
$c_d^p$	Cost of maximum average electric power during period $d$ [ $\$/\text{kW}_e$ ]
$k_{in}$	Annualized life cycle cost of storage for UTSS type $i$ at RTU $n$ [ $\$/\text{device-year}$ ]
<i>Miscellaneous Parameters</i>	
$\delta$	Duration of each timestep $t$ [hr]
$m_{in}$	Maximum number of UTSS type $i$ that may be installed at RTU $n$ [-]
$S_{in}^0$	Initial thermal storage inventory for UTSS type $i$ at RTU $n$ [ $\text{kW}_t$ ]
<i>Integer Variables</i>	
$Z_{in}$	Number of UTSS type $i$ installed at RTU $n$ [-]
<i>Continuous Variables</i>	
$\hat{P}_d$	Maximum aggregated power during period $d$ [ $\text{kW}_e$ ]
$P_t$	Total aggregated power at time $t$ [ $\text{kW}_e$ ]
$S_{int}$	Thermal storage energy inventory for UTSS type $i$ at RTU $n$ at time $t$ [ $\text{kWh}_t$ ]
$X_{int}$	Average thermal load added (charged) by UTSS type $i$ at RTU $n$ at time $t$ [ $\text{kW}_t$ ]
$Y_{int}$	Average thermal load reduced (discharged) by UTSS type $i$ at RTU $n$ at time $t$ [ $\text{kW}_t$ ]

### 6.4.3 UTSS model

Figure 6-2 provides a general sketch of how a UTSS interacts with existing building cooling equipment. The selected UTSS integrates a packaged thermal storage unit – containing an ice storage tank, ice-making equipment, and refrigerant management system – with the air-conditioning equipment in a roof-top unit (RTU).

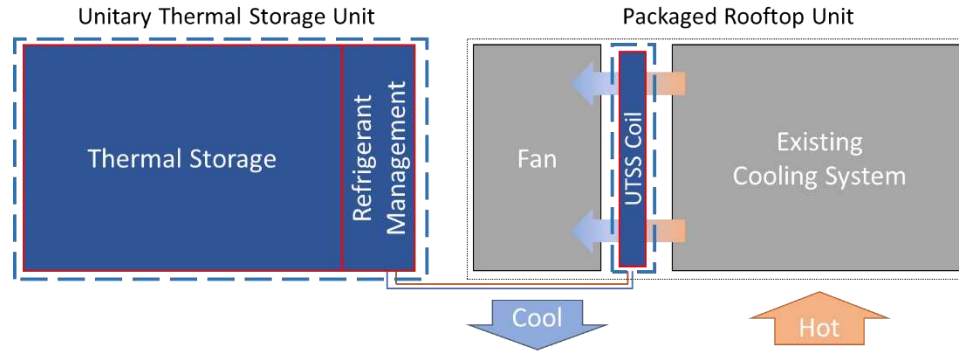


Figure 6-2: Depiction of a UTSS integrated with an RTU. Components of the UTSS are shown in blue. Note the placement of the UTSS evaporator coil within the RTU airstream [71].

The UTSS model is based on a set of non-linear performance curves found in the EnergyPlus Coil:Cooling:DX:SingleSpeed:ThermalStorage model object [36, 40] with additional detail provided in [103]. From this BEM object, we extract the performance curves and place them into an external Python script, to allow for workflow modularity and independence from any specific BEM software. The coefficients used in Equations 2-4 are based on the IceBear 30, formerly manufactured by Ice Energy Inc., and included with the EnergyPlus UTSS model [36].

The UTSS model outputs five parameter sets required by the optimization program: maximum rate of thermal storage discharging ( $\dot{q}_{it}^Y$ ), maximum rate of thermal storage charging ( $\dot{q}_{it}^X$ ), coefficient of performance for charging ( $COP_{it}^X$ ), discharge effectiveness ( $\epsilon_{int}$ ), and the tank thermal storage efficiency ( $\eta_{it}^S$ ). These parameters are calculated using equations (6-2) to (6-6), where the index of the UTSS type ( $i$ ) is set equal to 1, since the coefficients are unique to our UTSS model.

Equation (6-2) calculates the maximum rate of discharging ( $\dot{q}_{it}^Y$ ) as a function of nominal discharging rate and the wet-bulb temperature at the inlet of each roof-top unit ( $T_{in}^w$ ) [72].

Because each RTU has a different mix of return air from the building and fresh outside air, the inlet wet-bulb temperatures for each RTU at each timestep are obtained from the building energy simulation results, rather than from the ambient conditions in the weather file.

$$\dot{q}_{1nt}^Y = \dot{q}_1^{Y,nom} \left( -0.002765 \cdot (T_{nt}^w)^2 + 0.133949 \cdot T_{nt}^w - 0.561476 \right) \quad (6-2)$$

The maximum rate of charge is modeled as a function of nominal charging rate, tank state-of-charge (SOC), and ambient dry-bulb temperature ( $T_t^d$ ). However, to retain a linear formulation, the timestep variation of state-of-charge must be eliminated. For a fixed dry-bulb temperature, the maximum rate of charging varies  $\pm 7\%$  from the nominal rate as SOC fluctuates between 5% and 95%. Maximum charging rate decreases with SOC due to the growth of ice around the heat exchange coils within the tank, which slows the rate of heat transfer into storage. Rather than derive an approximate linearization of this relationship, we introduce a fixed parameter and set it equal to an expected value for the median state-of-charge of the ice tank ( $\tilde{s}_1$ ). We examine the validity of this assumption and the optimization sensitivity to this parameter in §6.6.4. The simplified curve, which assumes a median state-of-charge greater than 0.15, is given:

$$\dot{q}_{1t}^X = \dot{q}_1^{X,nom} \cdot (1.293 - 0.127 \cdot \tilde{s}_1 + 0.0186 \cdot \tilde{s}_1^2 - 0.0083 \cdot T_t^d - 0.0001 \cdot (T_t^d)^2 + 0.0013 \cdot \tilde{s}_1 \cdot T_t^d) \quad (6-3)$$

Equation (6-4) calculates coefficient of performance (COP) when UTSS is making ice (charging) as a function of nominal COP, tank SOC, and  $T_t^d$ . The value of  $COP_{1t}^X$  varies by  $\pm 3\%$  with SOC values between 5% and 95%. As in the  $\dot{q}_{1t}^X$  equation, we replace the timestep-varying SOC with an assumed median state-of-charge ( $\tilde{s}_1$ ) for calculation of optimization parameters.

$$COP_{1t}^X = COP_1^{X,nom} \cdot (0.6208 + 0.0211 \cdot \tilde{s}_1 - 0.0015 \cdot \tilde{s}_1^2 - 0.0026 \cdot T_t^d + 0.0007 \cdot (T_t^d)^2 + 0.0018 \cdot \tilde{s}_1 \cdot T_t^d)^{-1} \quad (6-4)$$

UTSS discharging COP is high ( $\sim 63.9$ ), since the compressor is off and only a small refrigerant circulation pump operates to provide cooling to the airstream. Our method combines RTU efficiency ( $COP_{nt}^N$ ) and UTSS discharging efficiency ( $COP_{it}^Y$ ) into a single discharge effectiveness value ( $\tilde{\epsilon}_1$ ) for each RTU in equation (6-5). We find this term more easily conceptualized than extremely high COPs that are not readily comparable to nominal RTU values. For example, if this UTSS were added to an ultra-high-efficiency RTU with a nominal COP of 4.4 (15 EER), the discharge effectiveness would be 93.1%. However, with a standard

efficiency RTU having a COP of 3.23 (11 EER), the discharge effectiveness increases to 94.9%. If sufficient fidelity in the UTSS model is possessed, discharge effectiveness may be calculated at each RTU and timestep ( $\epsilon_{int}$ ) according to the general form of equation (6-5). Because our model does not contain a performance curve for discharge efficiency, we assume a nominal value for discharge effectiveness ( $\tilde{\epsilon}_1$ ).

$$\epsilon_{int} = 1 - \left( \frac{COP_{nt}^N}{COP_{it}^Y} \right) \approx \tilde{\epsilon}_1 \quad (6-5)$$

Equation (6-6) defines the UTSS tank efficiency at each timestep as a function of  $T_t^d$ , heat transfer coefficient and surface area ( $UA_i$ ), tank freezing temperature ( $T_i^{fz}$ ), optimization timestep ( $\delta$ ), and maximum UTSS storage capacity ( $\bar{q}_i$ ). Losses through each thermal storage tank ( $\eta_{it}^s$ ) are relatively small, with approximately 5% capacity loss over a summer day.

$$\eta_{it}^s = 1 - \frac{\delta \cdot UA_i \cdot (T_t^d - T_i^{fz})}{\bar{q}_i} \quad (6-6)$$

## 6.4.4 Distributed storage optimization program

### 6.4.4.1 Objective function

Our optimization program provides both procurement and placement of UTSS within the community (design) and charge/discharge control signals (dispatch) over the course of the year. The formulation is a mixed-integer linear program (MILP) consisting of twelve equation sets (Equation (6-7) and Constraints (6-8) through (6-19)). The linear program ensures tractability and reasonable solution times when many buildings are simultaneously evaluated, and is similar to other strategic-level DER design-dispatch optimization tools [46, 108]. The objective function of the formulation minimizes total annual cost consisting of energy costs, demand charges, and the total annualized cost of storage, given by Equation (6-7).

$$\min \left[ \sum_{t \in \mathcal{T}} c_t^e (\delta \cdot P_t) + \sum_{d \in \mathcal{D}} c_d^p \hat{P}_d + \sum_{i \in \mathcal{I}} \sum_{n \in \mathcal{N}} k_{in} Z_{in} \right] \quad (6-7)$$

### 6.4.4.2 Constraints

Constraint (6-8) is the heart of this formulation and calculates the optimal power for the community at each timestep ( $P_t$ ) after applying thermal storage dispatch. It converts the linear decision variables ( $X_{int}, Y_{int}$ ) for thermal load (in kW<sub>t</sub>), used to charge or discharge individual UTSS devices, respectively, into deviations from the baseline community power draw ( $\tilde{p}_t$ ) at each timestep  $t$ . To accomplish this, each decision variable is divided by the appropriate efficiency parameter. Dividing the thermal energy added from ice charging ( $X_{int}$ ) is  $COP_{it}^X$ , provided by the UTSS model during pre-processing. The thermal energy reduced by discharging ( $Y_{int}$ ) is similarly divided by a COP; however, this value is from the RTU at which storage is placed and is obtained from the building energy simulation results ( $COP_{nt}^N$ ). The term is further modified by the nominal discharge effectiveness ( $\tilde{\epsilon}_1$ ) which accounts for the small amount of electric energy used to discharge the thermal storage. The complete  $Y_{int}$  term represents the electrical power avoided at a given RTU and timestep by discharging the UTSS. The full constraint is written such that charging may occur at any timestep, but discharging can only occur if a thermal load is present at a given RTU. Constraint (6-9) then captures the maximum power during each demand period  $d$ .

$$P_t = \tilde{p}_t + \sum_{i \in \mathcal{I}} \sum_{n \in \mathcal{N}} \left[ \frac{X_{int}}{COP_{it}^X} - \begin{cases} \frac{\tilde{\epsilon}_1 Y_{int}}{COP_{nt}^N} & \text{if } t \in \mathcal{T}_n^l \\ 0 & \text{otherwise} \end{cases} \right] \quad \forall t \in \mathcal{T} \quad (6-8)$$

$$\hat{P}_d \geq P_t \quad \forall d, t \in \mathcal{T}_d^p \quad (6-9)$$

Three constraints limit the performance of each UTSS during discharging. The total load reduced by discharging cannot exceed: (1) the cooling demand from the building at that RTU ( $l_{nt}$ ), given by Constraint (6-10); (2) the aggregated maximum rate of discharge of all the UTSS installed at each RTU, given by Constraint (6-11); and (3) the total available ice inventory at a given timestep ( $S_{int}$ ), given by Constraint (6-12).

$$\sum_{i \in \mathcal{I}} Y_{int} \leq l_{nt} \quad \forall n \in \mathcal{N}, t \in \mathcal{T}_n^l \quad (6-10)$$

$$Y_{int} \leq \dot{q}_{it}^Y \cdot Z_{in} \quad \forall \quad i \in \mathcal{I}, n \in \mathcal{N}, t \in \mathcal{T}_n^l \quad (6-11)$$

$$\delta \cdot Y_{int} \leq S_{int} \quad \forall \quad i \in \mathcal{I}, n \in \mathcal{N}, t \in \mathcal{T}_n^l \quad (6-12)$$

Constraint (6-13) limits the UTSS charging rate to be less than the aggregate maximum rate of charging for all UTSS installed at each RTU. Other restrictions on charging are provided by the inventory constraints.

$$X_{int} \leq \dot{q}_{it}^X \cdot Z_{in} \quad \forall \quad i \in \mathcal{I}, n \in \mathcal{N}, t \in \mathcal{T} \quad (6-13)$$

Thermal storage inventory ( $S_{int}$ ) is initialized by Constraint (6-14) and limited to the maximum nominal storage capacity of each tank by Constraint (6-15). Constraints (6-16) and (6-17) provide inventory balance during the applicable timesteps. Because the decision variables are in units of kW<sub>t</sub>, the optimization timestep  $\delta$  is used to convert all terms into units of energy. Energy losses due to heat transfer between the tank and ambient are applied to each previous timestep's final state-of-charge.

$$S_{in1} = S_{in}^0 \quad \forall \quad i \in \mathcal{I}, n \in \mathcal{N} \quad (6-14)$$

$$S_{int} \leq \bar{q}_i \cdot Z_{in} \quad \forall \quad i \in \mathcal{I}, n \in \mathcal{N}, t \in \mathcal{T} \quad (6-15)$$

$$S_{int} = \eta_{it}^S \cdot S_{in,t-1} + \delta \cdot X_{in,t-1} - \delta \cdot Y_{in,t-1} \quad \forall \quad i \in \mathcal{I}, n \in \mathcal{N}, t > 1 \text{ \& } \in \mathcal{T}_n^l \quad (6-16)$$

$$S_{int} = \eta_{it}^S \cdot S_{in,t-1} + \delta \cdot X_{in,t-1} \quad \forall \quad i \in \mathcal{I}, n \in \mathcal{N}, t > 1 \text{ \& } \notin \mathcal{T}_n^l \quad (6-17)$$

Constraints (6-18) and (6-19) ensure integrality and non-negativity. The number of UTSS units permitted at a given RTU is restricted by the parameter  $m_{in}$ , and is determined by physical system limitations.

$$X_{int}, Y_{int}, S_{int}, P_t, \hat{P}_d \geq 0 \quad \forall \quad i \in \mathcal{I}, n \in \mathcal{N}, t \in \mathcal{T}, t' \in \mathcal{T}_n^l, d \in \mathcal{D} \quad (6-18)$$

$$0 \leq Z_{in} \leq m_{in}, \text{integer} \quad \forall \quad i \in \mathcal{I}, n \in \mathcal{N} \quad (6-19)$$

#### 6.4.5 Limitations of this approach

There are four main limitations to our approach:

1. Median ice tank state-of-charge assumption. The first and most notable limitation to our approach is the UTSS model's independence of time-varying SOC. In reality, UTSS

efficiency and maximum rate of heat transfer are functions of both ambient conditions and SOC. However, inclusion of the SOC dependency in the optimization requires a non-linear formulation. For our UTSS Model, we assume a fixed parameter for median state of charge ( $\tilde{\delta}_1$ ) to maintain a linear optimization formulation, which helps maintain tractability, especially for community-scale problems. The quality of this assumption is examined in §6.5.4.

2. Fixed-speed compressor assumption. The second limitation of our approach is that we assume that a fraction of the cooling load can be subtracted from a specific air conditioning unit at a given timestep without affecting the baseline RTU efficiency. This assumption is valid only if the RTU in question uses a fixed-speed compressor. If so, part-load operation is achieved through equipment cycling and efficiency is only a function of air properties, which are treated as constants during a given timestep. If multi-stage compressors are used in the building models, our approach and formulation can still be applied, but efficiency changes between compressor stages will be neglected. To provide the most conservative estimate of UTSS performance, the highest efficiency stage should be used when calculating  $COP_{nt}^N$  parameters.
3. Unchanged zone loads assumption. The third limitation of our approach is that we do not account for the variation in zone air conditions that would occur when using UTSS compared to the baseline building cooling systems. Because UTSS discharge on a variable continuum to meet the cooling load, they will typically run continuously at part-load rather than frequently cycling. This will result in much more consistent dehumidification of the supply air compared to a direct-expansion air-conditioning unit, which in turn will affect the zone cooling loads over time. While this will affect cooling equipment energy use, it is unlikely to affect the optimization dispatch since it will result in a generally consistent change in zone air humidity for the full simulation period – there will be little, if any, differentiation between adjacent timesteps that would alter dispatching. If possible, this effect should be explored through re-simulation of the building models in BEM software. Such analysis is beyond the scope of this study.
4. No explicit accounting for changes in fan energy use. The final limitation of our approach is a lack of explicit accounting for the increased fan energy use when adding UTSS to the

airstream. Each cooling coil adds approximately 0.1 in. of water (25 Pa) in pressure drop to the airflow [111]. This addition is relatively small compared to other airstream components, such as air filters or fan system effects; but it will be felt for the entire life of the system and should not be neglected from final energy calculations. To accurately capture this effect, additional fan information is required. Such analysis is beyond the scope of this study.

## 6.5 Case study community

### 6.5.1 Building models and location

Our workflow is demonstrated using a community that consists of seven simulated buildings located in El Paso, TX, which lies within ASHRAE Climate Zone 3B (Warm-Dry). This location has significant seasonal and diurnal temperature variation resulting in large variability in cooling loads over the course of the year. Typical meteorological year weather data for El Paso International Airport is used [73] and the building models are generated using an OpenStudio measure that creates prototype commercial buildings [112-114]. We simulate these buildings using EnergyPlus v.9.3 using a timestep of 1 minute, which is the maximum fidelity of the software. HVAC system types are either packaged single zone air conditioners (PSZAC) or packaged variable-air-volume (PVAV) systems. Table 6-2 lists the seven buildings used in this case study, summarizing their ASHRAE Standard 90.1 vintage, HVAC system type, number of RTUs, and the maximum building occupancy.

Table 6-2: Summary of connected community building models

Building Type	Standard 90.1 Vintage	HVAC Type	No. RTU's	Max Occ.
Fast Food	2010	PSZAC	2	94
Midrise Apartment	Pre-2004	PVAV	3	79
Medium Office	2007	PVAV	3	286
Small Office	2013	PVAV	1	31
Outpatient	2010	PVAV	2	419
Restaurant	2004	PSZAC	2	287
Retail	Pre-2004	PSZAC	4	371

Figure 6-3 shows the weighted occupancy of the entire community over a summer weekday. Community aggregate occupancy peaks at 14:00 and remains above 50% until after 20:00.

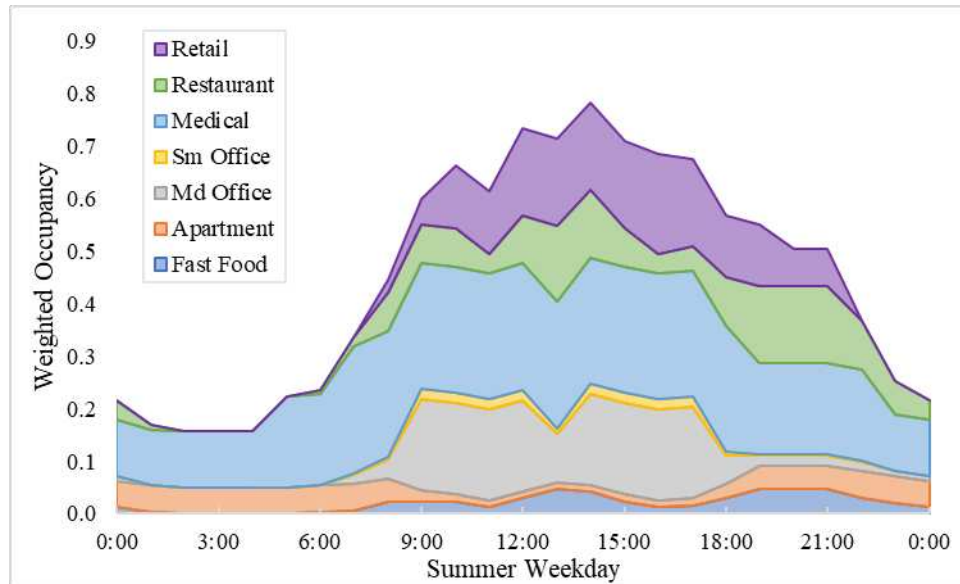


Figure 6-3: Aggregated weighted occupancies of each building type, presented to illustrate the temporal coincidence of building occupancy and relative sizes of each building

Table 6-3 lists the total annual electricity use and cooling-only electricity use for each building. The fraction of total annual electricity used for cooling ranges between 8.8% and 24.0% for individual buildings and is 17.2% for the entire community. Figure 6-4 shows the 15-minute-averaged aggregated load profiles for (a) total power demand and (b) cooling-only power demand for each building over a peak day in June. While the peak community occupancy occurs at 14:00, on this day the maximum cooling-only power demand occurs at 14:45 and total power demand peaks at 15:45. The fraction of total community power demand due to cooling loads on this day is 40%.

Table 6-3: Baseline building energy results

Building Type	Annual Cooling Electricity [MWh]	Annual Total Electricity [MWh]
Fast Food	14.1	159.9
Midrise Apartment	75.9	316.2
Medium Office	128.3	648.7
Small Office	6.4	44.3
Outpatient	234.6	1,243.9
Restaurant	46.9	401.5
Retail	72.7	554.0
<b>Totals</b>	<b>578.9</b>	<b>3,368.5</b>

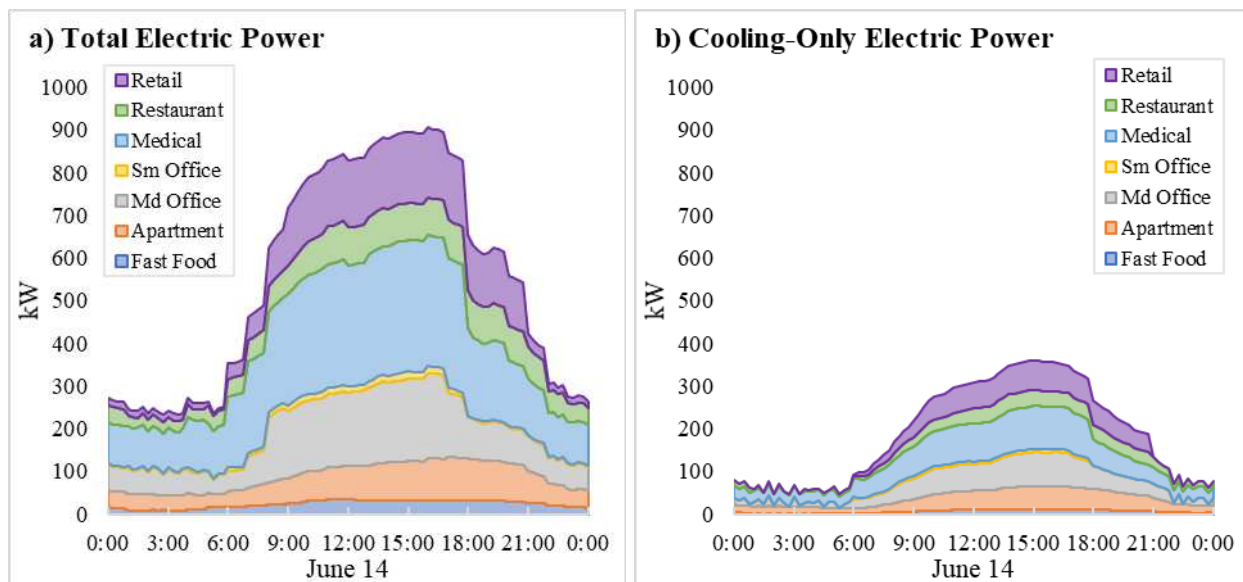


Figure 6-4: Aggregated electric power demand over a near-peak summer day from the baseline energy results: (a) total electric power demand; (b) cooling-only electric power demand

### 6.5.2 UTSS model data

In anticipation of new technologies, our optimization formulation is designed to handle multiple types of UTSS; however, this demonstration only evaluates one 40 ton-hour device formerly manufactured by Ice Energy [65, 115]. This device is well characterized through its limited market presence and has demonstrated both building-scale and grid-scale load-shifting

capabilities [37]. Table 6-4 lists its nominal performance characteristics, as well as the constants used in optimization parameter calculations.

Table 6-4: Performance characteristics for the selected UTSS (index  $i = 1$ )

Parameter	Value	Remarks
$\tilde{\epsilon}_1$	0.93	Assumes high-efficiency RTU
$COP_1^{X,nom}$	3.09	Rated COP of charging
$COP_1^{Y,nom}$	63.9	Rated COP of discharging
$\bar{q}_1$	133.6 kW <sub>t</sub>	95% of 40 ton-hours
$\dot{q}_1^{X,nom}$	17.6 kW <sub>t</sub>	5-tons cooling for ice-making
$\dot{q}_1^{Y,nom}$	35.2 kW <sub>t</sub>	10-tons cooling via ice discharge
$\tilde{s}_1$	0.55	Anticipated median tank state-of-charge
$S_{1n}^0$	0 kW <sub>t</sub>	All ice tanks are initially fully discharged
$T_1^{fz}$	0°C	Freezing temperature of ice tank
$UA_1$	0.007913 kW <sub>t</sub> /°C	Thermal loss rate as a function of temperature difference

### 6.5.3 Annualized life cycle cost estimate

The element of this analysis with the most uncertainty is the annualized life cycle cost (ALCC) of the UTSS unit. We use various sources [111, 116, 117] to obtain a realistic approximation for ALCC, itemized in Table 6-5. To address the uncertainty related to storage costs, we perform a parametric sweep over a broad range of possible ALCC values, discussed in §6.5.4.

Table 6-5: Cost components used in estimating the annualized life cycle cost

Cost Component	Value	Remarks
UTSS Device	\$17,500 <sup>[111, 116]</sup>	-
Installation	\$10,000 <sup>[111, 116]</sup>	-
Permitting/Engineering	\$2,500 <sup>[111, 116]</sup>	Cost shared with RTU retrofit
New HVAC	Not Included	-
Incentive	(\$12,500) <sup>[111, 117]</sup>	Government and utility incentives
Tax Credit	Not Included	20-30% + accelerated depreciation <sup>[111]</sup>
End-of-Life	Not Included	Included w/installation above
Life-Cycle Cost	\$17,500	-
Service Life	20 years <sup>[111]</sup>	-
Annual Maintenance	\$250 per year <sup>[111]</sup>	Includes major service at 10 years
Annualized Life Cycle Cost	\$1,125 per year	

#### 6.5.4 Solution method and sensitivity analyses

This case study is solved using IBM CPLEX v. 12.10.0.0 on an Intel Xeon E5440 2.83GHz dual Quad-core machine with 16 GB of RAM, operating Ubuntu 18.04.5 LTS. Due to large number of continuous variables (~1.27 million after pre-solve) and small number of general integer variables (17), this formulation is well suited to use Benders Decomposition [118], which we employ using the built-in ‘benderopt’ solver option [119]. Further improvement in solution time is achieved with symmetry elimination on the  $COP_{it}^X$  parameter values (via  $\leq 0.05\%$  perturbations), which we apply when reading the data into A Mathematical Programming Language (AMPL), the software used for MILP formulation and execution. Three small parametric analyses are performed to examine the program sensitivity to the UTSS model and formulation assumptions for the following parameters:  $\tilde{S}_1$ ,  $\mathcal{D}$ , and  $k_{in}$ .

To assess the potential impact of our assumed median UTSS state-of-charge ( $\tilde{S}_1$ ) on the optimization results, we execute the full workflow using three different values for  $\tilde{S}_1$ : 0.05,

0.55, and 0.95. When the ice tank is nearly empty, the contents are mostly water, and the heat transfer rates are much higher than when the tank is mostly solidified into ice. More conservative UTSS performance estimates will be obtained at higher  $\tilde{s}_1$  values. By bounding the UTSS at the near maximum and minimum states-of-charge, we quantify the potential significance of the  $\tilde{s}_1$  assumption.

The timesteps used for building energy simulation and optimization do not need to match, so long as the optimization timestep is an integer multiple of the simulation timestep. Because building power demand is billed over a rolling 15-minute horizon, we consider this the required optimization timestep ( $\delta = 0.25$  hours). However, previous literature has shown that modeling timestep can have a significant impact on calculated peak demand and the associated optimization results [120, 121]. By separating our building simulation process from the optimization, we take advantage of the highest available resolution in the energy modeling software (1-minute), but then apply the optimization over the 15-minute billing window used by many utilities. To explore the impact of longer optimization timesteps, we average the 1-minute building energy simulation data over 15, 30, and 60-minute windows ( $\delta = 0.25, 0.5, \text{ and } 1.0$ ) and evaluate the impact on the optimal solution. Shorter optimization timesteps result in exceedingly large matrices when performing full-year, multi-building analyses, and are not examined in this study.

As noted, the ALCC ( $k_m$ ) is the most ambiguous element of the case study. To address this uncertainty, we iteratively solve the optimization using progressively increasing values for ALCC. We begin with a minimum  $k_m$  of \$50 per UTSS per year, which makes the thermal storage essentially free to procure and operate. We then increment the value of  $k_m$  by \$50 and re-solve, repeating the process until we reach the point where the UTSS cost becomes prohibitive, and the optimized solution returns no thermal storage.

## 6.6 Results and discussion

### 6.6.1 Minimum annual cost

The optimization model solved in ~1.3 hours to a minimum annual cost of \$234,980 with 21 UTSS distributed across 11 of the 17 RTUs in five of the seven buildings. This provides \$12,420 in annual savings relative to the baseline community electric bill, which equates to a 4.9% annual savings in total electricity costs and a 17.8% savings in cooling-only electricity costs – even after accounting for the added \$23,625 in annual UTSS expenses. Figure 6-5 provides cost comparison between the optimal result and the baseline for (a) total electric and (b) cooling-only electric costs. The left columns on each plot are the sum of the remaining three cost components illustrated. While most savings are found in the reduction in demand charges, the optimization provides similar relative reductions for both energy and demand charges. Total energy charges are reduced 13.8% while demand charges are reduced by 14.8%. The energy and demand charges associated with cooling-only are reduced 45.2% and 54.4%, respectively.

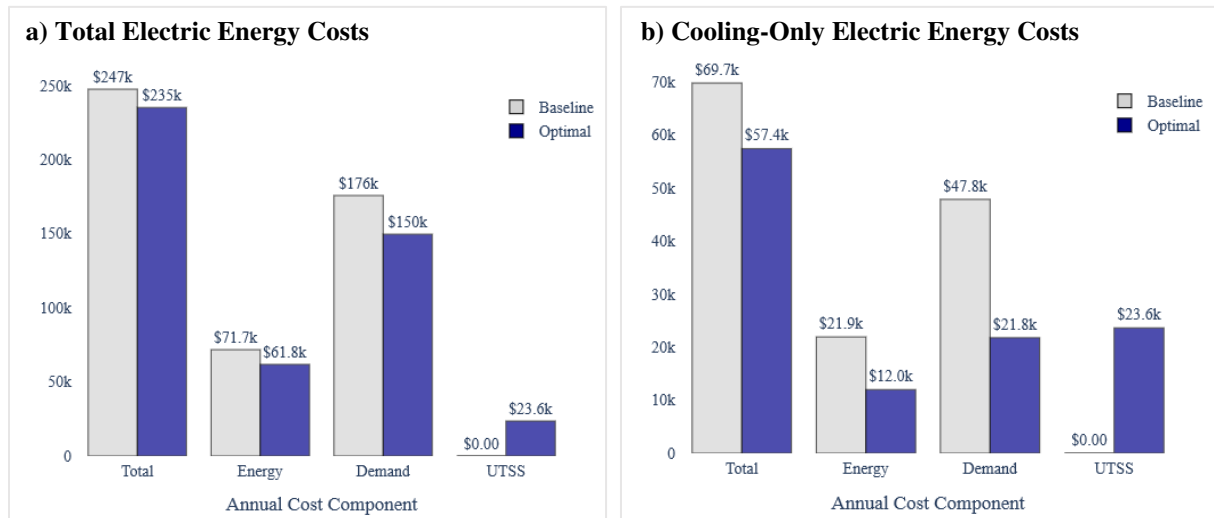


Figure 6-5: Cost comparison of the optimization program solution with baseline community energy bill. The total annual cost is the sum of the energy charges, demand charges, and ALCC for (a) [community aggregate] total electric energy costs and (b) cooling-only electric energy costs.

### 6.6.2 System design

The distribution of the 21 UTSS across the community is illustrated by Figure 6-6, where the gray bars indicate the maximum number of UTSS that can potentially be installed at a given

RTU (equal to the parameter  $m_{in}$ ), determined in pre-processing from the nominal capacities of each RTU. The blue bars are the number of UTSS installed at a given RTU. Because there was little cooling load diversity in our case study, the results generally conform to expectations, with more UTSS assigned to larger RTUs. However, not all results are intuitive. For example, RTU 17 receives thermal storage while RTU 14 does not, despite being smaller. RTU 11, which is by far the largest unit within the entire community, receives the same number of thermal storage devices as the much smaller RTU 15. The value of thermal storage is not determined solely by the magnitude of the cooling load that can be shifted at a given RTU, but also by how that load coincides with other electricity power demand across the community, and by the utility tariff.



Figure 6-6: Optimal UTSS placement by RTU, grouped by building. Each gray box depicts the maximum number of UTSS that could be assigned to given RTU, which is equivalent to the parameter  $m_{in}$ . The blue boxes depict the number and location of UTSS given by the optimized solution.

### 6.6.3 Optimal dispatch

The optimization program also provides RTU-level dispatch schedules for every UTSS within the community. Figure 6-7 shows the aggregate community electric demand profiles of

both the baseline and optimized cases for (a) the entire annual period and (b) a selected August week. In the annual demand profile comparison, the optimization response to the monthly demand charges is illustrated through the new maximum power values, most apparent during the summer months.

The optimization program also provides RTU-level dispatch schedules for every UTSS within the community. Figure 6-7 shows the aggregate community electric demand profiles of both the baseline and optimized cases for (a) the entire annual period and (b) a selected August week. In the annual demand profile comparison, the optimization response to the monthly demand charges is illustrated through the new maximum power values, most apparent during the summer months.

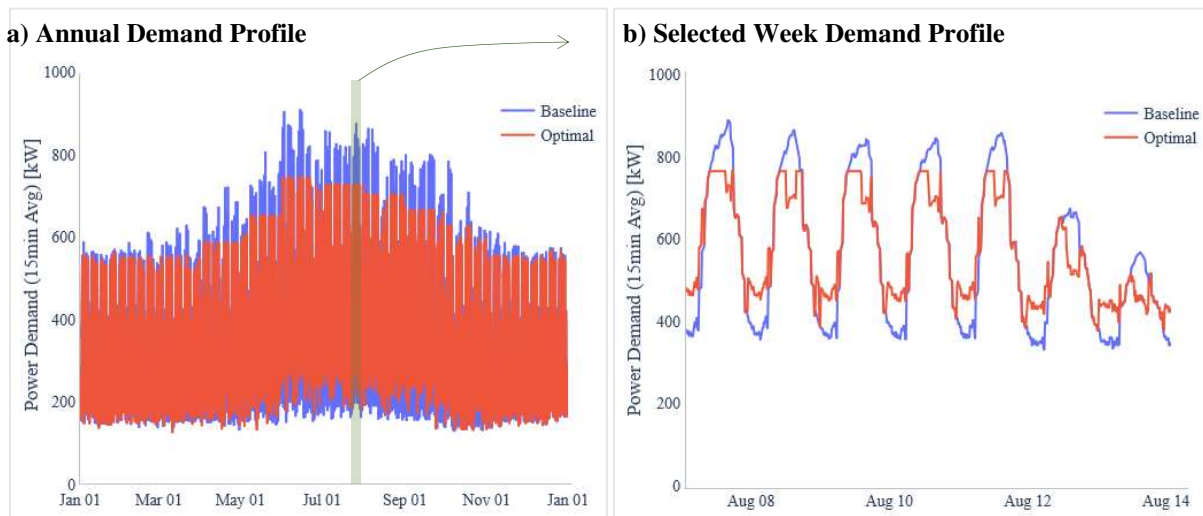


Figure 6-7: Comparison of Baseline and Optimal aggregated electric demand profiles. (a) shows the full-year profile, where optimized maximum values for each demand period  $d$  (one per month) are clearly visible. (b) shows one selected week, illustrating charge and discharge periods, as well as the optimization response to both demand charges and time-of-use energy charges.

The demand profile over the selected week of August 7-13 shows the daily performance of the optimized thermal storage relative to baseline. Here we see the response to both demand charges and time-of-use energy charges. Overnight charging does not immediately begin at the end of the day but occurs as late as possible. This maximizes charging efficiency as the ambient temperatures during early morning hours are typically lower than at late evening. It also minimizes thermal losses from the storage tank before the ice is used.

A load duration curve is the annual electric demand profile sorted from highest to lowest values. These curves provide a qualitative indication of the variation of the electric load over the course of the year. They also tell how much total time within the year that the load is above a certain value.

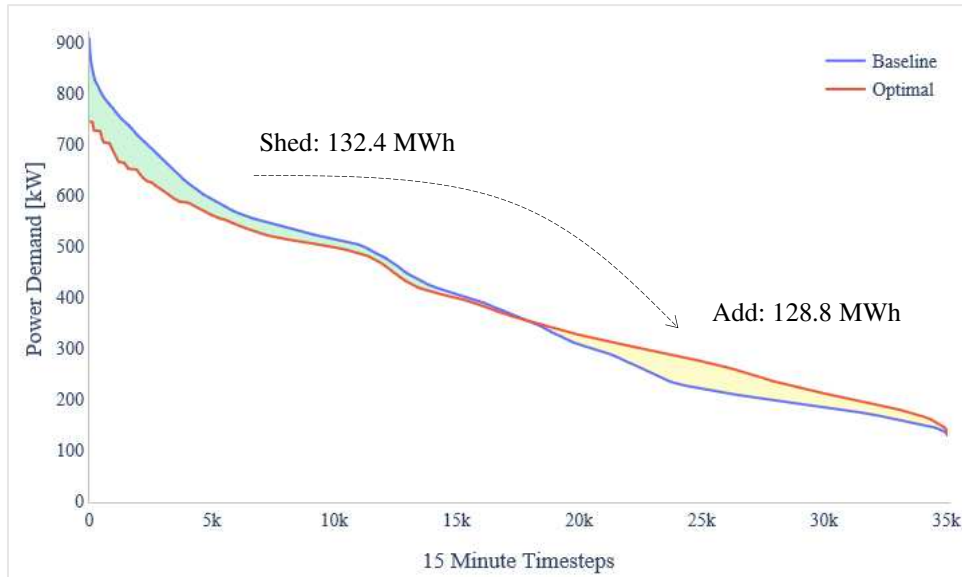


Figure 6-8: Annual load duration curve for the community aggregate power demand

Figure 6-8 presents the load duration curves for the community aggregate electric power demand for both the baseline and optimized cases. Deployment of UTSS has a flattening effect on the curve, producing a more stable load to the electric grid. It also reduces maximum annual power demand by 165 kW<sub>e</sub>. Load Shed (area between the curves when the optimal lies below the baseline) is 132.4 MWh while Load Add (area between the curves when the optimal falls above the baseline) is 128.8 MWh. Thus, the load shift efficiency ( $\eta_{shift}$ ), is 1.028. This decrease in annual energy use relative to baseline is achieved by the optimized control, which charges at times of maximum efficiency, rather than following a simple schedule-based charging signal. However,  $\eta_{shift}$  is highly dependent on the relative efficiencies of the ice-making compressor within the UTSS and the baseline cooling equipment. It is also a function of ambient weather and building thermal zone conditions. Because our location experiences large diurnal temperature swings, conditions are favorable for off-peak ice-making. The optimization formulation is not written to maximize energy efficiency, but rather to minimize total cost. Given a different set of

buildings in a different climate zone,  $\eta_{shift}$  may not exceed 1, especially if the electricity tariff promotes daytime ice charging.

Figure 6-9 shows the dispatch control signals for (a) each UTSS at its associated RTU for the whole year and for (b) the UTSS at RTUs 3 and 10 for the selected week of August 7-13. All values are normalized against the maximum rates of charging and discharging for each RTU. Positive values indicate charging; negative values indicate discharging. Individual UTSS dispatch signals reveal three insights into the charging rates, discharging rates, and seasonal importance of thermal storage. Figure 6-9a show all UTSS predominantly charge at the maximum possible rate. Unlike central chiller-ice plants which experience improved efficiency when ice charging rates are limited [38], the particular characteristics of UTSS encourage charging as quickly as possible when ambient conditions are favorable.

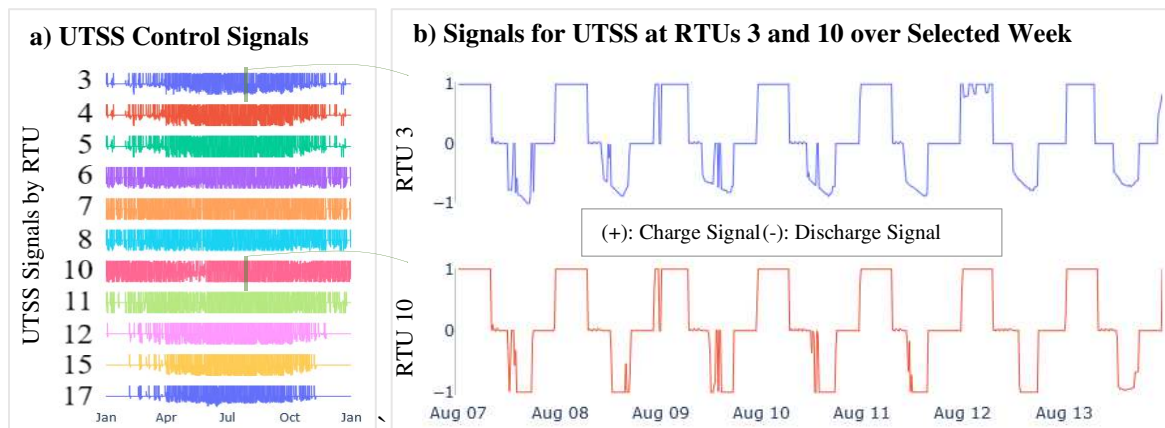


Figure 6-9: Control signals for each UTSS at their respective RTUs. Positive values are charging signals; negative values are discharging signals. All values are normalized against the appropriate maximum rate of heat transfer at each RTU and timestep ( $Z_{in} \cdot \bar{q}_{int}^X$  or  $Z_{in} \cdot \bar{q}_{int}^Y$ ). (a) shows all the UTSS signals for the entire year. (b) shows the dispatch signals for RTUs 3 and 10 for a selected August week.

Conversely, full-year profiles show discharging rates are often not at maximum values. Figure 6-9b shows UTSS at RTU 10 is discharged generally at its maximum rate, but over a narrower average daily window compared to RTU 3. The UTSS at RTU 3, which is much smaller, discharges at a limited rate over a longer period each day. An interesting observation emerges from these two examples: the larger RTU with more thermal storage is dispatched primarily during the on-peak hours of 12:00-18:00, when TOU charges are highest and peak

demand occurs. The storage at the smaller RTU is dispatched more slowly over the course of the day, providing a demand shaving role during both on-peak and off-peak hours. The requisite data analysis to confirm if this dispatch trend applies generally exceeds the scope of our present study.

#### 6.6.4 Sensitivity results

##### 6.6.4.1 Median UTSS state-of-charge

Changing the assumption for median UTSS state-of-charge does not alter the integer solution, nor does it appreciably change the linear solutions for charging and discharging. Variation in the optimization result is negligible between  $\tilde{s}_1$  values of 0.95 and 0.05, with minimum annual cost decreasing from \$235,076 to \$234,938, or a 0.04% change. All this change is manifest in the energy charges, with demand charges remaining constant between solutions. Furthermore, the change in energy charges is most significant at lower  $\tilde{s}_1$  values. The total change in cost between 0.95 and 0.55, the value we used in this case study, was only \$22 annually.

However, despite the negligible impact on optimized minimum cost, we find the value of  $\tilde{s}_1$  to be significant in determining overall system efficiency. Increasing  $\tilde{s}_1$  from 0.55 to 0.95 results in a reduction in  $\eta_{shift}$  from 1.028 to 0.995. Decreasing  $\tilde{s}_1$  from 0.55 to 0.05 results in a much higher  $\eta_{shift}$  of 1.14. This substantial increase in round-trip electric efficiency at lower  $\tilde{s}_1$  occurs because the calculated maximum rates and efficiencies for charging are higher at very low states-of-charge. Thus, the optimization can charge the tank more quickly at the times of highest efficiency.

Upon close examination of the UTSS charging efficiency curve, Equation 3, we find that COP for charging decreases linearly as state-of-charge increases from 0.15 to 0.95. However, when  $\tilde{s}_1 < 0.15$ , charging efficiency spikes. When normalized against our demonstration case assumption of  $\tilde{s}_1 = 0.55$ , the relative COP varies as shown in Figure 6-10. So long as ice tank state-of-charge is maintained above 0.15, the efficiency for ice charging varies by  $\pm 2\%$ ;

however, below that range, relative efficiency increases by  $>7\%$ . This, compounded with the increased charging capacity associated with lower states-of-charge, explains the exceedingly high load shift efficiency value obtained when optimizing with  $\tilde{s}_1 = 0.05$ .

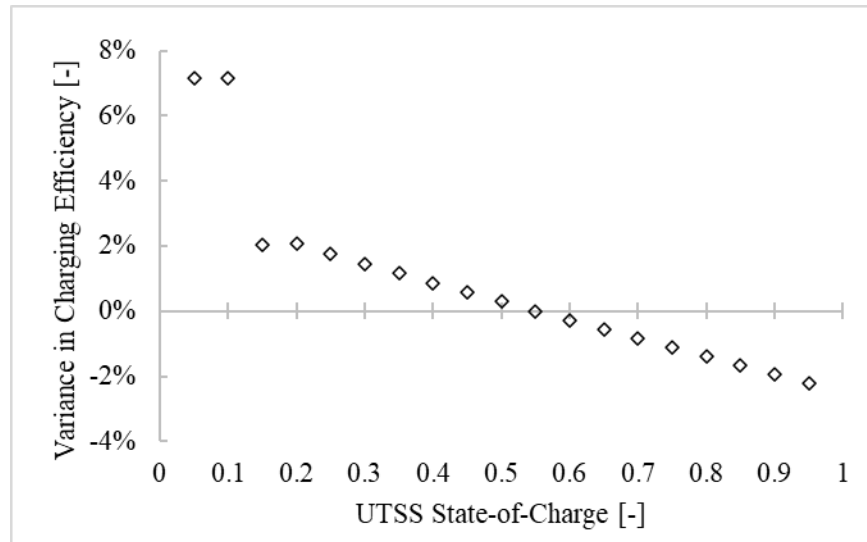


Figure 6-10: Variance in charging efficiency ( $COP_{ir}^x$ ) as a function of ice tank state-of-charge ( $\tilde{s}_1$ ) normalized against  $\tilde{s}_1 = 0.55$ , the value used in our demonstration optimization

Because the impacts of the  $\tilde{s}_1$  assumption are manifest in both charging and discharging, and off-peak energy costs are quite low, the total optimization results are essentially unchanged. However, the energy efficiency results vary significantly, especially at  $\tilde{s}_1$  values below 0.15. In our demonstration case, we partially mitigate this by reducing each UTSS nominal capacity to a usable capacity, and benefit from the fact that most of the time the UTSS states-of-charge are well above 15%. Nevertheless, the median state-of-charge assumption is significant, and can lead to an over-estimation of the electrical efficiency of the optimal design.

#### 6.6.4.2 Optimization timestep

Table 6-6 shows the capacity-normalized sensitivity results calculated using different optimization timesteps, with 15-minutes as the reference case. Though the building simulation timestep remains fixed at 1-minute, as optimization timestep changes from 15 to 30 to 60 minutes, the total number of UTSS in the solution increases. Energy charges do not vary as

timestep increases, but the maximum values for peak demand are somewhat reduced by the smoothing effect of the longer averaging window. This causes an increase in importance of energy charges relative to demand charges. The relative savings achieved by the optimization decreases by the values shown in Table 6-6. This confirms that the MILP is sensitive to the optimization timestep independent of the building energy simulation timestep, and should be set equal to the value required to accurately calculate the electricity bill.

Table 6-6: Comparison of results using different optimization timesteps

Optimization Timestep	Optimal Number of UTSS	Relative Change in Cost Savings
15 min	21	Reference
30 min	22	-3.1%
60 min	23	-5.6%

#### 6.6.4.3 Annualized life-cycle cost estimate

The parametric sweep over the full range of possible ALCC values provides insight into the potential maximum impact of using distributed UTSS within the community, and it reveals RTU prioritization for UTSS integration. Figure 6-11 shows the minimum annual cost results for 42 optimization runs with the ALCC ( $k_{in}$ ) ranging from \$50 to \$2150 per device per year. The red dashed line is the maximum possible cost from the optimization, which is equal to the baseline annual energy bill of \$247,400. The green dashed line is the minimum possible cost if (1) all cooling electric energy is purchased at off-peak rates and dispatched assuming  $\eta_{shift} = 1$ , and (2) demand charges are dictated only by non-cooling loads. For our community, this value is \$180,600, which represents a 29.7% potential reduction in the total annual electric bill. As the ALCC increases, the total number of UTSS procured decreases, shown by the blue diamonds in Figure 6-11b. When  $k_{in}$  exceeds \$2150 per device per year, the optimization determines thermal storage to be too expensive and returns the baseline, no-storage case.

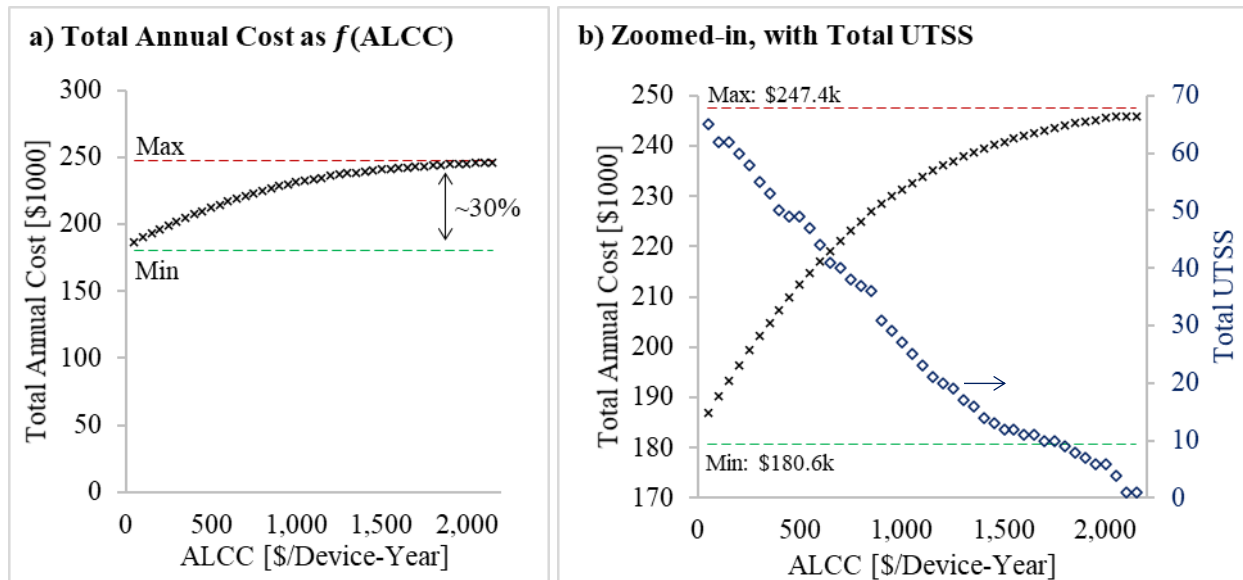


Figure 6-11: Optimization results as a function of ALCC, bounded by the baseline annual energy bill (Max) in red and the minimum possible energy bill (Min) in green. (a) Total annual cost shown at full scale relative to the energy bill, illustrating a potential 29.7% savings. (b) Zoomed-in results with the total number of UTSS determined by the optimization plotted on the secondary axis.

This parametric sweep also provides information on the relative priority of each RTU for receiving thermal storage. Figure 6-12 shows the total number of UTSS procured as a function of ALCC but broken out by RTU assignment. Moving from right-to-left on Figure 6-12 identifies the price point at which each UTSS is added at a given RTU. For example, we see that RTU 15 (light gray, near the top) should be the first one to receive UTSS at an annualized cost of \$2,100, while RTU 16 in the same building (yellow, top) should not receive UTSS until the price drops below \$1,100 per device per year. Similarly, RTU 10 (gold, middle) should be prioritized over RTU 11 (blue, middle), even though both are in the same building and RTU 11 is larger.

On a shared machine this parametric sweep of 42 complete optimization runs took approximately 63 hours using 15-minute optimization timesteps, but only 4.5 hours using 60-minute timesteps (with somewhat different results, as discussed above). As this type of analysis is strategic in scope and belongs early in a new construction or retrofit design process, we find the insight that it provides for UTSS placement priorities to be well worth the computer run time.

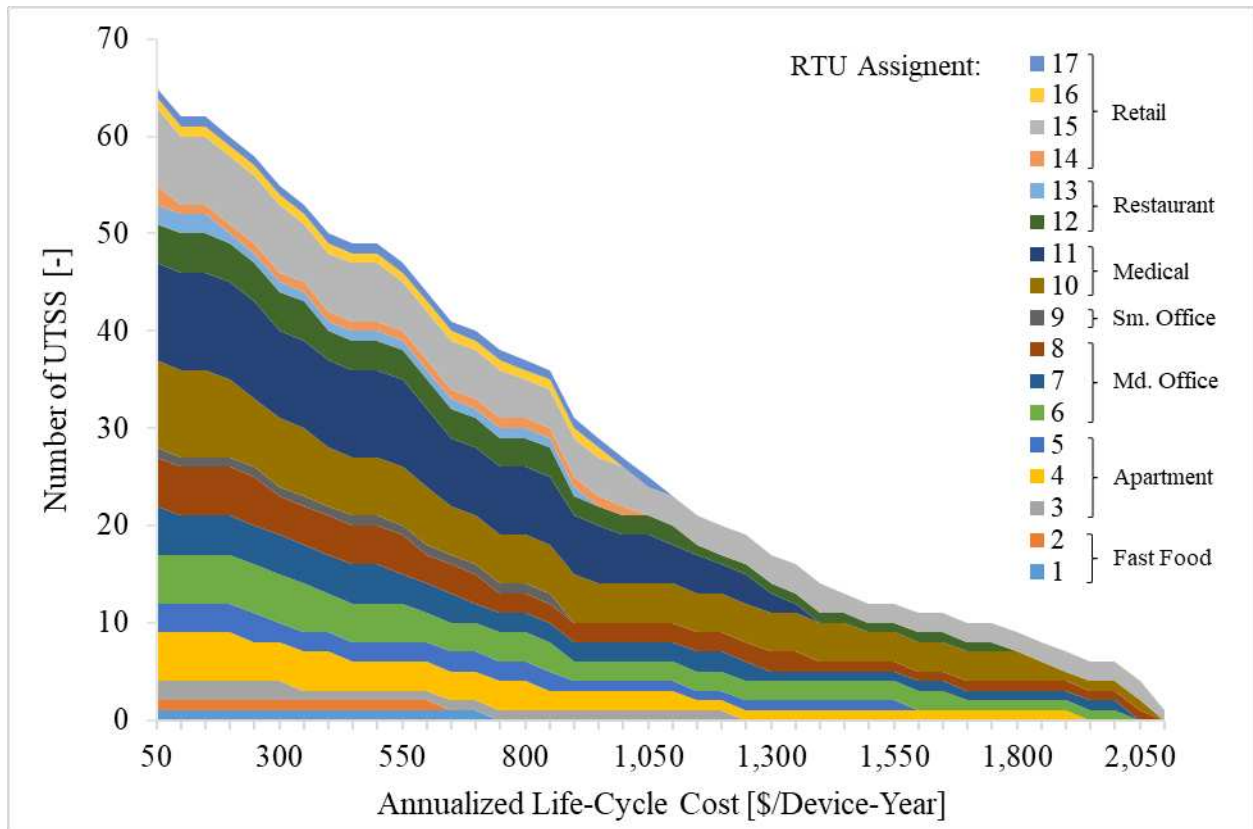


Figure 6-12: Total number of UTSS determined by the optimization, divided by RTU assignment, as a function of annualized life-cycle cost of the UTSS

## 6.7 Utility of the community optimization approach

This optimization workflow is designed to be highly scalable, equally applicable to a single building with a single RTU or to a multitude of buildings with many RTUs. As the community increases in size the number of variables also necessarily increases. To retain problem tractability without modifying the formulation as the problem size grows, the optimization timestep may be lengthened, with the noted loss in solution fidelity, discussed previously. Other methods, such as reducing the optimization horizon ( $\mathcal{T}$ ) from the full-year to a shorter operating season, aggregation of similar HVAC systems/loads across the community, or using a multi-step optimization which dissociates the design and dispatch aspects may also be useful; however, they are not assessed within this paper.

Considering the large size of a multi-building HVAC optimization problem, one may question the value of this aggregated approach. To demonstrate the utility of our approach, we

apply the optimization individually for each of the seven buildings in our demonstration case, aggregate those individual results, and compare them with our connected community optimization. The significant differences in the results for each approach illustrate the value of our method, despite the additional computation time required by the solver.

Table 6-7: Comparison between community and individual building optimization approaches

Optimization Approach	Total UTSS	Baseline Annual Cost	Optimal Annual Cost	Relative Savings	Solve Time
Community	21	\$247,404	\$235,054	5.0%	85 min
Individual Building	19	\$253,294	\$243,987	3.7%	25 min

Table 6-7 shows a few of the differences in the optimization results obtained between the two methods. It is important to note that the value of the baseline energy bill is lower for the community approach due to the difference in demand charges assessed by the two methods. Nevertheless, even though it is optimizing against a lower baseline energy bill, the community approach can capitalize on the diversity in building loads to obtain greater relative (and absolute) annual savings. If only the energy bills are considered (excluding hardware costs), the community optimization produces a savings of \$35,975 (14.5%) vs. \$30,682 (12.1%) for the aggregated individual building optimizations. The individual building approach results in fewer total UTSS installed, and it places them differently than the community approach does. RTUs 3, 6, 11, and 12 receive one fewer UTSS each; and RTUs 9 and 10 each receive one additional UTSS. This results in less overall storage placed in the Midrise Apartment, the Medium Office, and the Restaurant with the individual optimization approach. Surprisingly, the Small Office receives storage under the individual optimization, which it does not when using the community approach. While the solution time is ~3.5 times greater than that required for an individual building optimization approach, the community approach produces different design and dispatch results for greater cost savings.

## 6.8 Conclusions

We present a new simulation-optimization workflow that employs building energy modeling software and a mixed-integer linear program to optimally design and dispatch ice-based unitary thermal storage systems within connected communities. The workflow is modular and allows for any BEM or optimization solver to be used. The UTSS regression model is extracted from the EnergyPlus source code and placed into a separate Python script, allowing for custom tuning, should sufficient data be available. This workflow is useful in evaluating the economic potential of packaged ice storage systems within the GEB context and is scalable from a single building to large communities.

We demonstrate the workflow using a seven-building case study in El Paso, TX, with 17 RTUs at which UTSS might be placed. Using realistic electric rates and capital costs, our optimization workflow finds an optimal distribution of 21 UTSS across 11 of the available RTUs in five buildings. Annualized expenditures for the UTSS are \$23,625, but energy bill savings are \$36,045, resulting in a net annual savings of \$12,420 across the district. Cooling-only electricity costs are reduced 51.6%, excluding UTSS costs, compared to baseline through the optimized dispatch. Including the hardware costs, the cooling-only energy savings remain quite substantial at 17.8% annually.

To assess the validity of our workflow assumptions, we perform three small parametric studies. We find the median UTSS SOC parameter ( $\tilde{S}_i$ ) to be insignificant in affecting the optimized design or dispatch, but it does affect any whole system efficiency calculations made during post-processing. The optimization timestep ( $\mathcal{D}$ ) is significant, independent of the building simulation timestep, and should be set at a value adequate for accurate energy bill calculations. We also perform a broad sweep over the full range of possible ALCC values ( $k_{in}$ ) and examine the design results as a function of cost.

Based on the analyzed community, we conclude that the design and dispatch of UTSS at the community scale out-performs individual building optimization by taking advantage of the load diversity across multiple buildings. In our demonstration case, the optimal design produces 5% savings in the annual energy bill, after accounting for UTSS hardware costs, which compares favorably to only 3.7% savings obtained using an individual building approach. If hardware costs

are excluded, the community optimization produced an annual savings of 14.5% vs. 12.1% when using an individual building approach.

Future work associated with this project includes adding a re-simulation step following the optimization to evaluate the UTSS design and dispatch signals within the building energy modeling platform. This will capture the building-specific non-linear effects that are not captured in our MILP. Additionally, this approach is based on known weather inputs, and is therefore useful for early design analysis and the development of heuristic control strategies. Additional data analysis to develop these heuristic controls for UTSS operating dynamically throughout the day should be performed. The utility of the optimization model for business-case analyses could benefit by reformulating the objective to be a function of required payback period instead of annualized capital cost. Finally, future analyses would benefit from more thoroughly validated UTSS models, especially ones that capture partial charging and discharging operation. We hope that our workflow provides a useful starting place in helping answer how packaged cool thermal storage should be distributed and controlled in the GEB future.

## **6.9 Acknowledgements**

We would like to acknowledge the National Renewable Energy Laboratory for funding this research through the Alliance Partner University Program contract number UGA-0-41025-152. We would also like to thank Dr. Alexandra Newman of Colorado School of Mines for her contributions to improve our optimization program formulation.

## CHAPTER 7

### DESIGN AND DISPATCH OF CENTRAL ICE STORAGE SYSTEMS ACROSS MULTIPLE CHILLED WATER PLANTS

The previous chapter presents half of the integrated simulation-optimization workflow; what remains is to apply the optimization to central chilled water plants that may exist within the connected community. However, as noted in §6.4.5, the unitary thermal storage system (UTSS) program assumes that cooling load modulation on the rooftop unit (RTU) is met by cycling the compressor. This assumption is inappropriate for central chilled water plants, as chiller efficiency is variable and non-linearly related to both the ambient conditions and the cooling load being met. This chapter develops a method to use the same chiller performance curves used in building energy simulation within the optimization program.

#### **7.1 Methodology for central CTES simulation-optimization**

The optimization program for central cool thermal energy storage program has the same objective as the distributed UTSS program (see §6.4.4), and functions in a similar manner by deviating from the baseline chiller performance via charging or discharging, where the baseline performance is obtained from the building energy simulation. However, chiller and ice tank performance parameters are calculated differently (§6.2.1 and §6.2.2) and the optimization formulation requires modification (§7.4). A mixed-integer linear program (MILP) is retained for relatively fast workflow execution. The formulation is further improved by adding a demand-response (DR) cost to the objective function, which applies separate financial penalties associated with special periods when electrical load reduction is required by the utility.

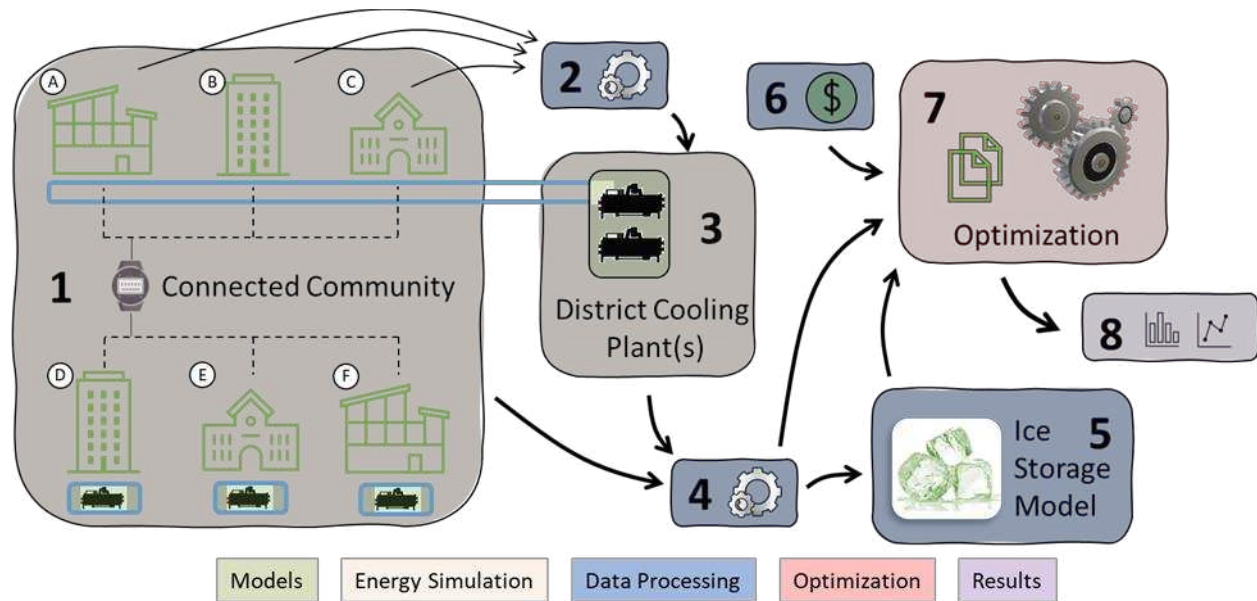


Figure 7-1: Simulation-optimization workflow for ice thermal storage in a connected community with multiple chilled-water loops. To illustrate the workflow capabilities, buildings A, B, and C are shown thermally connected to a district cooling plant; buildings D, E, and F, each have their own chiller(s). The bold numbers serve as references for further discussion the text.

The workflow illustrated in Figure 7-1 optimizes ice thermal storage design and dispatch for any centrally-metered collection of buildings that use chilled water loops for space cooling. The buildings may be thermally connected to a district cooling plant, or they may have their own chillers. In the figure, the various models for buildings, plants, ice storage, cost, and optimization are highlighted in green. Energy simulation steps are highlighted in pink; data processing steps are shown in blue; optimization is highlighted in red; and results are indicated by purple. The workflow is managed via a series of Python scripts which handle all aspects of the workflow except the optimization performed in step 7. A common weather data file containing ambient wet-bulb and dry-bulb temperatures for a one-year period is required for all steps of the workflow, which are described below.

**Step 1:** Building energy simulation. The first step of the workflow is to simulate each individual building within the community to obtain the building energy use and cooling loads over the entire year. If a building contains its own chillers, the energy and performance data from each chiller is also captured in this step. If a building is connected to a district loop, its contribution to the district cooling load is stored and

used as an input for the district cooling plant calculations in step 2. In our workflow, all building simulations are performed using OpenStudio version 3.2 [122]. To facilitate the capturing of chiller performance data, we write and apply a custom measure (script) to each building that extracts the chiller performance curves and specifications from the building model. This allows the later optimization to use the same chiller performance models used in the original building energy simulation for greater accuracy. The measure is also used in the plant loop simulations performed in step 3.

- Step 2: District cooling plant load calculation. For buildings that are connected to a district cooling plant, additional processing and simulation steps are required. Within the workflow, users may specify what buildings are connected to each plant loop through a simple csv file. The script then aggregates the required cooling and chilled water mass flow rates for all buildings within each assigned district and generates schedule files to be used by the plant loop simulation in step 3. This aggregation does not account for any thermal losses in the distribution network, which must be handled separately in the plant loop simulations.
- Step 3: District cooling plant simulation. Plant loop simulations are also performed using OpenStudio. A separate model is required for each district cooling plant. A series of custom measures are used to automatically read-in the required cooling and mass flow rates generated in step 2. The simulation generates timeseries data for chiller and pump electricity use over the course of the year.
- Step 4: Building and chiller parameter calculation. This step of workflow takes the timeseries data output by the building energy simulation engine and calculates the following parameters required by the optimization program at each optimization timestep: total building electricity use, cooling rate provided by each chiller, chiller electricity use. The potential to reduce or increase electricity use as a function of changing the chiller operating point (for either ice charging or discharging), as well as the maximum rate of ice charging, are also calculated for each timestep. The specific methodology for these calculations is discussed in §7.2.
- Step 5: Ice thermal energy storage parameter calculation. From the ice thermal energy storage model, we require a maximum rate of charging and a maximum rate of

discharging at each timestep. These values are dependent on the return water temperature and the available cooling capacity more than any existing cooling load for each chiller at each timestep. The equations used to derive these values are presented in §7.3.

- Step 6: Creating utility rates with flexibility drivers. The optimal solution for ice storage system design is driven primarily by the cost parameters. An annualized cost of thermal storage in units of \$/device-year and an electric utility rate are required. The utility rate may contain any combination of demand periods and time-of-use variations, though tiered utility rates will require additional constraints when executing the optimization. The workflow can also be used with non-monetary units for cost, but an equivalent price for the thermal storage would be required to provide meaningful results.
- Step 7: Mathematical optimization via mixed-integer linear programming. A thermal storage system design and dispatch that produces a minimum annual cost is obtained through a MILP. A linear program is used to obtain rapid solution times and ensure problem tractability. The mathematical optimization model is written as a set of text files and executed within AMPL software [123]. AMPL manages the data communication with the solver, which may be any integer-linear solver to which the user has licensed access.
- Step 8: Post-process results. The results from the optimization workflow are a minimum-annual-cost design and dispatch schedule of ice thermal energy storage tanks at each cooling plant in the community. The step is managed by Python script which generates convenient data summaries and figures.

## **7.2 Chiller performance model**

The optimization program requires several pieces of information from each chiller at each timestep in order to dispatch the thermal storage: (1) the electrical energy reduction that corresponds to any thermal load reduction, which occurs during ice discharge; (2) the electrical energy increase that corresponds to the chiller operating at the ice-tank charging temperature; (3) the minimum part-load ratio (PLR) of the chiller; and (4) the available capacity of each chiller to make ice while simultaneously meeting existing cooling loads. Using these pieces of

information, the MILP will select one of four operating modes for each chiller within the community:

1. Bypass: This operating mode retains existing chiller performance and bypasses any thermal storage that is installed on the plant loop.
2. Charging: The chiller evaporator outlet temperature setpoint is changed to a user-defined ice-charging temperature. The chiller nominal capacity is de-rated according to its associated performance curves. Any capacity above existing cooling loads is then available for CTES charging.
3. Full-storage discharge: In this mode, the chiller is completely bypassed, and the full cooling load is met by the thermal storage.
4. Partial-storage discharge: The chiller evaporator outlet temperature setpoint is elevated above the supply water temperature setpoint. The thermal storage is discharged to reduce the fluid temperature down to the supply water temperature setpoint. This mode only applies above the minimum (PLR) of the chiller.

The optimization program assumes a storage-downstream configuration with the ice-tank placed in series with the chillers, as illustrated by Figure 7-2. This generally provides higher chiller efficiency relative to a storage-upstream configuration, due to the lower temperature lift requirements placed on the chiller when operating under partial-storage control, and is a common design used by the CTES industry [17, 124].

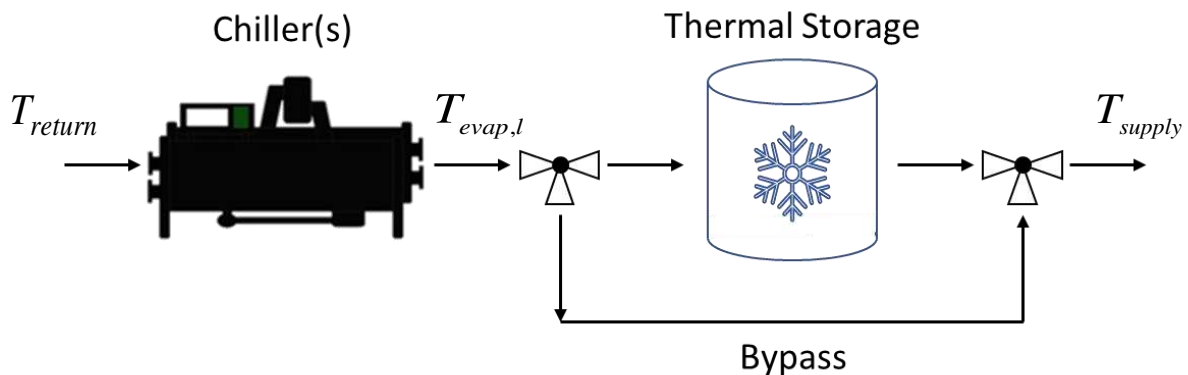


Figure 7-2: Assumed chiller-storage configuration with return, evaporator-leaving, and supply temperatures indicated

### 7.2.1 Getting the chiller performance models from building energy simulation

The workflow requires details about each chiller that are typically not present in building energy simulation outputs. While working fluid temperatures, chiller electricity use, and the cooling rate of the evaporator are easily accessed as simulation outputs, the performance curve coefficients will not be provided without explicit instruction before the energy simulation is run. To ensure all outputs are fully accessible to the optimization pre-processor, an OpenStudio measure is used [125]. The complete code for this measure is available online as noted in APPENDIX B. Timeseries outputs are added to the EnergyPlus simulation output file (.eso); static values are written to chiller-specific text files.

The workflow automatically handles air-cooled and water-cooled chillers, so long as their performance is modeled as a function of the temperature of the fluid leaving the evaporator and the temperature of the fluid entering the condenser. In the EnergyPlus simulation engine, this is referred to as the Chiller:Electric:EIR model, and originated with the DOE-2 energy simulation tool [39]. Performance curves are experimentally derived and are unique to each mode, though typical curves for various chiller types have been developed and are available in standard libraries [114]. Above the minimum PLR, equations (7-1) to (7-5) are used to compute the electric power used by the chiller to meet a given thermal load ( $\dot{q}_{load}$ ), where  $\dot{q}_{ref}$  is the reference cooling capacity,  $\dot{q}_{avail}$  is the cooling capacity available at specific operating conditions,  $COP_{ref}$  is the reference coefficient of performance,  $CAP(temp)$  is a capacity multiplier that is a function of temperatures,  $EIR(temp)$  is the energy-input-to-cooling-output ratio multiplier as a function of temperatures,  $EIR(PLR)$  is the energy-input-to-capacity-output multiplier as a function of chiller part-load ratio,  $T_{evap,l}$  is the temperature of the fluid leaving the evaporator,  $T_{cond,e}$  is the temperature of the fluid entering the condenser, and  $c_x$  are chiller-specific coefficients.

$$Chiller\ Power = \frac{\dot{q}_{ref}}{COP_{ref}} \cdot CAP(temp) \cdot EIR(temp) \cdot EIR(PLR) \quad (7-1)$$

$$CAP(temp) = c_1 + c_2 \cdot T_{evap,l} + c_3 \cdot T_{evap,l}^2 + c_4 \cdot T_{cond,e} + c_5 \cdot T_{cond,e}^2 + c_6 \cdot T_{evap,l} \cdot T_{cond,e} \quad (7-2)$$

$$EIR(temp) = c_7 + c_8 \cdot T_{evap,l} + c_9 \cdot T_{evap,l}^2 + c_{10} \cdot T_{cond,e} + c_{11} \cdot T_{cond,e}^2 + c_{12} \cdot T_{evap,l} \cdot T_{cond,e} \quad (7-3)$$

$$EIR(PLR) = c_{13} + c_{14} \cdot PLR + c_{15} \cdot PLR^2 \quad (7-4)$$

$$PLR = \frac{\dot{q}_{load}}{\dot{q}_{avail}} = \frac{\dot{q}_{load}}{\dot{q}_{ref} \cdot CAP(temp)} \quad (7-5)\S$$

If the chiller is water-cooled, the temperature of the fluid entering the condenser is assumed to be the ambient wet-bulb temperature. For air-cooled chillers,  $T_{cond,e}$  is assumed to be the ambient dry-bulb. Complete documentation on the Chiller:Electric:EIR model is available in the EnergyPlus Engineering Reference Manual, Section 14.3.9 [126]. If a different chiller performance model is required, the optimization program remains valid, but parameters for charging performance (§7.2.2) and discharging performance (§7.2.3) must be processed manually outside this workflow.

## 7.2.2 Charging performance

To obtain the available cooling capacity of the chiller for making ice at a given timestep ( $\dot{q}_{chg}$ ), we use equation (7-2), but adjust the temperature of the chilled water leaving the evaporator to one suitable for charging the thermal storage. Typical charging temperatures range from -9.4°C to -3.3°C (15°F to 26°F) depending on the type of ice storage system [17]. The condenser entering temperature is a constant at each timestep and is equal to the ambient temperature appropriate for the chiller type. Using these lower evaporator leaving temperatures, the available chiller cooling capacity decreases. This reduction in chiller performance is called the de-rate. Typical de-rate values are ~0.65-0.7, though they vary with chiller type and ambient conditions. Therefore, the chiller capacity for making ice is approximately 30% less than its nominal rating. In our formulation, available ice charging capacity ( $\dot{q}_{chg}$ ) can only exist if the chiller's derated available capacity ( $\dot{q}_{de-rate}$ ) at a given timestep exceeds the current cooling load ( $\dot{q}_{load}$ ), given by equation (7-6).

$$\dot{q}_{chg} = \max\{\dot{q}_{de-rate} - \dot{q}_{load}, 0\} \quad (7-6)$$

The chiller power required to make ice is calculated according to equation (7-7), where  $P_{chg}$  is the additional power that would be used by the chiller if it switched to ice-making mode,

$\tilde{P}_{chiller}$  is the chiller power required to meet the existing cooling load,  $COP_{ref}$  is the nominal coefficient of performance for the chiller, and  $EIR_{chg}$  is the value of equation (7-3) at charging conditions. It is assumed that the chiller operates at a PLR of 1 during ice charging.

$$P_{chg} = \tilde{P}_{chiller} - \left( \frac{\dot{q}_{de-rate}}{COP_{ref}} \cdot EIR_{chg} \right) \quad (7-7)$$

### 7.2.3 Discharging performance

When the ice tank is discharged, some, or all, of the cooling load on the chiller is reduced. This reduction in load results in a non-linear reduction in chiller power. To model this relationship, we generate a chiller power reduction curve for every timestep using the original plant loop simulation outputs. Because ambient conditions are held constant within each simulation timestep and the cooling demand from the building is fixed, a reduction in chiller electric power ( $\Delta P_{dcg}$ ) as a function of the reduction in cooling load is calculated solely as a function of evaporator leaving fluid temperature.

Figure 7-3 (page 103) illustrates an example chiller power reduction curve. The origin represents the chiller operating point in the baseline simulation at a specific timestep. The x-axis represents the reduction in thermal load on the chiller, achieved by elevating the temperature of the water leaving the evaporator. In the optimization program, any such reduction in chiller load must be met by discharging the ice tanks. As the chiller load is reduced, the electric power is reduced according to the line plotted. The curve is valid anywhere above the minimum PLR of the chiller. Below the minimum PLR, the curve is modified by a chiller cycling ratio to produce a linear trend towards zero cooling load.

To linearize this curve for use within our optimization MILP, we segment the curve to create piece-wise linear approximations. New parameters are introduced to capture the slope ( $\lambda_s^-$ ) and range of each segment ( $\bar{y}_s$ ), as illustrated in Figure 7-4. To ensure proper optimization execution, it is imperative that the slopes of each successive segment decrease in magnitude, this ensures that the solver shaves chiller load and power in physically correct sequence. If the slopes of each segment do not decrease, additional binary operators are required during optimization.

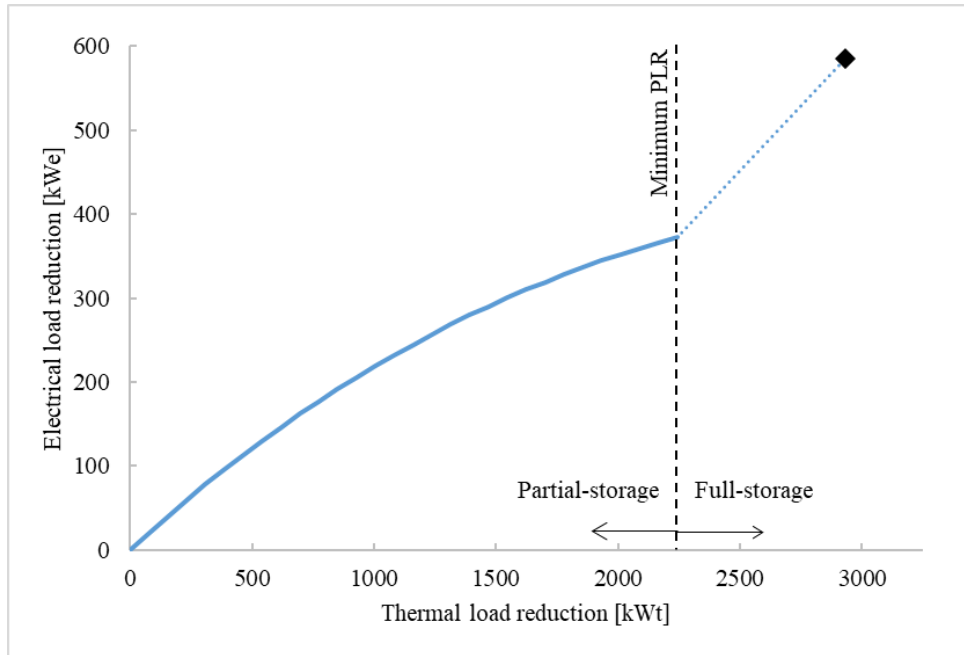


Figure 7-3: Example chiller power reduction curve with partial and full-storage regions indicated. The black diamond is the point at which the chiller is turned-off, representing the maximum possible reduction in both thermal and electrical loads for a given timestep.

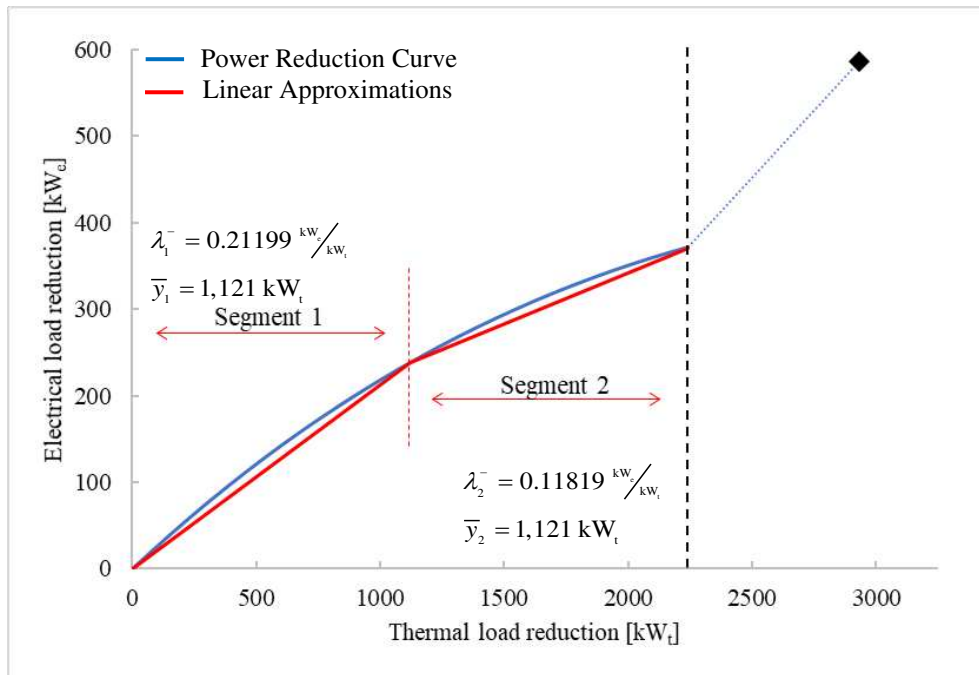


Figure 7-4: Example linearization of the chiller power reduction curve using two segments for the partial-storage region above the minimum part-load ratio.  $\lambda_s^-$  are the segment slopes and  $\bar{y}_s$  terms are the applicable ranges.

Increasing the number of segments used to approximate the chiller power reduction curve will rapidly increase the number of variables within the optimization problem. Fortunately, these are all continuous and are handled with relative ease by modern solvers such as IBM ILOG CPLEX and Gurobi [127, 128]. Nevertheless, it is useful to keep the number of segments as small as possible while still retaining a high level of accuracy. Table 7-1 summarizes the absolute and root mean squared errors of the linear approximation as a function of the number of segments for the example chiller curve shown in Figure 7-4.

Table 7-1: Linear approximation errors for the example chiller power reduction curve

No. segments	Maximum absolute error [kW <sub>e</sub> ]	Root mean squared error [kW <sub>e</sub> ]
1	54.5	39.5
2	20.9	14.7
3	7.0	4.5
4	4.2	3.1

While increasing the number of segments reduces the overall error, a balance between accuracy and solution speed must be maintained. The acceptable threshold for linearization error depends significantly on the accuracy of the underlying chiller models used within the building energy simulation. If those models are well calibrated, increasing the segmentation during this step will produce more accurate results. If generic models are used for a first-pass analysis, less resolution may be acceptable and will improve optimization solve times. Generally, using three segments provides a good balance between accuracy and speed.

### 7.3 CTES performance model

The required parameters for ice storage at each timestep are the maximum rates of charging and discharging. Except for high states-of-charge, above 90%, and low states of charge, below 15%, the maximum rate of charging and discharging can be held relatively invariant with state-of-charge for internal-melt ice-on-coil tanks [129]; therefore, we neglect this term in our parameter calculation and assume a median tank state-of-charge ( $\hat{s}$ ) of 0.55. The dominant factor in estimating the maximum heat transfer rates into and out of the tank is the maximum temperature difference (delta-T) between the tank inlet and outlet. During ice tank charging, this

delta-T is fixed. However, when discharging, the maximum delta-T is the difference between the return water temperature and the supply water temperature setpoint, which varies by cooling plant and by timestep. Using our assumed  $\tilde{s}$ , we estimate the heat transfer coefficient (i.e., UA) using a polynomial function developed by Henze and Krarti [130] and coefficients derived by King and Potter [131], given in equation (7-8);  $\bar{q}_{ice}$  is the nominal thermal storage capacity of the ice tank in GJ and the 10 in the divisor is a temperature difference normalization factor. We then solve equation (7-9) to obtain the maximum possible rate of heat transfer across the ice tank using the mass flow rate of the chiller and the nominal capacity of each tank.

$$UA \approx \frac{(1.39 - 7.63 \cdot \tilde{s} + 26.34 \cdot \tilde{s}^2 - 47.61 \cdot \tilde{s}^3 + 41.85 \cdot \tilde{s}^4 - 14.29 \cdot \tilde{s}^5)}{3600 \cdot 10 \cdot \bar{q}_{ice}} \text{ [W/K]} \quad (7-8)$$

$$\dot{q}_{ice} = UA \cdot (T_{evap,i} - T_{supply}) \text{ [W]} \quad (7-9)$$

#### 7.4 Central CTES optimization program

The equations presented so far within this chapter have not included any form of indexing. For the optimization, the parameters vary both by chiller plant and by timestep. To properly capture these dependencies in a concise manner, the nomenclature for the optimization program is revised and presented in Table 6-2 below. Parameters are defined using lower-case letters; upper-case letters are reserved for variables. Script letters are used to define sets. Superscripts are used for descriptors and subscripts are used for indexing.

Table 7-2: Notation for the central thermal energy storage optimization program

<i>Sets</i>	
$d \in \mathcal{D}$	Set of utility demand periods in the optimization horizon
$n \in \mathcal{N}$	Set of cooling plants within the community
$s \in \mathcal{S}$	Set of linear segments into which each chiller power reduction curve is divided
$t \in \mathcal{T}$	Set of all timesteps within the optimization period
$t \in \mathcal{T}_d^{\mathcal{D}}$	Indexed set of timesteps within each utility demand period $d$
$t \in \mathcal{T}^{\mathcal{R}}$	Set of timesteps during which demand response event(s) occur

Table 7-2 continued

<i>Building Simulation Parameters</i>	
$l_{nt}$	Thermal cooling load served by cooling plant $n$ at time $t$ [ $\text{kW}_t$ ]
$\tilde{p}_t$	Average total power demand for the community during timestep $t$ [ $\text{kW}_e$ ]
$\tilde{p}_{nt}^{\text{chiller}}$	Average chiller power demand to meet full cooling load at plant $n$ at time $t$ [ $\text{kW}_e$ ]
<i>Central CTES Parameters</i>	
$\eta_t^{\text{ice}}$	Ice thermal storage tank ambient-loss efficiency at time $t$ [-]
$\epsilon_n$	Electric load shed effectiveness of the ice storage installed at pant $n$ [-]
$\lambda_{nt}^+$	Coefficient for thermal storage charging at plant $n$ at time $t$ [-]
$\lambda_{nst}^-$	Coefficient for partial-storage load reduction segment $s$ at plant $n$ at time $t$ [-]
$\bar{l}_{nst}$	Maximum rate of partial-storage discharge at plant $n$ over segment $s$ at time $t$ [ $\text{kW}_t$ ]
$\dot{q}_{nt}^{+, \text{chiller}}$	Maximum available charging rate from the chillers at plant $n$ at time $t$ [ $\text{kW}_t$ ]
$\dot{q}^{+, \text{ice}}$	Nominal maximum rate of charging for each thermal storage tank [ $\text{kW}_t$ ]
$\dot{q}_t^{-, \text{ice}}$	Maximum rate of discharging for thermal storage at time $t$ [ $\text{kW}_t$ ]
$\bar{q}$	Maximum usable thermal storage capacity of each thermal storage tank [ $\text{kWh}_t$ ]
<i>Cost Parameters</i>	
$c_t^r$	Additional cost of electric energy during a demand response event at time $t$ [ $\$/\text{kWh}_e$ ]
$c_t^e$	Cost of electric energy at time $t$ [ $\$/\text{kWh}_e$ ]
$c_d^p$	Cost of maximum average electric power demand during period $d$ [ $\$/\text{kW}_e$ ]
$k_n$	Annualized cost of storage installed at plant $n$ [\\$]
<i>Miscellaneous Parameters</i>	
$\mathcal{D}$	Duration of each timestep $t$ [hr]
$\bar{z}_n$	Maximum number of thermal storage tanks that may be installed at plant $n$ [-]

Table 7-2 continued

<i>Binary and Integer Variables</i>	
$\alpha_{nt}$	Binary; 1 iff. full-storage discharge is used at plant $n$ at time $t$ [-]
$Z_n$	Number of thermal storage tanks installed at plant $n$ [-]
<i>Continuous Variables</i>	
$L_{nt}^+$	Thermal load added by charging the thermal storage at plant $n$ at time $t$ [ $\text{kW}_t$ ]
$L_{nt}^{-F}$	Thermal load reduced at plant $n$ via full-storage at time $t$ [ $\text{kW}_t$ ]
$L_{nst}^{-P}$	Thermal load reduced at plant $n$ via partial-storage over segment $s$ at time $t$ [ $\text{kW}_t$ ]
$\hat{P}_d$	Maximum aggregated power demand during period $d$ [ $\text{kW}_e$ ]
$P_t$	Total aggregated power demand at time $t$ [ $\text{kW}_e$ ]
$P_{nt}^+$	Electric power added through CTES charging by plant $n$ at time $t$ [ $\text{kW}_e$ ]
$P_{nt}^{-F}$	Electric power reduced through full-storage discharge at plant $n$ at time $t$ [ $\text{kW}_e$ ]
$P_{nt}^{-P}$	Electric power reduced through partial-storage discharge at plant $n$ at time $t$ [ $\text{kW}_e$ ]
$Q_{nt}$	Thermal storage inventory for thermal storage at plant $n$ at time $t$ [ $\text{kW}_t$ ]

#### 7.4.1 Central CTES formulation

The optimization objective is to minimize total annual cost by procuring and placing ice thermal storage tanks on any of the available plant loops within the community (design) and then dispatching those tanks in response to time-variant cost signals and special demand-response events. Our program is a MILP, with one general integer variable for each plant loop and one binary for each plant and timestep during which cooling load exists, and all other variables are continuous. The objective function in equation (7-10) contains four labeled terms: (1) annualized capital expenditure to purchase, install, and maintain the ice storage tanks at a given plant; (2) total energy costs; (3) total demand charges; and (4) total cost penalties associated with failing to mitigate energy use during demand-response events.

$$\min \left[ \sum_{n \in \mathcal{N}} k_n \cdot Z_n + \sum_{t \in \mathcal{T}} c_t^e \cdot \delta \cdot P_t + \sum_{d \in \mathcal{D}} c_d^p \cdot \hat{P}_d + \sum_{t' \in \mathcal{T}^R} c_{t'}^r \cdot \delta \cdot P_{t'} \right] \quad (7-10)$$

The minimization objective is constrained by efficiency, energy-balance, inventory, and heat-transfer limit equations. The power variables that appear in the objective function are auxiliary variables calculated from the chiller efficiency equations associated with charging and discharging the thermal storage. The total community electric power demand at each timestep ( $P_t$ ) is calculated in equation (7-11) by summing the deviations from the baseline community electric power ( $\tilde{p}_t$ ). The power increase terms ( $P_{nt}^+$ ) for ice charging are given by (7-12); and the power decrease terms ( $P_{nt}^{-F}$  and  $P_{nt}^{-P}$ ) for discharging are computed in (7-13) and (7-14). A binary term required to actuate the full-storage operating mode. Peak demand for a given period ( $\hat{P}_d$ ) is captured by equation (7-15).

$$P_t \geq \tilde{p}_t + \sum_{n \in \mathcal{N}} (P_{nt}^+ - P_{nt}^{-F} - P_{nt}^{-P}) \quad \forall \quad t \quad (7-11)$$

$$P_{nt}^+ \geq \lambda_{nt}^+ \cdot L_{nt}^+ \quad \forall \quad n, t \quad (7-12)$$

$$P_{nt}^{-F} \leq \epsilon_n \cdot \tilde{p}_{nt}^{chiller} \cdot \alpha_{nt} \quad \forall \quad n, t \quad (7-13)$$

$$P_{nt}^{-P} \leq \epsilon_n \cdot \sum_{s \in \mathcal{S}} \lambda_{nst}^- \cdot L_{nst}^- \quad \forall \quad n, t \quad (7-14)$$

$$\hat{P}_d \geq P_t \quad \forall \quad t \in \mathcal{T}_d^D \quad (7-15)$$

Heat transfer rates are limited both by the chillers and by the thermal storage devices. The maximum rate of charging is limited by equations (7-16) and (7-17).

$$L_{nt}^+ \leq \dot{q}_{nt}^{+,ice} \cdot Z_n \quad \forall \quad n, t \quad (7-16)$$

$$L_{nt}^+ \leq \dot{q}_{nt}^{+,chiller} \quad \forall \quad n, t \quad (7-17)$$

The maximum rates of heat transfer for discharging depend on the operating mode of the system, governed by equations (7-18) to (7-21). Note the use of the binary operator ( $\alpha_{nt}$ ) to toggle between the two modes.

$$L_{nt}^{-F} \leq l_{nt} \cdot \alpha_{nt} \quad \forall \quad n, t \quad (7-18)$$

$$L_{nt}^{-F} \leq \dot{q}_t^{-,ice} \cdot Z_n \quad \forall \quad n, t \quad (7-19)$$

$$L_{nst}^{-P} \leq (1 - \alpha_{nt}) \cdot \bar{l}_{nst} \quad \forall \quad n, s, t \quad (7-20)$$

$$\sum_{s \in \mathcal{S}} L_{nst}^{-P} \leq \dot{q}_t^{-,ice} \cdot Z_n \quad \forall \quad n, t \quad (7-21)$$

Inventory balance is maintained by equation (7-22), limited by the total installed storage capacity in (7-23), and used to restrict the maximum rates of discharging in (7-24) and (7-25).

$$Q_{nt} = \eta_t^{ice} \cdot Q_{n,t-1} + \delta \cdot (L_{n,t-1}^+ - L_{n,t-1}^{-F} - \sum_{s \in \mathcal{S}} L_{ns,t-1}^{-P}) \quad \forall \quad n, t > 1 \quad (7-22)$$

$$Q_{nt} \leq \bar{q} \cdot Z_n \quad \forall \quad n, t \quad (7-23)$$

$$\delta \cdot L_{nt}^{-F} \leq Q_{nt} \quad \forall \quad n, t \quad (7-24)$$

$$\delta \cdot \sum_{s \in \mathcal{S}} L_{nst}^{-P} \leq Q_{nt} \quad \forall \quad n, t \quad (7-25)$$

The formulation is completed by adding a constraint to initialize the state-of-charge of each newly installed storage as empty (7-26), and to enforce non-negativity (7-27), integrality (7-28), and binary (7-29) constraints.

$$Q_{n0} = 0 \quad \forall \quad n \quad (7-26)$$

$$L_{nt}^+, L_{nt}^{-F}, L_{nst}^{-P}, P_t, P_{nt}^+, P_{nt}^{-F}, P_{nst}^{-P}, \hat{P}_d, Q_{nt} \geq 0 \quad \forall \quad d, n, s, t \quad (7-27)$$

$$0 \leq Z_n \leq \bar{z}_n, \text{ integral} \quad \forall \quad n \quad (7-28)$$

$$\alpha_{nt} \text{ binary} \quad \forall \quad n, t \quad (7-29)$$

The equations above are written such that both full-storage and partial-storage are available to the solver at every timestep. This is generally not the case, as often chillers operate on both seasonal and diurnal schedules. Additionally, it is likely that operators may wish to exclude full-storage operation during certain times of the day. To restrict the timesteps when certain operating modes are permitted, we introduce two indexed sets defined in Table 6-3. These indexed sets are applied at optimization run-time and greatly improve the solver performance, especially by reducing unused binary variables. Note that partial-storage is always permitted when a cooling load exists at a plant.

Table 7-3: Indexed sets introduced to restrict available operating modes

<i>Special Indexed Sets</i>	
$t \in \mathcal{T}_n^l$	Indexed set of timesteps during which cooling loads exist at plant $n$
$t \in \mathcal{T}_n^F$	Indexed set of timesteps during which full-storage operation is available at plant $n$

#### 7.4.2 Assumptions and limitations of the central CTES program

While this workflow is designed to be flexible, capable of handling a wide variety of chiller types and multiple cooling loops, it relies on several major assumptions of which users must be aware:

1. Chiller-storage configuration is assumed to be chiller-upstream. This layout generally provides the highest-average chiller efficiency but is not appropriate for all plant designs.
2. Chiller performance is automatically modeled as a function of the fluid temperature leaving the evaporator and the fluid temperature entering the condenser. Other chiller models may be used to obtain the chiller performance parameters at each timestep, but these calculations must be performed outside the automated workflow.
3. Pumping power is not explicitly calculated. Rather, the load shed effectiveness term ( $\epsilon_n$ ) is used to account for all inefficiencies added within the plant when the storage is being discharged. This includes ancillary electrical systems and the increased pump power required to divert the working fluid through the thermal storage heat exchangers.

#### 7.5 Demonstrating the revised formulation with a two-loop campus

The Central CTES workflow is demonstrated using two chilled water plants on the Colorado School of Mines (Mines) campus, namely chiller loops 6 and 7. The remainder of this section describes the two loops in question, summarizes the energy simulation results for all the buildings and the two plant loops, presents three utility rates for examination, and explores the optimization results and implications.

### 7.5.1 Description of campus



Figure 7-5: Colorado School of Mines main campus with chiller loops 6 and 7 marked in green and red, respectively [132]

For this analysis, seven buildings on chiller loop 6 and two buildings on chiller loop 7 are simulated and calibrated against utility data for total energy use and peak electric demand in 2019. Figure 7-5 presents a map of the Mines campus with both loops indicated by colored dashed lines. Within loop 7, a calibrated building energy model was not available for the Green Center at the time of this analysis, so it is excluded from optimization set. Table 7-4 and Table 7-5 summarize the annual energy use in kWh and the peak electricity demand in kW for each building and chiller plant used in the optimization scenario.

Table 7-4: 2019 energy use data for chiller loop 6

Building/Plant	Annual Energy Use (kWh)	Peak Energy (kW)
Berthoud Hall	855,428	194
Brown Hall	2,312,792	254
CoorsTek	1,738,010	315
Elm Hall	1,671,105	360
Maple Hall	575,228	116
Weaver Towers	413,916	87
Welcome Center	378,753	125
Chiller Plant 6	1,785,936	684
Total	9,731,168	2,136

Table 7-5: 2019 energy use data for chiller loop 7, excluding the Green Center

Building/Plant	Annual Energy Use (kWh)	Peak Energy (kW)
Coolbaugh Hall	2,265,402	505
Hill Hall	3,313,395	595
Chiller Plant 7	854,254	300
Total	6,433,051	1,400

Figure 7-6 presents a comparison of the energy simulation results for electric and thermal energy use of the buildings within each chiller loop. The electric energy use for each building is obtained directly from the simulation results and used to compare against the 2019 data displayed in Table 7-4 and Table 7-5. The thermal cooling loads are aggregated and simulated according to steps 2 and 3 of the workflow, described above.

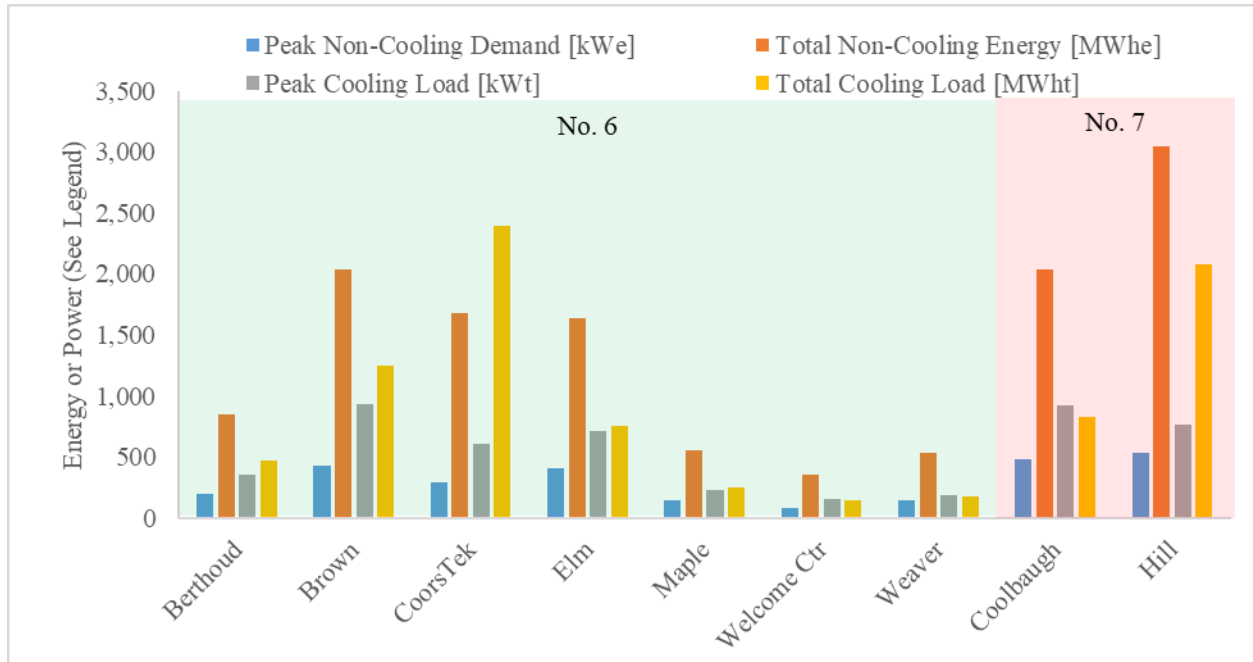


Figure 7-6: Energy use comparison between buildings on chiller loops 6 and 7, with categories for peak non-cooling electricity demand in kW<sub>e</sub> (blue), total annual non-cooling electric energy in MWh<sub>e</sub> (orange), peak thermal cooling load in kW<sub>t</sub> (gray), and total annual thermal cooling load in MWh<sub>t</sub> (yellow).

The two chiller plants serving loops 6 and 7 are simulated in OpenStudio as stand-alone models with a “LoadProfile:Plant” object added to demand the equivalent sum of the building cooling loads on the chillers. Chiller loop 6 is simulated using 647-ton York YK series chillers with a nominal COP of 6.32, provided within the EnergyPlus program [40]. Chiller loop 7 is simulated using a generic water-cooled chiller model with a nominal COP of 5.5, obtained from the OpenStudio standards library [72]. These models were selected and calibrated to match the total annual electric energy use and peak electric demand within 10% of the 2019 data. The performance curves for each of these chiller models are extracted from the simulation results and processed for optimization according to the method described in §7.2.

### 7.5.2 Ice thermal storage tanks

The ice thermal storage tanks for which these plants are optimized are CALMAC 1190C internal-melt, ice-on-coil tanks with a nominal capacity of 162 ton-hours (570 kWh) [133]. These tanks are of moderate size and have been used previously in other campus installations [100]. The freezing point of the water within the tank is assumed to be 32°F (0°C). The ice

charging temperature is set to 23°F (-5°C), and the outlet temperature of the working fluid leaving the tank is 30°F (-1°C). The cost of each tank, including installation is estimated at \$140 per ton-hour (\$39.81 per kWh<sub>t</sub>) of storage, which results in an installed cost of \$22,690 per tank [134]. Assuming a 20-year lifespan of each tank, the annualized cost ( $k_n$ ) of each tank is \$1,135. Thermal losses are estimated at 5% stored capacity lost per 24-hour period.

### 7.5.3 Interruptible service utility rates

Three rates are explored for this demonstration case. In addition to the historic 2019 utility rates, which serve as a baseline (Base Rate), two interruptible service scenarios are examined. 80-hour and 160-hour scenarios are used, during which the Mines campus must effectively disconnect from the grid and meet all electric loads internally. To facilitate this, Mines has installed a generator plant. These generators are considered sunk cost, so only the price of fuel is used to determine the cost of electricity during the service interruption periods.

Mines is billed for electricity under both energy (\$ per kWh) and demand (\$ per monthly maximum kW) charges. For 2019, the average monthly cost of electric energy varied from \$0.038 to \$0.077 per kWh, with an annual average of \$0.067 per kWh. The demand charges varied from a low of \$14.46 per kW in winter months, up to \$17.47 per kW in summer months, with an annual average of \$15.53 per kW. This is referred to as the Base Rate for this optimization scenario.

Mines simultaneously operates under an interruptible service operation contract (ISOC) with the local utility provide (i.e., Xcel Energy). Under the ISOC, the utility provides campus with an annual credit in exchange for a commitment to cease drawing power from the grid as required by the utility within 10-minutes of notification. We assume this credit is applied to the cost of the generator plant, to include capital and maintenance costs, and therefore exclude it from the optimization. To meet their electricity requirements during interruption periods, Mines turns-on their generator plant to meet any load that cannot be eliminated or shifted. In this case, we assume that the only load reduction measure applied to campus is the discharge of thermal storage. Therefore, when in an ISOC event, the cost of electrical power for campus becomes the cost of operating the on-site generator plant. Table 7-6 summarizes the fuel cost calculation for 2019.

Table 7-6: Calculating the cost of generating electricity via Mines’ diesel generators in 2019

Generator power <sup>[135]</sup>	473 kW
Approximate fuel burn rate <sup>[136]</sup>	29.61 gal/hr
Fuel per energy <sup>[137]</sup>	0.0626 gal/kWh`
Cost of fuel without road taxes <sup>[138, 139]</sup>	2.594 \$/gal
Calculated cost per energy ( $c_i^r$ )	0.1624 \$/kWh

To explore the impact of demand-response events on district thermal-storage designs, two ISOC scenarios are also optimized and evaluated. First, an 80-hour scenario using the 2019 diesel costs shown in Table 7-6; second, a 160-hour scenario with a 50% increase in fuel costs ( $c_i^r = 0.2436 \text{ } \$/_{\text{kWh}}$ ). These are subsequently referred to as ISOC80 and ISOC160+ for brevity; the “+” is used to indicate elevated fuel costs. The number of hours in each scenario corresponds to the total number of hours throughout the year during which service is interrupted. By contract, the duration of individual events may be restricted by the consumer to periods as short as 4-hours [140].

The total number of hours for service interruption are divided into 20 events selected to occur on above-average-energy-use days between June 1 and September 29. The days of interruption are kept consistent between scenarios, but for the 80-hour scenario, the four-hour period of 14:00-18:00 is used; and for the 160-hour scenario, an eight-hour period of 12:00-20:00 is used. Table 7-7 lists the dates on which service interruption events are assumed to occur.

Table 7-7: Dates of ISOC service interruption events

Month	Service Interruption Dates
June	13, 27, 28
July	3, 11, 13, 18, 19
August	3, 9, 14, 15, 19, 25, 31
September	1, 2, 5, 20, 29

## 7.6 Central CTES optimization results

The three main outputs of the optimization program are minimum annual cost, optimal design, and optimal dispatch. The Mines chiller plants are iteratively optimized for each of the three utility rates using Gurobi v. 9.0.0 solver with an absolute optimization gap of less than \$1000. This gap must be set to a value less than the annualized capital cost of each storage tank to ensure that the optimal design is accurately obtained. The optimization execution is managed through AMPL on an eight-core server running Ubuntu 18.04.5 LTS. Solutions are obtained in less than two minutes using 1-hour timesteps.

Because each utility rate has its own baseline reference with no storage installed, scenarios are compared by their potential savings and relative improvement over their respective reference cases. Table 7-8 compares the savings between the three utility rates in absolute values.

Table 7-8: Annual savings for optimized scenarios by cost component

Scenario	Net [\$]	Energy [\$]	Demand [\$]	Storage cost [\$]
Base Rate	11,066	-880	22,162	10,215
ISOC80	11,626	-39	23,014	11,350
ISOC160+	13,852	2,325	27,417	15,890

Figure 7-7 shows the relative savings after optimization for total, energy, and demand cost components for each scenario. In the Base Rate case, the flat energy charges assessed to Mines in 2019, which do not vary throughout the day, disincentivize thermal storage usage. This is because of the energy losses associated with charging and discharging the ice tanks and the lack of any cost incentive to motivate usage of the system. However, when ISOC events occur, they effectively become “on-peak” time-of-use periods during which energy is more expensive. In the ISOC80 case, the negative effect of the flat energy charge is almost completely negated; in the ISOC 160+ scenario, the demand response events dominate the flat rate, providing a significant cost incentive to purchase additional storage.

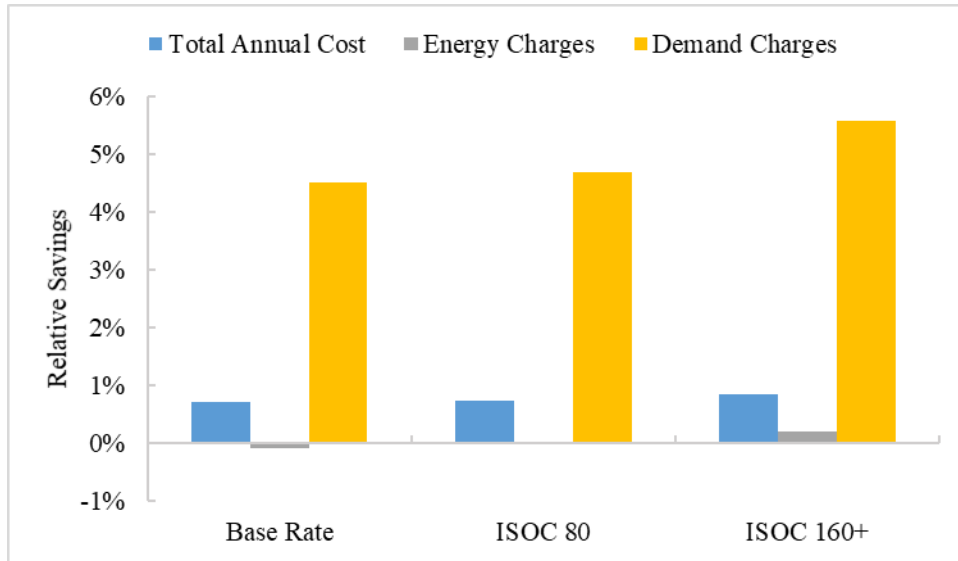


Figure 7-7: Relative annual savings for optimized scenarios by cost component

The optimal design required to achieve the cost savings presented above is given simply by the number of thermal storage tanks installed at each chiller loop, given by the values  $Z_n$  in the formulation. Figure 7-8 summarizes the optimal design by Chiller Loop for each utility rate scenario.

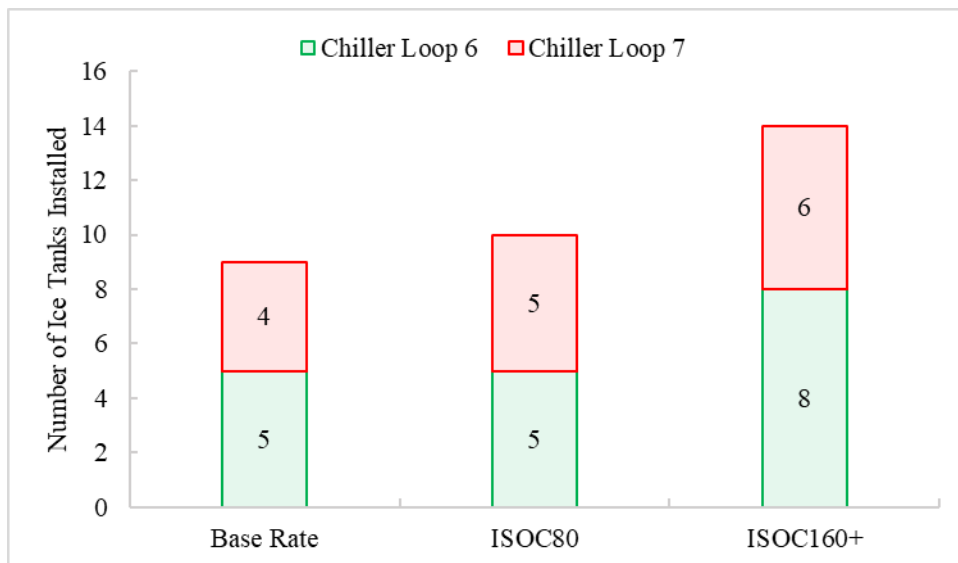


Figure 7-8: Optimal design as a function of utility rate

Using just the 2019 Base Rate, installing nine tanks provides the minimum cost solution, with five at chiller loop 6 and four at chiller loop 7. While chiller loop 6 serves approximately

twice the cooling load at chiller loop 7, the differences in optimal design between the two are only 20%. This is because demand charges are the only factor in the Base Rate which incentivize thermal storage. As more load is reduced at a given chiller, up to the point of minimum PLR, the associated energy savings has diminishing returns. This is shown by the decreasing slope of the chiller power reduction curves, discussed in §7.3. Therefore, when operating in a partial-storage mode, it is advantageous in terms of energy savings at a given timestep to partially reduce load at all operating chillers than to drastically reduce the load on only one chiller.

As ISOC events are added, the increased cost of energy during the service interruption periods incentivizes the use of thermal storage. If the cost of energy and the duration of additional ISOC events exceeds the annualized capital cost of a storage tank, the additional tank is purchased. Thus, when 80 hours of service are interrupted, a total of 10 tanks are purchased for both chiller loops. When 160 hours are interrupted, and the escalated cost of diesel is included, the optimal number of tanks increases to 14.

The final optimization output is the thermal storage dispatch to achieve the minimum cost. Figure 7-9 through Figure 7-11, on the following pages, show the reference baseline and optimized total electric power profiles for all three scenarios over the months of chiller and CTES operation.

In the Base Rate scenario, Figure 7-9, thermal storage is used almost exclusively for peak shaving and is discharged for only 225 hours throughout the year. Monthly peak electricity demand is reduced an average of 5.88% (170 kW) from the reference baseline. Due to the inefficiencies associated with operating the chiller at part-load and while charging ice, combined with the absence of a time-of-use energy charge, the thermal storage is not used for daily load shifting.

In ISOC80, shown in Figure 7-10, though only one additional storage tank has been added, the demand-response events produce a 7.1% increase in the total number of hours of CTES discharge and reduce the average monthly peak demand by 6.1% (176 kW) from baseline. The relatively small additional use of thermal storage is due to the coincidence of the ISOC periods with days during which the thermal storage was previously used for peak demand reduction under the base rate.

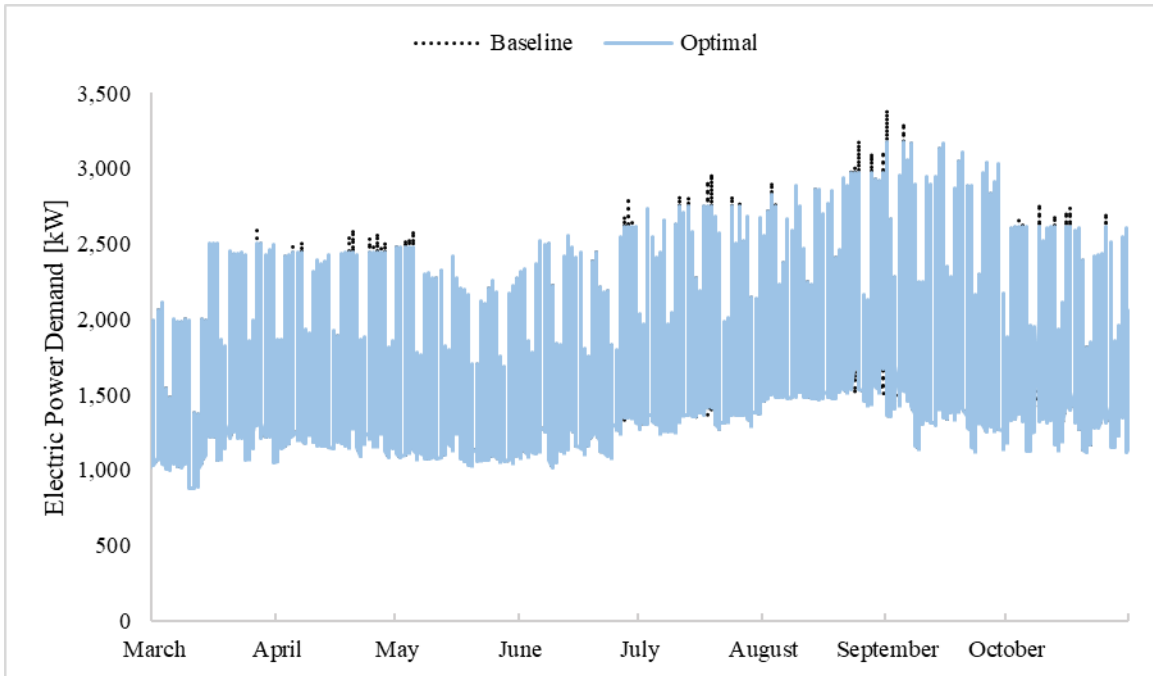


Figure 7-9: Base Rate scenario community aggregate electric power demand profiles from March to October, the months of thermal storage operation

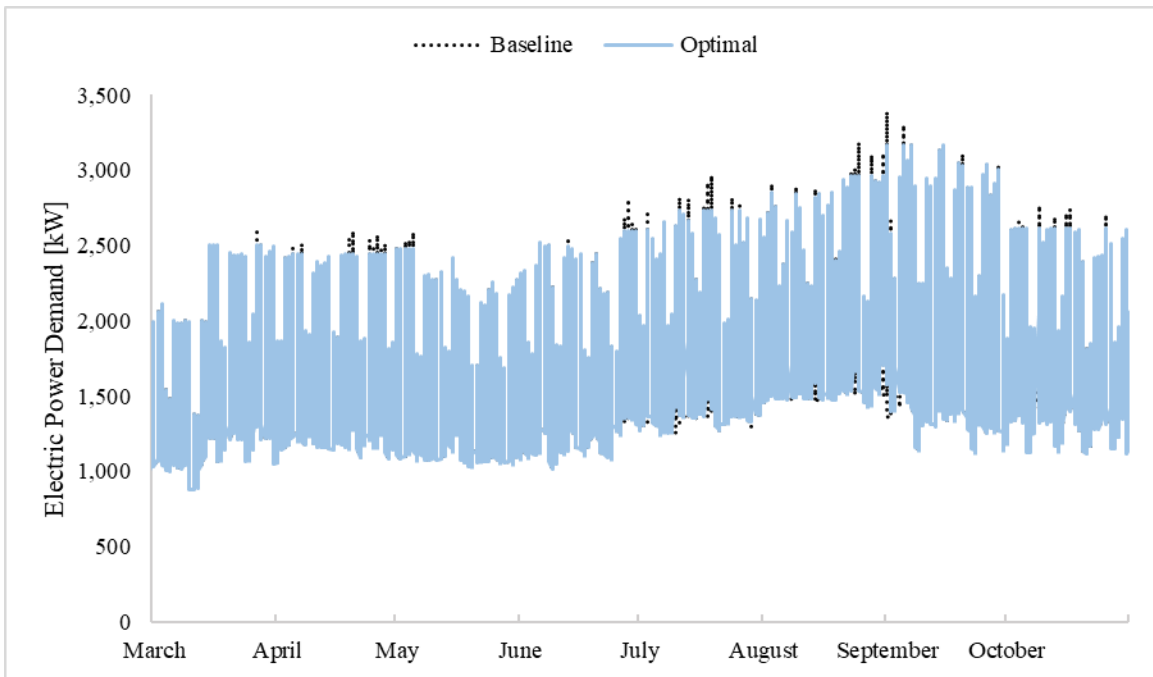


Figure 7-10: ISOC80 scenario community aggregate electric power demand profiles from March to October, the months of thermal storage operation

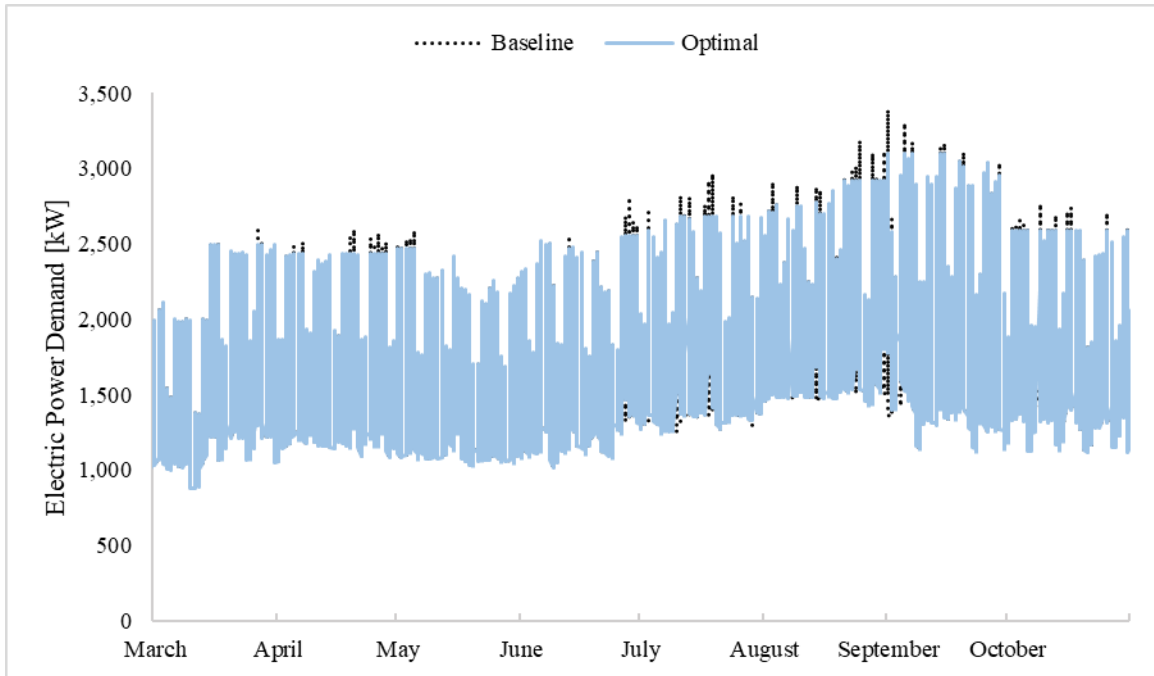


Figure 7-11: ISOC160+ scenario community aggregate electric power demand profiles from March to October, the months of thermal storage operation

In the ISOC160+ scenario, Figure 7-11, the elevated cost of fuel and the greater number of hours for service interruption encourage thermal storage usage as a load-shifting tool to avoid energy charges, as well as reduce peak demand. Thermal storage is discharged over 65% more hours than the reference baseline (371 hours) and monthly peak demand is reduced by an average of 7.2% (210 kW).

The figures above qualitatively indicate that the increased requirement for demand response, as signaled through a service interruption event, results in a greater ability to use ice thermal storage in a cost-effective manner. Quantitatively, we find that as a greater number of ISOC hours incentivizes the procurement of thermal storage, the additional capacity can then be used to offset additional demand charges at other times. When increasing from 80 to 160 hours of service interruption, the total number of hours of thermal storage discharge increases from 241 to 371. This is equivalent to 1.625 hours of ice usage for every 1 hour of added service interruption, which exceeds the fuel cost multiplier of 1.5. This indicates is a synergistic effect between the two cost signals to incentivize thermal storage usage.

In this chapter, the simulation-optimization workflow for central thermal storage systems is developed and demonstrated. The performance of chillers operating at various part-loads is linearized into a segmented chiller power reduction curve for every timestep, and the optimization framework initially developed in CHAPTER 6, is revised to employ this new set of constraints. Yet as written, this formulation only applies to central systems, further modification is required to both the formulation and the pre-processing steps of the workflow to simultaneously accommodate both technologies.

## CHAPTER 8

### INTEGRATED SIMULATION-OPTIMIZATION WORKFLOW COMBINING DISTRIBUTED AND CENTRAL THERMAL STORAGE SYSTEMS

The previous two chapters present individual simulation-optimization workflows for distributed UTSS and central thermal storage systems. Both are demonstrated on example building sets which exclusively contain cooling systems compatible with the respective workflow. However, to be fully applicable to connected communities, these two workflows must be integrated into one, illustrated in Figure 8-1. Fortunately, the main methodologies previously presented for UTSS and chiller modeling are still applicable, so only two elements require substantial modification in the final workflow: first, the optimization formulation must be modified to handle both types of thermal storage; and second, the data-management within the preprocessor must be updated accordingly.

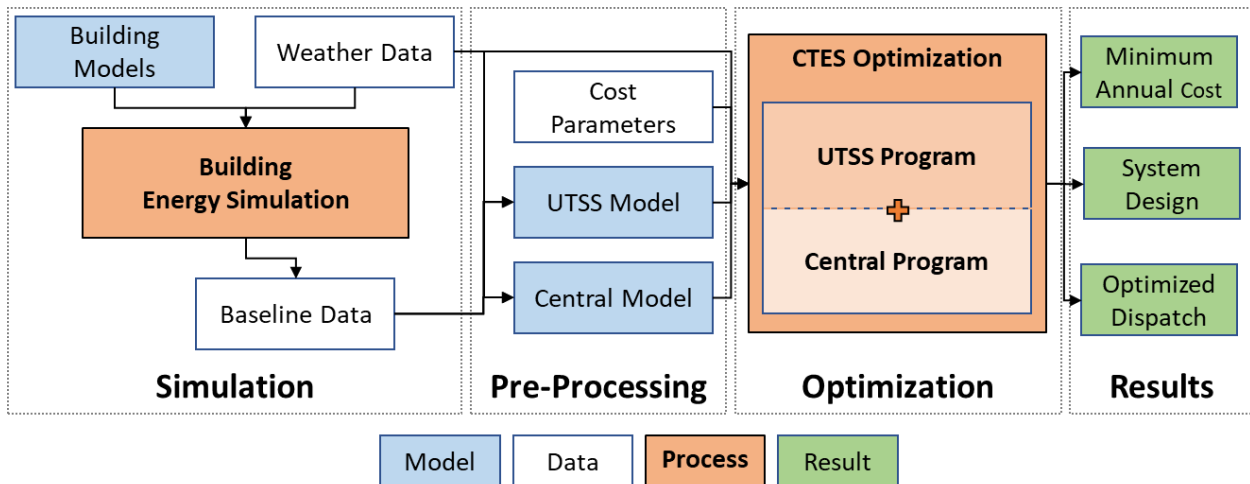


Figure 8-1: Integrated simulation-optimization workflow

This chapter presents the integrated workflow and demonstrates it using a selection of buildings that contain both central chillers and distributed rooftop units. To better illustrate the potential applications of this work, two demand-response cost signals are compared to a baseline utility rate, including an existing critical peak pricing (CPP) rate and a modeled future real-time pricing (RTP) scheme.

## 8.1 Integrated optimization program

Unlike the initial UTSS formulation presented in §6.4.3, the central storage program in §7.4 is generalizable to cooling equipment with both variable-speed and fixed-speed compressors. Therefore, the latter formulation serves as the foundation for the integrated Central-UTSS workflow.

### 8.1.1 Optimization program notation

The final notation required for the integrated formulation is presented in Table 8-1. As with two previous formulations, parameters are defined with lowercase letters, variables are uppercase, subscripts are used for indexing, and superscripts are reserved for descriptors. To differentiate between the types of thermal storage system, the index  $i$  is introduced, where  $i=1$  when the applicable storage system is UTSS and  $i=2$  for central tank compatible devices.

Table 8-1: Notation for integrated CTES formulation

<i>Sets</i>	
$d \in \mathcal{D}$	Set of utility demand periods in the optimization horizon
$i \in \mathcal{I}$	Set of thermal storage devices: 1 = UTSS, 2 = central tank
$n \in \mathcal{N}$	Set of all rooftop units and chiller plants within the community
$s \in \mathcal{S}_n$	Set of linear segments into which cooling system $n$ performance curve is divided
$t \in \mathcal{T}$	Set of all timesteps within the optimization period
$t \in \mathcal{T}_d^{\mathcal{D}}$	Indexed set of timesteps within each utility demand period $d$
$t \in \mathcal{T}_n^{-F}$	Indexed set of timesteps during which full storage is available at system $n$ ,
	$\mathcal{T}_n^{-F} \subset \mathcal{T}_n^{-P}$
$t \in \mathcal{T}_n^{-P}$	Indexed set of timesteps during which cooling load exists at system $n$
$t \in \mathcal{T}^{\mathcal{R}}$	Set of timesteps during which demand response event(s) occur

Table 8-1 continued

<i>Building Simulation Parameters</i>	
$l_{nt}$	Thermal cooling load served by cooling plant $n$ at time $t$ [ $\text{kW}_t$ ]
$\tilde{p}_t$	Average total power demand for the community during timestep $t$ [ $\text{kW}_e$ ]
$\tilde{p}_{nt}^N$	Average cooling system power to meet full cooling load at plant $n$ at time $t$ [ $\text{kW}_e$ ]
<i>Thermal Storage Parameters</i>	
$\eta_{nt}^I$	Thermal storage tank ambient-loss efficiency at pant $n$ at time $t$ [-]
$\epsilon_n$	Electric load shed effectiveness of the thermal storage installed at pant $n$ [-]
$\lambda_{nt}^+$	Coefficient for thermal storage charging at plant $n$ at time $t$ [-]
$\lambda_{nst}^-$	Coefficient for partial-storage load reduction segment $s$ at plant $n$ at time $t$ [-]
$\bar{l}_{nst}$	Maximum rate of partial-storage discharge at plant $n$ over segment $s$ at time $t$ [ $\text{kW}_t$ ]
$\dot{q}_{nt}^{N+}$	Maximum available charging rate from the coolers at plant $n$ at time $t$ [ $\text{kW}_t$ ]
$\dot{q}_i^{I+}$	Nominal maximum rate of charging for storage type $i$ [ $\text{kW}_t$ ]
$\dot{q}_{int}^{I-}$	Maximum rate of discharging for thermal storage type $i$ at plant $n$ at time $t$ [ $\text{kW}_t$ ]
$\bar{q}_i$	Maximum usable capacity for each thermal storage type $i$ [ $\text{kWh}_t$ ]
<i>Cost Parameters</i>	
$c_t^r$	Additional cost of electric energy during a demand response event at time $t$ [ $\$/\text{kWh}_e$ ]
$c_t^e$	Cost of electric energy at time $t$ [ $\$/\text{kWh}_e$ ]
$c_d^p$	Cost of maximum average electric power demand during period $d$ [ $\$/\text{kW}_e$ ]
$k_{in}$	Capacity cost of storage of type $i$ installed at plant $n$ [ $\$/\text{kWh}_t$ ]

Table 8-1 continued

<i>Miscellaneous Parameters</i>	
$\delta$	Duration of each timestep $t$ [hr]
$\psi_t$	Required electric power reduction at time $t$ in the event of a demand response signal [kW <sub>e</sub> ]
$y_i$	Expected lifespan of thermal storage device type $i$ [years]
$\bar{z}_{in}$	Maximum number of thermal storage devices of type $i$ that may be installed at plant $n$ [-]
<i>Binary and Integer Variables</i>	
$\alpha_{nt}$	Binary; 1 iff. full-storage discharge is used at plant $n$ at time $t$ [-]
$Z_{in}$	Number of thermal storage tanks of type $i$ installed at plant $n$ [-]
<i>Continuous Variables</i>	
$L_{nt}^+$	Thermal load added by charging the thermal storage at plant $n$ at time $t$ [kW <sub>t</sub> ]
$L_{nt}^-$	Thermal load reduced at plant $n$ via full-storage at time $t$ [kW <sub>t</sub> ]
$L_{nst}^-$	Thermal load reduced at plant $n$ via partial-storage over segment $s$ at time $t$ [kW <sub>t</sub> ]
$\hat{P}_d$	Maximum aggregated power demand during period $d$ [kW <sub>e</sub> ]
$P_t$	Total aggregated power demand at time $t$ [kW <sub>e</sub> ]
$P_{nt}^+$	Electric power added through CTES charging by plant $n$ at time $t$ [kW <sub>e</sub> ]
$P_{nt}^-$	Electric power reduced through full-storage discharge at plant $n$ at time $t$ [kW <sub>e</sub> ]
$P_{nt}^{-P}$	Electric power reduced through partial-storage discharge at plant $n$ at time $t$ [kW <sub>e</sub> ]
$Q_{nt}$	Thermal storage inventory for thermal storage at plant $n$ at time $t$ [kW <sub>t</sub> ]

### 8.1.2 Integrated CTES formulation

The integrated CTES optimization formulation presents several improvements over the previous stand-alone UTSS and CTES iterations presented in CHAPTER 6 and CHAPTER 7,

including a modification of the storage cost parameters in the objective function, explicit use of indexed sets where applicable, and the introduction of a required power reduction constraint.

### 8.1.2.1 Objective function

The objective function given in equation (8-1) minimizes (1) the total annual cost of storage, (2) annual energy charges, (3) annual demand charges, and (4) any special energy costs associated with demand response events. The cost of storage term (1) is revised so that the cost parameter  $k_{in}$  may be specified as a function of capacity, with units of \$/kWh<sub>t</sub>. This is more analogous to other forms of storage, such as batteries, allowing for more direct comparison when evaluating technologies.

$$\min \left[ \underbrace{\sum_{i \in \mathcal{I}} \sum_{n \in \mathcal{N}} k_{in} \cdot \frac{\bar{q}_i}{y_i} \cdot Z_{in}}_{(1)} + \underbrace{\sum_{t \in \mathcal{T}} c_t^e \cdot \delta \cdot P_t}_{(2)} + \underbrace{\sum_{d \in \mathcal{D}} c_d^p \cdot \hat{P}_d}_{(3)} + \underbrace{\sum_{t \in \mathcal{T}^R} c_t^r \cdot \delta \cdot P_t}_{(4)} \right] \quad (8-1)$$

### 8.1.2.2 Constraints

Constraints (8-2) through (8-6) are the power conversion constraints, through which thermal load reductions or increases at each timestep are converted into a new electric power demand for each timestep. The indexed sets  $T_n^{-F}$  and  $T_n^{-P}$  define the timesteps during which full-storage and partial-storage operation are possible, respectively, at a given cooling system.  $T_n^{-P}$  contains all the timesteps during which cooling load exists at a specific device;  $T_n^{-F}$  is always a subset of  $T_n^{-P}$ .

$$P_t \geq \tilde{p}_t + \sum_{n \in \mathcal{N}} P_{nt}^+ - \begin{cases} (P_{nt}^{-F} + P_{nt}^{-P}) & \text{if } t \in T_n^{-F} \\ P_{nt}^{-P} & \text{if } t \in T_n^{-P} \text{ \& } \notin T_n^{-F} \\ 0 & \text{otherwise} \end{cases} \quad \forall t \in \mathcal{T} \quad (8-2)$$

$$P_{nt}^+ \geq \lambda_{nt}^+ \cdot L_{nt}^+ \quad \forall n \in \mathcal{N}, t \in \mathcal{T} \quad (8-3)$$

$$P_{nt}^{-F} \leq \epsilon_n \cdot \tilde{p}_{nt}^N \cdot \alpha_{nt} \quad \forall n \in \mathcal{N}, t \in T_n^{-F} \quad (8-4)$$

$$P_{nt}^{-P} \leq \epsilon_n \cdot \sum_{s \in \mathcal{S}_n} \lambda_{nst}^- \cdot L_{nst}^- \quad \forall n \in \mathcal{N}, t \in T_n^{-P} \quad (8-5)$$

$$\hat{P}_d \geq P_t \quad \forall \quad t \in \mathcal{T}_d^D \quad (8-6)$$

The thermal charging and discharging performance are constrained by equations (8-7) through (8-12). Full-storage remains actuated by the binary operator  $\alpha_{nt}$ .

$$L_{nt}^+ \leq \sum_{i \in \mathcal{I}} \dot{q}_{in}^{I+} \cdot Z_{in} \quad \forall \quad n \in \mathcal{N}, t \in \mathcal{T} \quad (8-7)$$

$$L_{nt}^+ \leq \dot{q}_{nt}^{N+} \quad \forall \quad n \in \mathcal{N}, t \in \mathcal{T} \quad (8-8)$$

$$L_{nt}^{-F} \leq l_{nt} \cdot \alpha_{nt} \quad \forall \quad n \in \mathcal{N}, t \in \mathcal{T}_n^{-F} \quad (8-9)$$

$$L_{nt}^{-F} \leq \sum_{i \in \mathcal{I}} \dot{q}_{it}^{I-} \cdot Z_{in} \quad \forall \quad n \in \mathcal{N}, t \in \mathcal{T}_n^{-F} \quad (8-10)$$

$$L_{nst}^{-P} \leq \begin{cases} (1 - \alpha_{nt}) \cdot \bar{l}_{nst} & \text{if } t \in \mathcal{T}_n^{-F} \\ \bar{l}_{nst} & \text{otherwise} \end{cases} \quad \forall \quad n \in \mathcal{N}, s \in \mathcal{S}_n, t \in \mathcal{T}_n^{-P} \quad (8-11)$$

$$\sum_{s \in \mathcal{S}} L_{nst}^{-P} \leq \sum_{i \in \mathcal{I}} \dot{q}_{it}^{I-} \cdot Z_{in} \quad \forall \quad n \in \mathcal{N}, t \in \mathcal{T}_n^{-P} \quad (8-12)$$

Thermal storage inventory is maintained and limited via equations (8-13) to (8-17). All thermal storage devices are initialized with an empty state-of-charge.

$$Q_{nt} = \eta_{nt}^I \cdot Q_{n,t-1} + \delta \cdot \left( L_{n,t}^+ - \begin{cases} \left( L_{nt}^{-F} + \sum_{s \in \mathcal{S}_n} L_{nst}^{-P} \right) & \text{if } t \in \mathcal{T}_n^{-F} \\ \sum_{s \in \mathcal{S}_n} L_{nst}^{-P} & \text{if } t \in \mathcal{T}_n^{-P} \text{ \& } t \notin \mathcal{T}_n^{-F} \\ 0 & \text{otherwise} \end{cases} \right) \quad (8-13)$$

$$\forall \quad n \in \mathcal{N}, t \in \mathcal{T} \text{ \& } > 1$$

$$Q_{nt} \leq \sum_{i \in \mathcal{I}} \bar{q}_i \cdot Z_{in} \quad \forall \quad n \in \mathcal{N}, t \in \mathcal{T} \quad (8-14)$$

$$\delta \cdot L_{nt}^{-F} \leq \eta_{nt}^I \cdot Q_{n,t-1} \quad \forall \quad n \in \mathcal{N}, t \in \mathcal{T}_n^{-F} \quad (8-15)$$

$$\delta \cdot \sum_{s \in \mathcal{S}_n} L_{nst}^{-P} \leq \eta_{nt}^I \cdot Q_{n,t-1} \quad \forall \quad n \in \mathcal{N}, t \in \mathcal{T}_n^{-P} \quad (8-16)$$

$$Q_{n1} = 0 \quad \forall \quad n \in \mathcal{N} \quad (8-17)$$

A new constraint, added to explore the effect of load reduction requirements, is given in equation (8-18). Here the new parameter  $\psi_t$  is used to enforce a specific electrical load

reduction, relative to the baseline power demand, during each of the demand response timesteps contained within set  $\mathcal{T}^R$ .

$$P_t \leq \tilde{p}_t - \psi_t \quad \forall t \in \mathcal{T}^R \quad (8-18)$$

Equations (8-19) to (8-21) enforce the positive linearity, integrality, and binary nature of the variables.

$$L_{nt}^+, L_{nt}^-, L_{nst}^-, P_t, P_{nt}^+, P_{nt}^-, P_{nt}^*, P_{nst}^-, \hat{P}_d, Q_{nt} \geq 0 \quad (8-19)$$

$$\forall d \in \mathcal{D}, n \in \mathcal{N}, s \in \mathcal{S}_n, t \in \mathcal{T}, t^* \in \mathcal{T}_n^{-F}, t' \in \mathcal{T}_n^{-P}$$

$$0 \leq Z_{in} \leq \bar{z}_{in}, \text{ integral} \quad \forall i \in \mathcal{I}, n \in \mathcal{N} \quad (8-20)$$

$$\alpha_{nt} \text{ binary} \quad \forall n \in \mathcal{N}, t \in \mathcal{T}_n^{-F} \quad (8-21)$$

### 8.1.2.3 UTSS Parametrization

No changes are needed to use the formulation above with centralized storage tanks ( $i = 2$ ) at any number of chiller plants. However, for UTSS ( $i = 1$ ), a few adjustments are needed in the pre-processing methodology. When using UTSS, the entire region of both full- and partial-storage discharge is governed by a single linear variable for each timestep,  $L_{nst}^-$ . No binary-actuated full-storage variables are required. For any cooling system compatible with UTSS, the number of segments,  $\mathcal{S}_n$ , is set to 1, and the maximum rate of partial-storage discharge for that segment,  $\bar{l}_{nl}$ , is set equal to the existing cooling load,  $l_{nt}$ . The maximum number of central ice tanks for the specific RTU,  $\bar{z}_{2n}$ , must then be set to 0.

## 8.2 Demonstrating the complete workflow on a mixed case

To illustrate the efficacy and potential uses of the integrated CTES optimization program, a selection of buildings is taken from the URBANopt example project, originally devised and publicly shared by the National Renewable Energy Laboratory (NREL) [109]. Of the 18 buildings in the example project, five are selected with similarly-scaled total electric energy use. These five are then simulated in climate zone 4B, with a thirty-year typical meteorological year weather file from Prescott, AZ [73].

## 8.2.1 Description of buildings and plants

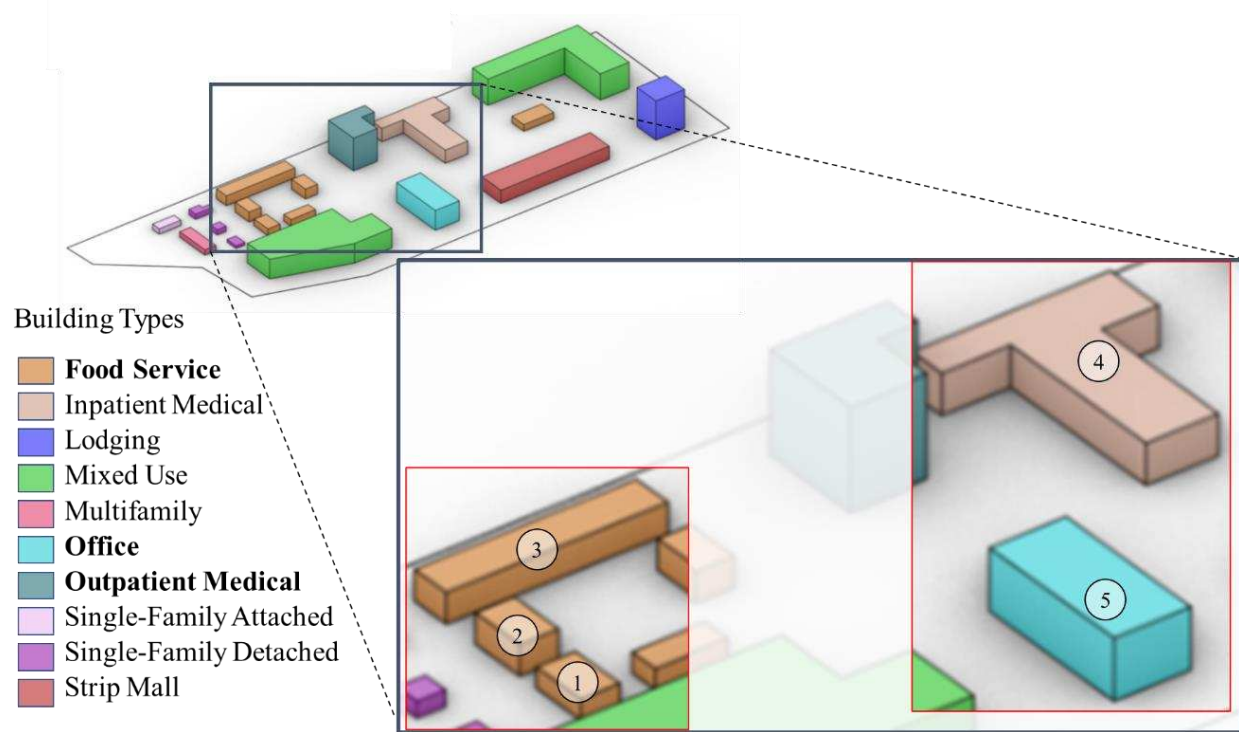
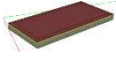
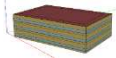

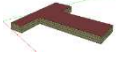
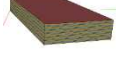


Figure 8-2: Selected buildings from the URBANopt example project used to demonstrate the integrated simulation-optimization workflow [109]. The five selected building models are identified in the inset and numbered for identification throughout the remainder of this chapter.

Figure 8-2 shows the full URBANopt example project and an inset identifying the five buildings selected for this demonstration. Buildings 1-3 are food service with varying numbers of packaged rooftop units; building 4 is an outpatient medical facility with a central chiller; and building 5 is an office, also with a central chiller. Table 8-2 summarizes the results of the simulation step of the workflow, including the annual electricity use, the annual cooling electricity use, and the cooling system types for each building in the scenario.

Table 8-2: Summary of annual energy use and cooling systems for selected buildings

ID	Building	Annual Electricity [MWh]	Total Cooling Electricity [MWh]	Cooling Systems	Chiller/RTU Indices ( <i>n</i> )
1	 Restaurant 1	978	110	5 RTUs (PSZAC)	3-7
2	 Restaurant 2	5,526	753	3 RTUs (PVAV)	8-10
3	 Restaurant 3	1,457	156	15 RTUs (PSZAC)	11-25
4	 Outpatient Medical	6,682	685	Chiller 440 tons	1
5	 Office	2,951	440	Chiller 400 tons	2
Aggregate		17,594	2,144	25 devices	-

### 8.2.2 Utility rates for flexibility

Three electric utility rates are examined in this case study. The first is a traditional time-of-use energy and demand charge rate based on the Arizona Public Service large commercial E-32 tariff [141]. The second rate takes the E-32 tariff and applies a critical peak pricing (CPP) rider. This rider provides an energy charge reduction during summer off-peak hours but requires a minimum of 200 kW power demand reduction during critical events, which are identified 24-hours in advance by the utility company. Between six to 18 CPP events may occur over the summer months, and any electricity used during the critical event hours is billed at an escalated rate [142]. In our scenario, nine CPP events are used. Table 8-3 lists the off-peak and on-peak

energy prices for the E-32 and CPP utility rates. The third rate, derived from the Cambium energy futures studies bills energy use via real-time pricing (RTP), and is discussed further below [143].

Table 8-3: Summary of energy charges for the three utility rates examined in this scenario. All units are in \$/kWh.

Utility Rate	Winter (Nov-Apr)		Summer (May-Oct)		
	Off-Peak	On-Peak	Off-Peak	On-Peak	Critical Event
E-32	0.04264	0.05552	0.05730	0.07018	-
CPP	0.04264	0.05552	0.04872	0.07018	0.25
Cambium	Varies by hour - min: 0.00295, max: 0.9375, mean: 0.03978				

All three utility rates use time-of-use based demand charges, calculated monthly. During off-peak hours, electric power demand is billed at \$3.272 per kW. During on-peak hours, the charge increases to \$11.71 per kW.

The Cambium RTP energy charges are obtained from a suite of forward-looking scenarios modeled and published by NREL. The future data is obtained from the Cambium tool, which assembles structured data sets of hourly cost, emission, and operational data for possible futures of the U.S. electric sector [144]. The specific hourly cost signal is obtained from the 2030 Mid-case data for the state of Arizona. The modeled future end-use total cost in \$/MWh is then converted into an hourly electricity cost and used as a real-time pricing structure. Figure 8-3, on the following page, shows the hourly energy price profile over the course of the year. Much of the time, energy prices fall below \$0.05 per kWh, but occasionally escalate as high as \$0.93 per kWh. To enforce the electrical power reduction requirement during the critical events,  $\psi_t$  is set equal to 200kW  $\forall t \in \mathcal{T}^R$ .

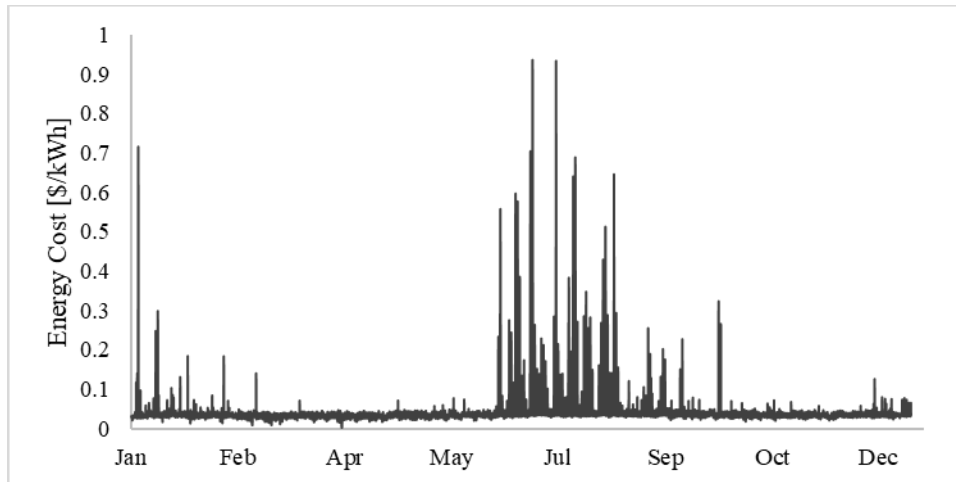


Figure 8-3: Predicted future real-time pricing (RTP) hourly costs of energy over the course of the year for the Cambium Mid-Case 2030 scenario [143]

### 8.2.3 Thermal storage devices and costs

The thermal storage devices for this optimization are the same as those described in §6.5.2 and §7.5.2. For the central chillers, CALMAC 1190C internal-melt, ice-on-coil tanks with a nominal capacity of 162 ton-hours (570 kWh) are used [133]. The cost per capacity of each tank is \$140 per ton-hour, or \$39.81 per kWh<sub>t</sub> [134]. For UTSS, the IceBear 40 packaged system with a nominal usable capacity of 38 ton-hours (133 kWh<sub>t</sub>) is used. Ice charging is performed by an internal 5-ton (17.6 kW<sub>t</sub>) compressor [36]. The cost of the packaged system is estimated to be \$265 per ton-hour, or \$75.19 per kWh<sub>t</sub> [111]. The large discrepancy in cost between the central tanks and the UTSS is due to the cost of the ice-making compressor.

As with the case studies in the previous chapters, the CTES devices examined here are ice-based. This provides a more interesting constraint set for optimization as chiller performance is more heavily impacted when charging ice thermal storage rather than a stratified chilled water tank. Additionally, when considering CTES for individual buildings, ice storage is often favored over sensible storage technologies due to its smaller space requirement.

### 8.3 Integrated workflow optimization results

The three main outputs of the integrated optimization program are the same as the previous UTSS and Central programs: minimum annual cost, optimal design, and optimal dispatch. The example scenario is optimized with each of three utility rates using Gurobi v. 9.0.0

solver. The optimization execution is managed through AMPL on an eight-core server running Ubuntu 18.04.5 LTS. Solutions within an absolute gap of \$100 are obtained in approximately 15 minutes using 1-hour timesteps.

### 8.3.1 Minimum cost

The baseline costs (before optimization) vary by utility rate, so minimum cost performance is expressed in terms of relative savings. The maximum relative savings is achieved using the Cambium RTP rate, with a 3.54% reduction in total annual costs. The 3.16% reduction is obtained under the E-32 rate. However, the CPP rate only achieves an overall annual savings of 1.82%. These results are compared in Figure 8-4, along with the total annual costs, including storage.



Figure 8-4: Minimum annual cost and relative savings before and after optimization for the E-32, CPP, and Cambium utility rates. The red diamonds represent relative savings between the baseline and optimized cases.

Compared to the E-32 rate, the CPP savings is significantly smaller. This is because of the hard power reduction constraint required by the utility rider. This requirement enforces the procurement of more thermal storage than would be purchased if a cost-signal alone is used to motivate load shifting. Conversely, the Cambium real-time pricing scheme produces greater savings when optimized. This implies that highly variable energy charges – in this case ones that

change hourly (Cambium) compared to twice daily (E-32) – are more conducive to load flexibility via thermal storage.

### 8.3.2 Optimal design

The second result of interest from the MILP is the optimal design. We find significant differences in the number and distribution of the two types of thermal storage systems across the 25 possible locations in the five buildings. The breakdown of number of thermal storage units by building is given in Table 8-4.

Table 8-4: Optimal number and type of CTES devices installed at each building using the E-32, CPP, and Cambium utility rates

ID	Building	Number of Applicable CTES Devices			
		Type	E-32	CPP	Cambium
1	Restaurant 1	UTSS	0	5	1
2	Restaurant 2	UTSS	3	26	7
3	Restaurant 3	UTSS	0	7	2
4	Outpatient Medical	Central	2	2	2
5	Office	Central	1	1	1
Total			6	41	13

In terms of total capacity, the E-32 rate uses 600 ton-hours of TES capacity and Cambium uses 864 ton-hours. However, the CPP rate dwarfs those figures, using 1,923 ton-hours of thermal storage. It is this much greater thermal storage capacity which contributes to the reduced relative savings obtained by the CPP scenario. The reason for this greater capacity is entirely due to the introduction of a hard power-reduction requirement in equation (8-18). By requiring sufficient thermal storage to meet a 200kW electrical power reduction over 5-hour CPP events, the thermal storage requirements are nearly seven times greater than what was determined without the CPP rider.

It is also noteworthy that the thermal storage applied at the chillers is consistent across the three utility rates. This occurs for two reasons: first, while the chillers in the Outpatient Medical center and the Office meet greater cooling loads than individual RTUs in the

Restaurants, they do so at higher efficiencies as well. When turning down a chiller to a reduced part-load, the electricity savings is proportionately smaller than turning off an RTU. Therefore, after peak shaving is achieved on the larger central systems, additional financial benefit is obtained through adding more distributed UTSS across the community.

The second reason is best explained in the context of the CPP scenario. In this case, many UTSS are added where intuition might suggest that additional central tanks would be more cost-effective. The reason for this is that the critical events occur in the afternoon hours, from 15:00-20:00, which are not coincident with high cooling loads from the two buildings with chillers. Instead, cooling loads comprise a larger fraction of the energy use in the restaurants, making them more-ideal candidates for additional thermal storage during those hours.

### **8.3.3 Optimal dispatch**

Achieving minimum cost is not only a function of purchasing and installing thermal storage, but also a function of control. Traditional thermal storage controls charge the CTES at night and subsequently discharge it over the course of the day, or during specific on-peak hours [ref]. However, the optimized dispatch balances energy costs, device efficiencies, and loads met by individual cooling systems across the community. Inspection of these results reveals that a traditional schedule-based control scheme may not achieve the minimum cost result.

Figure 8-5 through Figure 8-7 present the hourly dispatch signals for the thermal storage installed at individual cooling systems over the course of the entire year. Presented in this manner, it is easy to observe general trends in thermal storage usage across the various chillers and RTUs. Each cooling system is labeled using either a “C,” for chiller, or an “R,” for rooftop unit, and the index used within optimization formulation (see Table 8-2 for building assignment). Positive values are charging signals and negative values are discharging signals; the magnitude of each signal is equal to the normalized rate of charging or discharging for each timestep. A value of  $\pm 1$  is equal to the maximum rate of heat transfer.

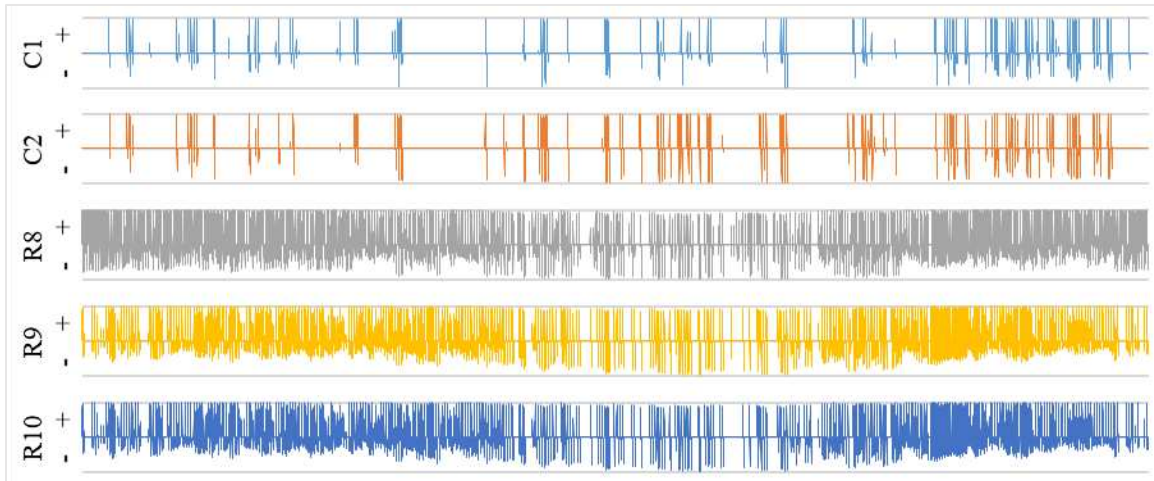


Figure 8-5: E-32 optimal hourly thermal storage dispatch signals by cooling system over the course of the full year. Positive values are charging signals, negative values are discharging signals. All values are normalized against the maximum rate of charge or discharge at each timestep.

Figure 8-5 shows the dispatch results for the five locations at which thermal storage installed under the E-32 utility rate. Notably, the thermal storage at the central tanks (C1 in the Outpatient Medical center and C2 in the Office) is relatively infrequently used. In general, it is employed for peak shaving, to reduce peak demand charges. On non-peak days, the thermal storage at the central chiller plants is often unused. This is because the energy cost difference between on-peak and off-peak energy prices is insufficient to overcome the inherent inefficiencies incurred through charging and discharging the thermal storage with the existing chillers. Conversely, at the large PVAV systems found in Restaurant 2 (R8-R10), the installed UTSS is used nearly every day of the year. This indicates that the round-trip efficiencies of the packaged UTSS, coupled with RTU's that are relatively less efficient than central chillers, allow them to affect a daily savings in energy charges in circumstances where chillers cannot.

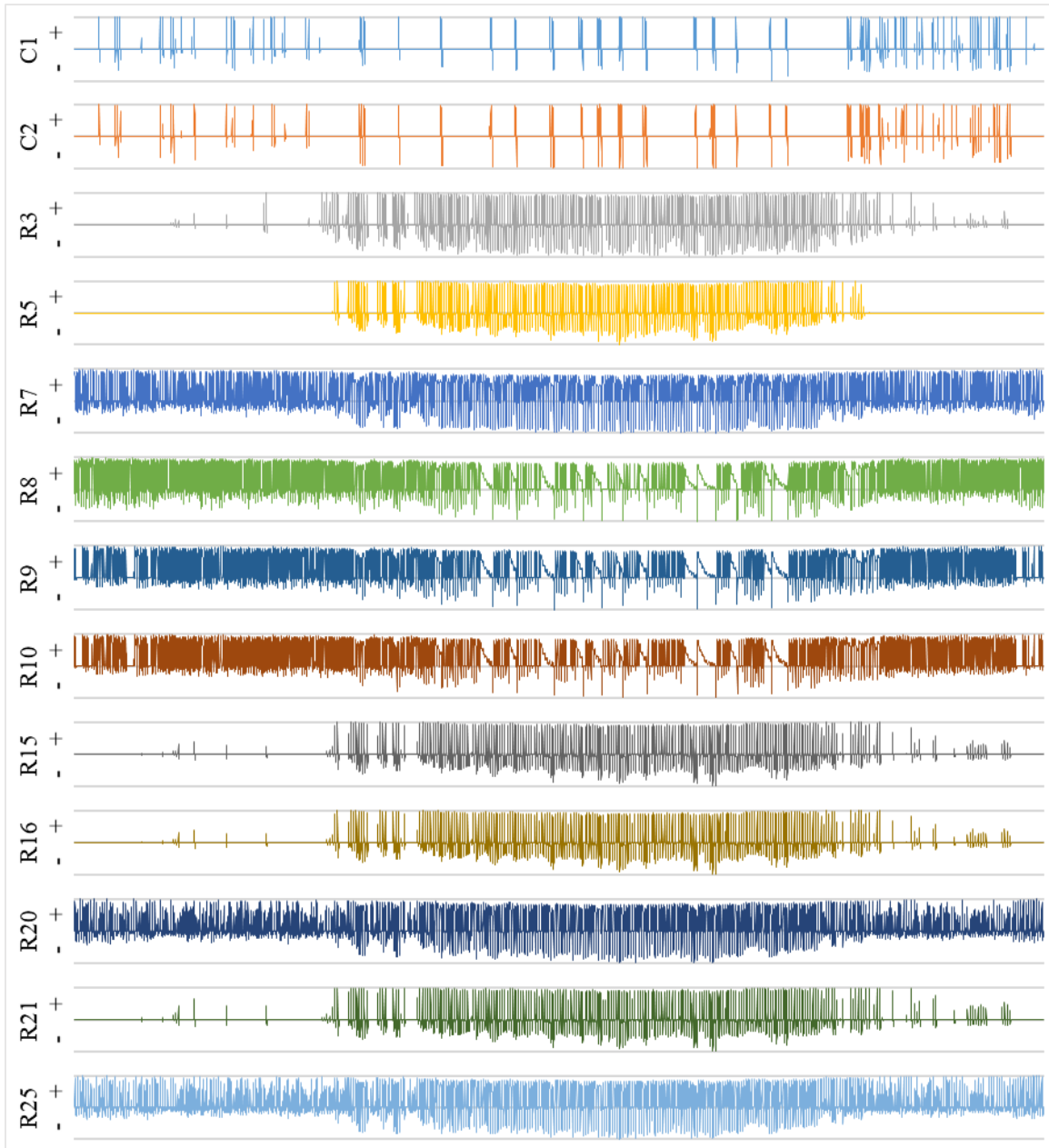


Figure 8-6: CPP optimal hourly thermal storage dispatch signals by cooling system over the course of the full year. Positive values are charging signals, negative values are discharging signals. All values are normalized against the maximum rate of charge or discharge at each timestep.

The thermal storage dispatch under the critical peak pricing rider is shown in Figure 8-6. Beyond the obvious increase in the number of locations for storage, two interesting features are illustrated in this figure. First, the central storage at the chillers is used even less frequently than under the E-32 rate. Similarly, this is due to the relative efficiencies of the baseline cooling

equipment. Because the CPP necessitates a much larger amount of storage to meet the 200kW electricity load reduction, additional UTSS are procured. Once installed, these devices offer a higher energy charge savings than when turning down a chiller, therefore they are used nearly every day if cooling load is present. This highlights the second feature of interest: while the central storage at the chillers is used for peak shaving, the UTSS are used daily to mitigate the time-of-use energy charges. This implies that after absorbing the increased cost of hardware, UTSS may offer greater daily savings potential than central chillers for daily operation.

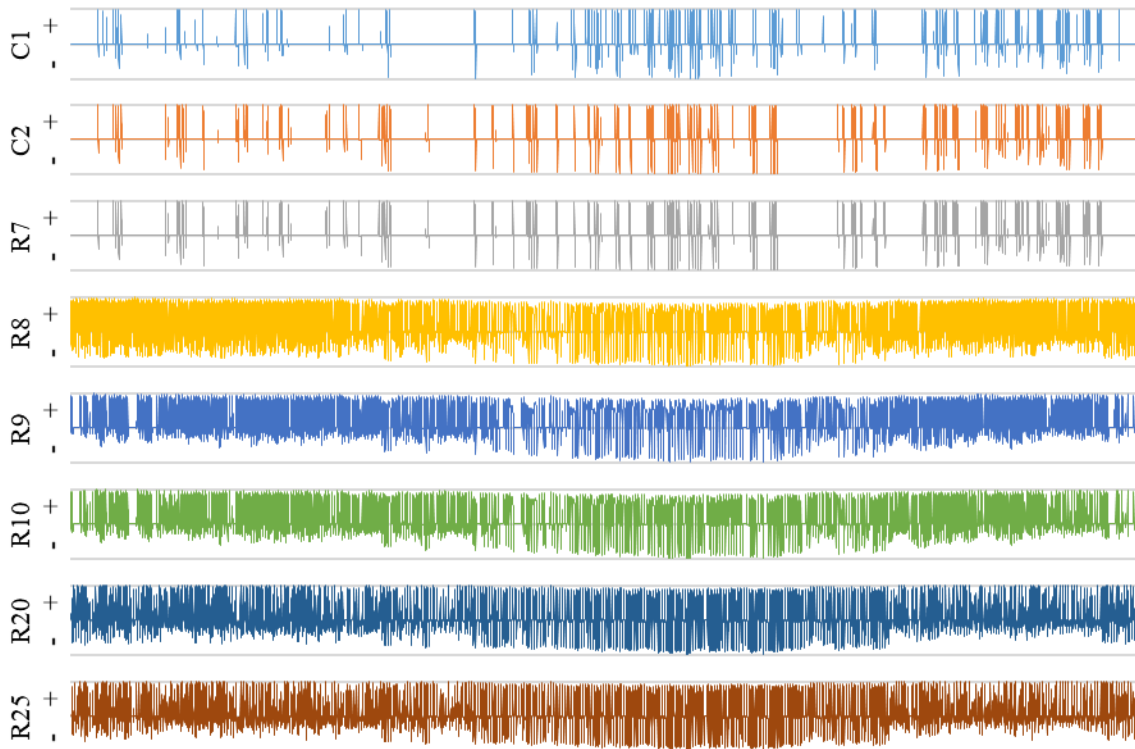


Figure 8-7: Cambium optimal hourly thermal storage dispatch signals by cooling system over the course of the full year. Positive values are charging signals, negative values are discharging signals. All values are normalized against the maximum rate of charge or discharge at each timestep.

Contrary to what was observed in the CPP scenario, under the real-time pricing of the Cambium rate (Figure 8-7), thermal storage at the chillers increases relative to the scheduled on-peak and off-peak periods of the E-32 rate. The Cambium rate is also more conducive to storage utilization than E-32, as evidenced by the additional use of storage at R7 (Restaurant 1), R20 (Restaurant 3), and R25 (Restaurant 3).

These dispatch signals are manifest in changes in the electric power profile of the five-building community over the course of the year. To illustrate the efficacy of the thermal storage, a sample day during which a critical event occurs is selected and the total electric power is plotted in Figure 8-8. By policy, critical event hours coincide with the normal summer on-peak period of 15:00-20:00.

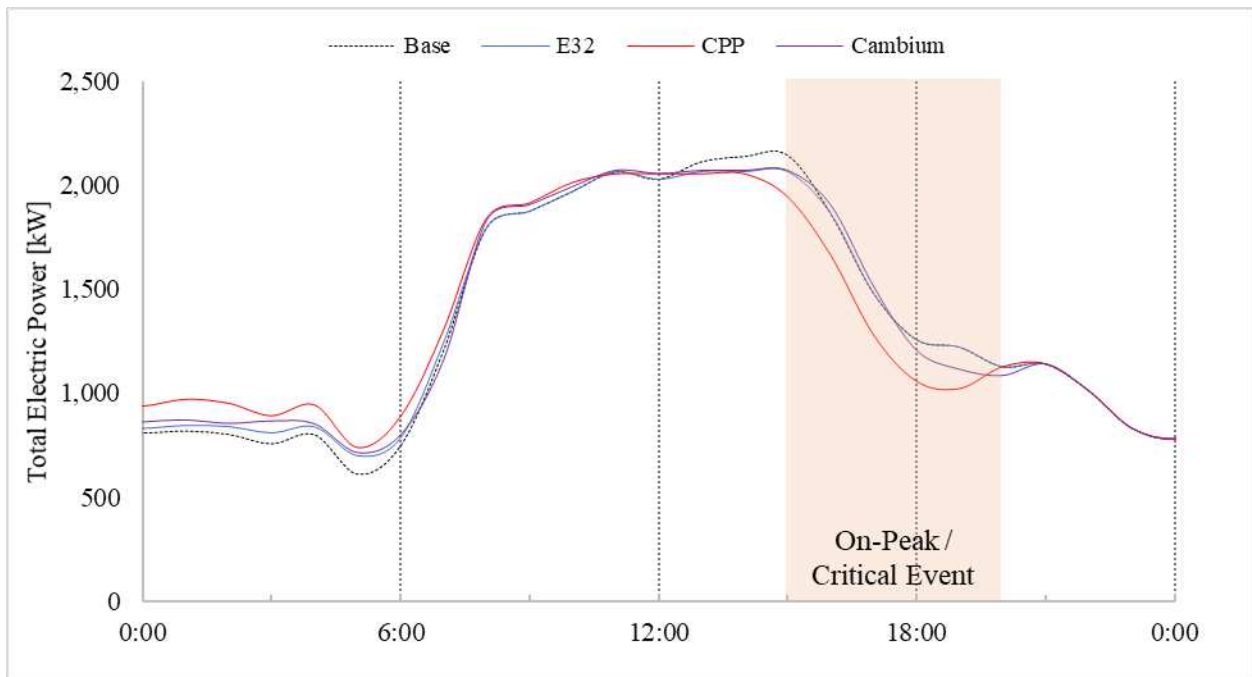


Figure 8-8: Comparison of the community electric power profiles over August 4, during which a critical event occurs coincident with the normal on-peak period

In Figure 8-8, the baseline electric power is plotted as a dotted black line and the three optimized cases are in blue, red, and purple for E-32, CPP, and Cambium, respectively. All three optimized cases perform some peak shaving for two-to-three hours prior to the on-peak period beginning at 15:00. During on-peak hours, the E-32 profile performs approximately one hour of additional peak shaving and then follows the baseline power profile. The CPP profile falls substantially below the baseline profile since it is forced to reduce the power demand by at least 200kW from 15:00-20:00. The Cambium scenario is unusual in that the thermal storage is first discharged for peak shaving around 13:00-14:00 but is then not discharged again until after 18:00. This is due to the delayed peak in electricity prices under the real-time pricing, shown in Figure 8-9. Even though electricity loads are much smaller across the community at that time of

day, the financial signal provided by the RTP dictates that storage be used in the early evening, rather than mid-day.

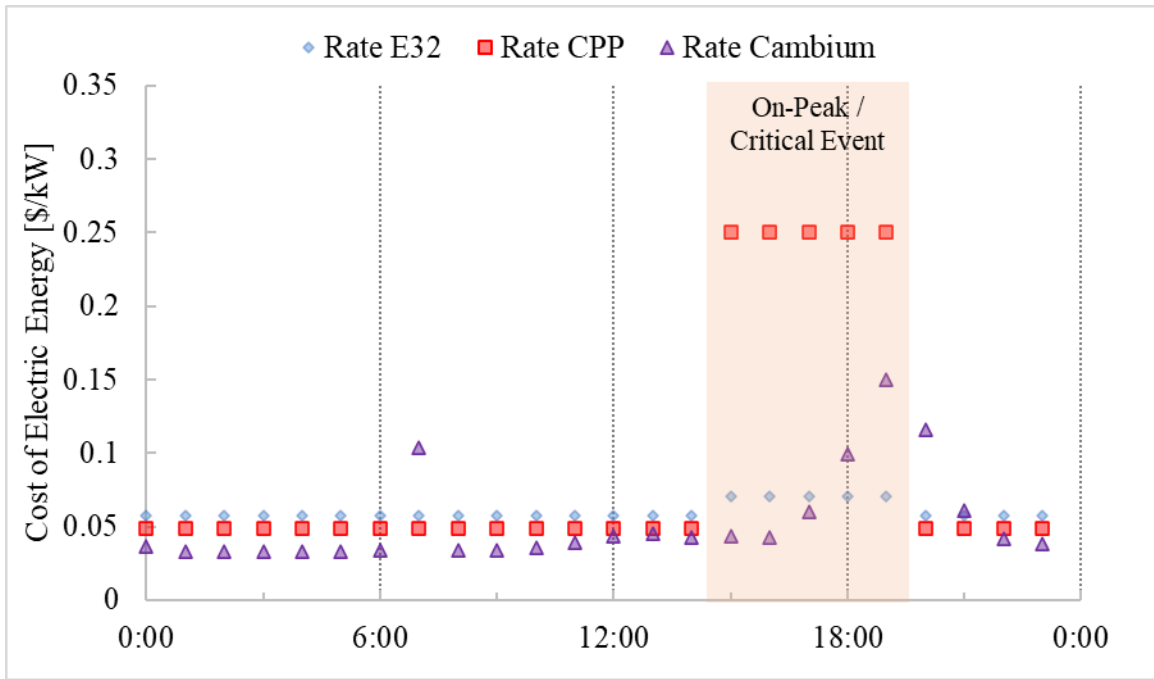


Figure 8-9: Hourly cost of electricity on August 4, for the E-32, CPP, and Cambium utility rates

The results shown for the integrated simulation-optimization workflow provide unique insights into the potential value of two different thermal storage technologies in a small, five-building case study. Though these results are specific to the buildings and utility rates explored here and were obtained using exclusively ice-based thermal storage technologies, they demonstrate the value of the community-scale optimization approach to exploring possible thermal storage integrations. The addition of an electrical load reduction requirement during demand-response events ( $\psi_t$ ) is useful for exploring the impacts of using thermal storage under dynamic utility rates that vary in response to critical grid events. By including both central thermal storage tanks and distributed UTSS, the tradeoffs between their cost and performance can be explored.

Two final conclusions can be drawn from this example: (1) explicit power reduction constraints associated with demand-response programs can be more effective incentives than cost signals alone, and (2) different thermal storage systems are more suited to specific load

shaping applications due to the inherent charging and discharging performance differences between UTSS and central tanks.

## CHAPTER 9

### CONCLUSIONS AND FUTURE WORK

This thesis provides a simulation-optimization workflow for distributed and centralized cool thermal energy storage technologies within a connected community. To achieve this, the research began through modeling and analysis of distributed unitary thermal storage systems and central chiller-ice systems using OpenStudio. Subsequently, a mixed-integer linear program was developed to optimize UTSS design and dispatch to achieve minimum annual cost. Using a similar methodology, the MILP was modified to apply to central tanks installed at chiller plants. Finally, both MILPs are integrated, and the simulation-optimization workflow revised so that both distributed UTS and centralized tanks may be simultaneously optimized within a multi-building, connected community context. Each aspect of this research process is applied to a unique case study, allowing for examination of the CTES performance in a variety of contexts and demonstrating the versatility of the integrated workflow.

The research conducted is based on several knowledge gaps that have emerged in the context of a future grid dominated by variable renewable energy resources: (1) insufficient capability to model distributed UTSS using open-source building energy modeling platforms, (2) a complete absence of UTSS optimization frameworks, and (3) a lack of general CTES optimization within a connected community context. By addressing these gaps, CTES may now be evaluated through both an iterative simulation approach and mathematical optimization for a collection of electrically connected buildings.

#### **9.1 Summary of key conclusions**

In the previous five chapters, different case studies are presented to illustrate different aspects of CTES modeling and optimization. While all numerical results are case-study specific, the several general conclusions can be derived from each chapter.

Based on the limited data analyzed for UTSS in CHAPTER 4, we conclude that packaged variable air volume systems are generally more conducive to CTES integration than packaged single zone air-conditioners. This is due to their comparatively greater thermal storage utilization and a smaller increase in fan energy use because of the additional thermal storage components in the system. However, future work should expand this analysis.

When modeling central ice tanks in CHAPTER 5, the improved ability to simulate realistic chiller-ice controls over the analyzed case reveals that ~10% of daily electricity use may be shifted via thermal storage with negligible changes in total annual electricity use, when coupled with a smaller chiller. The use of in-simulation demand-response testing reveals the significant impact of specific control decisions on the immediate and delayed energy use of the facility.

UTSS community optimization in CHAPTER 6, reveals two key promising conclusions: (1) a parametric optimization approach can be used to identify thermal storage installation priorities as a function hardware costs, and (2) community-scale optimization shows greater potential for both CTES utilization and cost savings compared to optimizing buildings individually.

In CHAPTER 7, a method is devised to develop a chiller power reduction curve for each timestep in the simulation-optimization workflow. This curve is linearized so that the mixed-integer linear program structure developed in CHAPTER 6 may be extrapolated to include central CTES technologies. By using three curve segments instead of one, the approximation error for chiller efficiency is reduced nearly ten-fold. A synergistic effect between the number of interrupted service hours (one of the ways utilities can implement demand-response for those who can otherwise temporarily generate their own power) and CTES utilization is observed.

Finally, from the integrated simulation-optimization workflow developed and the case studies demonstrated in CHAPTER 8, we draw two conclusions: (1) power reduction requirements associated with critical peak pricing schemes can be more significant drivers of thermal storage utilization than elevated cost signals; and (2) the higher average efficiencies of chillers lend themselves to CTES installations for the purposes of demand charge reduction, while the lower relative efficiencies of RTUs lend themselves to time-of-use charge avoidance. Under three different cost signals, a combination of central and distributed CTES is required to achieve the minimum cost, indicating the value of the integrated workflow.

## **9.2 Research contributions**

The work performed in development of this thesis provides the following contributions to the cool thermal storage field of study:

- Two OpenStudio measures to model UTSS and central CTES technologies within specific building energy models. These scripts are maintained on an NREL GitHub repository, are integrated with other OpenStudio-based tools, and are available for public download at RubyGems.org. At the time of publication, these measures have been downloaded 17,945 times.
- An optimization approach is developed for UTSS within the connected community context, which will provide the minimum-cost design and dispatch of packaged thermal storage systems at the individual HVAC system level.
- A method to extract chiller performance curves from building energy simulation and linearize them for use in a central storage optimization program.
- An integrated simulation-optimization approach, which employs open-source building energy simulation and a new mixed-integer linear program to optimally design CTES systems for a given community context. Both UTSS and central tanks are simultaneously optimized.

### **9.3 Areas for future research**

While the work presented here helps provide the tools to address how CTES can be cost-effectively integrated into the future grid, they need to be investigated with more case studies, and there are several areas of potential future work that can expand or improve upon what has been presented here.

In terms of CTES modeling with OpenStudio (and EnergyPlus), there is potential to improve the available thermal storage models within the program. The models that are available are the result of previous work that is many years old and limited to two manufacturers. It is probable that recent technology improvements have allowed real hardware to exceed the performance of the simulated models, especially for novel phase-change material devices. This work will be experimental in nature, as performance curves are device-specific. While the capability to use custom CTES models is always available, unless they are built-into the software, they remain generally unavailable to energy modelers and engineers.

For the linearization of the chiller performance curves, additional work is needed to expand the capability to include chiller models that are derived as functions of the condenser

leaving water temperature (known as “Chiller:Electric:ReformulatedEIR” within EnergyPlus). These models can be more accurate than those based on the condenser entering water temperature but are also more device-specific. Adding functionality to the workflow to automatically pre-process alternative chiller models will improve the general usability of the workflow.

Within the MILP, some formulation improvements are worth future examination: the addition of alternative demand-response constraints beyond simple load reduction requirements and the use of non-financial cost signals, such as emissions profiles. The linear formulation allows CTES analysis when the chiller capacities are fixed, since they are a fixed parameter obtained from the building energy simulation results. However, this assumes CTES as a retrofit, rather than combined with a new chiller installation. Additional cost-benefit can be obtained by simultaneously optimizing the chiller capacity with the thermal storage capacity and control. The MILP presented here should be reformulated to include chiller re-sizing. Additionally, the program structure should be examined to improve solver run-time. Neither pricing schemes, nor scaling, were evaluated as part of this work but a careful examination of both may help identify ways to reduce solution times. Depending on the type of community under analysis, chilled water thermal storage may need to be evaluated as well. To do this, an alternative performance model for stratified chilled water tanks must be added to the pre-processor.

Finally, these new tools should be exercised on a much larger scale and across a variety of contexts to examine the potential aggregate benefits that CTES can provide at the utility and grid scales. When large reference data sets, such as ComStock [145] and ResStock [146] become publicly available, there may be excellent opportunity to conduct such analysis. Direct integrations with URBANopt may be feasible, allowing for higher fidelity and more complex analysis CTES in the urban context [109]. Doing so will generate a sufficient body of data to develop direct cost comparisons with other electrical storage technologies, particularly batteries. Because of the scalability of the workflow, from single buildings to large districts, several possible use-cases are worth investigation. In particular, the workflow should be employed to help identify or develop utility rates that incentivize both the acquisition of thermal storage, as well as its consistent utilization for the purposes of energy flexibility – as dictated by the local mix of variable renewable energy generation assets on the grid.

## REFERENCES

1. Bowers, R. *Updated Renewable Portfolio Standards Will Lead to More Renewable Electricity Generation*. Today in Energy, February 27, 2019. Available from: <https://www.eia.gov/todayinenergy/detail.php?id=38492/>
2. *California ISO - Today's Outlook*. California Independent System Operator (CAISO), 2019. Available from: <http://www.caiso.com/TodaysOutlook/Pages/default.aspx/>
3. *Locational Marginal Prices*. Open Access Same-time Information System (OASIS), 2019. Available from: <http://oasis.caiso.com/mrioasis/logon.do/>
4. Fink, M. *Testing the Value of Energy Efficiency in the Renewable Ramp Challenge*. Efficiency Vermont, 2017. p. 14.
5. *Unlocking Our Nation's Wind Potential*. U.S. Department of Energy Office of Energy Efficiency & Renewable Energy (EERE), May 15, 2019. Available from: <https://www.energy.gov/eere/articles/unlocking-our-nation-s-wind-potential/>
6. Neukomm, M., V. Nubbe, and R. Fares. *Overview of Research Challenges and Gaps*, in *Grid-Interactive Efficient Buildings Technical Report Series*. DOE/GO-102019-5227. U.S. Department of Energy Office of Energy Efficiency and Renewable Energy (EERE), 2019. p. 44.
7. *Standards and Codes: Net-Zero Energy, High Performance Buildings*. National Institute of Standards and Technology (NIST), 2011. Available from: <https://www.nist.gov/el/standards-and-codes-net-zero-energy-high-performance-buildings/>
8. *Criteria for the Passive House*, EnerPHit and PHI Low Energy Building Standard, version 9f. Passive House Institute, 2020. p. 27. Available from: [http://passiv.de/downloads/03\\_building\\_criteria\\_en.pdf/](http://passiv.de/downloads/03_building_criteria_en.pdf)
9. Tabares-Velasco P.C., A. Speake, M. Harris, A. Newman, T. Vincent, and M. Lanahan. A Modeling Framework for Optimization-Based Control of a Residential Building Thermostat for Time-of-Use Pricing. *Applied Energy*, vol. 242, 2019. p. 1346-1357.
10. *Commercial Building Energy Consumption Survey (CBECS) 2012*. U.S. Energy Information Administration (EIA), 2012. Available from: <https://www.eia.gov/consumption/commercial/>

11. *NETEnergy Partnerships*. NetEnergy, November 26, 2019. Available from: <http://www.netenergytes.com/#partnerships/>
12. *Energy Storage Grand Challenge*. U.S. Department of Energy (DOE), 2020. Available from: <https://www.energy.gov/energy-storage-grand-challenge/energy-storage-grand-challenge/>
13. Spector, J. *Ice Energy, Thermal Storage Evangelist, Files for Bankruptcy*. Greentech Media, February 7, 2020. Available from: <https://www.greentechmedia.com/articles/read/thermal-storage-evangelist-ice-energy-files-for-bankruptcy/>
14. *AHRI Standard 900: Performance Rating of Thermal Storage Equipment Used for Cooling*. Air-Conditioning Heating and Refrigeration Institute (AHRI), 2014. p. 68.
15. Willis, R. and B. Parsonnet. *Energy Efficient TES Designs for Commercial DX Systems*. ASHRAE 2010 Winter Conference, Orlando, FL. ASHRAE, 2010. p. 147-157.
16. MacCracken, M. *Thermal Energy Storage Myths*. ASHRAE Journal, vol. 45(9). 2003. p. 6.
17. Glazer, J. *ASHRAE Design Guide for Cool Thermal Storage: 2nd Edition*. ASHRAE, Atlanta, GA, 2019. p. 312.
18. Ulbig, A., and G. Andersson. *On Operational Flexibility in Power Systems*. 2012 IEEE Power and Energy Society General Meeting. San Diego, CA. Institute of Electrical and Electronics Engineers (IEEE), 2012. p. 8.
19. Ottesen, S., and A. Tomasgard. A Stochastic Model for Scheduling Energy Flexibility in Buildings. *Energy* vol. 88, 2015. p. 364-376.
20. Siebert, N., et al. *Scheduling Demand Response and Smart Battery Flexibility in a Market Environment: Results from the Reflexe Demonstrator Project*. 2015 IEEE Eindhoven PowerTech. Institute of Electrical and Electronics Engineers (IEEE), 2015. p. 6.
21. Alcázar-Ortega, M., C. Calpe, T. Theisen, and J.F. Carbonell-Carretero. Methodology for the Identification, Evaluation and Prioritization of Market Handicaps Which Prevent the Implementation of Demand Response: Application to European Electricity Markets. *Energy Policy* vol. 86, 2015. p. 529-543.
22. Hall, C. *Optimizing Ice Thermal Storage to Reduce Energy Cost*. UMI Number: 1557852. Masters Thesis, North Carolina A&T State University. ProQuest Dissertations Publishing, 2014. p. 104.

23. Song, X., L. Liu, T. Zhu, S. Chen, and Z. Cao. Study of Economic Feasibility of a Compound Cool Thermal Storage System Combining Chilled Water Storage and Ice Storage. *Applied Thermal Engineering* vol 133, 2018. p. 613-621.
24. Song, X., T. Zhu, L. Liu, and Z. Cao. Study on Optimal Ice Storage Capacity of Ice Thermal Storage System and Its Influence Factors. *Energy Conversion and Management* vol. 164, 2018. p. 288-300.
25. Sanaye, S, and A. Shirazi. Four E Analysis and Mmulti-Objective Optimization of an Ice Thermal Energy Storage for Air-Conditioning Applications. *International Journal of Refrigeration* vol 36, 2013. p. 828-841.
26. Abdullah, M.O., L.P. Yii, E. Junaidi, G. Tambi, and M.A. Mustapha. Electricity Cost Saving Comparison Due to Tariff Change and Ice Thermal Storage (ITS) Usage Based on a Hybrid Centrifugal-ITS System for Buildings: A University District Cooling Perspective. *Energy and Buildings* vol. 67, 2013 p. 70-78.
27. Henze, G. Evaluation of Optimal Control for Ice Storage Systems. UMI Number 9613262. PhD Thesis, University of Colorado. ProQuest Dissertations and Theses, 1995. p. 266.
28. Niu, J., Z. Tian, Y. Lu, and H. Zhao. Flexible Dispatch of a Building Energy System Using Building Thermal Storage and Battery Energy Storage. *Applied Energy* vol. 243, 2019. p. 274-287.
29. Cox, S.J., D. Kim, H. Cho, and P. Mago. Real Time Optimal Control of District Cooling System with Thermal Energy Storage Using Neural Networks. *Applied Energy* vol. 238, 2019. p. 466-480.
30. Van Asselt, A, D. Reindl, G. Nellis, and S. Klein. *Design and Utilization of Thermal Energy Storage to Increase the Ability of Power Systems to Support Renewable Energy Resources*. ASHRAE 1607-RP, ASHRAE, 2017. p. 174.
31. Henze, G.P., B. Biffar, D. Kohn, and M.P. Becker. Optimal Design and Operation of a Thermal Storage System for a Chilled Water Plant Serving Pharmaceutical Buildings. *Energy and Buildings* vol 40, 2008. p. 1004-1019.
32. Shan, K., C. Fan, and J. Wang. Model Predictive Control for Thermal Energy Storage Assisted Large Central Cooling Systems. *Energy* vol 179, 2019. p. 916-927.
33. Tang, R., S. Wang, and L. Xu. An MPC-Based Optimal Control Strategy of Active Thermal Storage in Commercial Buildings during Fast Demand Response Events in Smart Grids. *Energy Procedia* vol 158, 2019 p.2506-2511.

34. Powell, K.M., et al. Thermal Energy Storage to Minimize Cost and Improve Efficiency of a Polygeneration District Energy System in a Real-Time Electricity Market. *Energy* vol 113, 2016 p.52-63.
35. Chavez, P., and D. Stingelin. *Thermal Energy Storage New Mexico State University*. Rocky Mountain APPA, 2019. Available from: [http://rma.appa.org/wp-content/uploads/2019/09/RMA-2019\\_1-3-Thermal-Energy-Storage-System.pdf/](http://rma.appa.org/wp-content/uploads/2019/09/RMA-2019_1-3-Thermal-Energy-Storage-System.pdf/)
36. Kung, F., M. Deru, and E. Bonnema. *Evaluation Framework and Analyses for Thermal Energy Storage Integrated with Packaged Air Conditioning*. NREL/TP-5500-60415. National Renewable Energy Laboratory (NREL), October, 2013. p. 102.
37. Hunt, E. *Ice Energy Completes First Phase of Largest Distributed Thermal Storage System Installation in U.S.* Global News Wire, February 6, 2019. Available from: <https://www.globenewswire.com/news-release/2019/02/06/1711475/0/en/Ice-Energy-Completes-First-Phase-of-Largest-Distributed-Thermal-Storage-System-Installation-in-U-S.html/>
38. Henze G.P., M. Krarti, M.J. Brandemuehl. Guidelines for Improved Performance of Ice Storage Systems. *Energy and Buildings* vol. 35, 2003. p. 111-127.
39. Hirsch, J.J. *DOE-2.3: Building Energy Use and Cost Analysis Program*. Lawrence Berkeley National Laboratory (LBNL), Camarillo, CA, 2017. p. 293. Available from: <https://www.doe2.com/DOE2/>
40. *EnergyPlus 9.3.0*. U.S. Department of Energy (DOE), 2020. Available from: <http://energyplus.net/>
41. *TRACE Software Feature Comparison*. TRANE, 2019. Available from: <https://www.trane.com/commercial/north-america/us/en/products-systems/design-and-analysis-tools/analysis-tools/TRACE-Software-Feature-Comparison.html>
42. *TRNSYS Thermal Storage Components*. TRNSYS, 2003. Available from: <https://sel.me.wisc.edu/trnsys/trnlib/thermal.htm>
43. *TRNSYS - Official Website*. TRNSYS, 2017. Available from: <http://www.trnsys.com/>
44. *REopt Capabilities*. National Renewable Energy Laboratory (NREL), December 30, 2020. Available from: <https://reopt.nrel.gov/about/capabilities.html>
45. Montuori, L., M. Alcázar-Ortega, C. Álvarez-Bel, and A. Domijan. Integration of Renewable Energy in Microgrids Coordinated with Demand Response Resources: Economic Evaluation of a Biomass Gasification Plant by Homer Simulator. *Applied Energy* vol 132, 2014. p. 15-22.

46. *Distributed Energy Resources Customer Adoption Model (DER-CAM)*, Grid Integration Group. Lawrence Berkeley National Laboratory (LBNL), 2020. Available from: <https://gridintegration.lbl.gov/der-cam/>
47. *Microgrid Decision Support Platform*. Xendee, 2020. Available from: <http://xendee.com>
48. Naranjo Palacio, S., K.F. Valentine, M. Wong, and K.M. Zhang. Reducing Power System Costs with Thermal Energy Storage. *Applied Energy* vol 129, 2014. p. 228-237.
49. Hao, L., et al. Study of Operation Strategies for Integrating Ice-Storage District Cooling Systems into Power Dispatch for Large-Scale Hydropower Utilization. *Applied Energy* vol 261, 2020. p. 114477.
50. Heine, K., R. Meyer. *openstudio-load-flexibility-measures-gem*, version 0.3.1, National Renewable Energy Laboratory (NREL), 2021. Available from: <https://rubygems.org/gems/openstudio-load-flexibility-measures>
51. Heine, K., P.C. Tabares-Velasco, and M. Deru. Energy and Cost Assessment of Packaged Ice Energy Storage Implementations Using OpenStudio Measures. *Energy and Buildings* vol 248, 2021. p. 111189.
52. Le Varlet, T., et al. Comparative Life Cycle Assessment of Lithium-Ion Battery Chemistries for Residential Storage. *Journal of Energy Storage* vol 28, 2020. p. 101230.
53. Heine, K., A. Thatte, P.C. Tabares-Velasco. A Simulation Approach to Sizing Batteries for Integration with Net-Zero Energy Residential Buildings. *Renewable Energy* vol 139, 2019. p. 176-185.
54. Tam, A, D. Ziviani D, J.E. Braun, and N. Jain. Development and Evaluation of a Generalized Rule-Based Control Strategy for Residential Ice Storage Systems. *Energy and Buildings* vol 197, 2019. p. 99-111.
55. Torres-Toledo, V., K. Meissner, A. Coronas, and J. Müller. Performance Characterisation of a Small Milk Cooling System with Ice Storage for PV Applications. *International Journal of Refrigeration* vol 60, 2015. p. 81-91.
56. Selvnes, H., Y. Allouche, R.I. Manescu, and A. Hafner. Review on Cold Thermal Energy Storage Applied to Refrigeration Systems Using Phase Change Materials. *Thermal Science and Engineering Progress* vol 22, 2021. p. 100807.
57. Yokoyama, R. and K. Ito. Effect of Inlet Air Cooling by Ice Storage on Unit Sizing of a Gas Turbine Cogeneration Plant. *Journal of Engineering for Gas Turbines and Power* vol 126, 2004. p. 351-357.

58. Cole W.J., J.D. Rhodes, K.M. Powell, and T.F. Edgar. Turbine Inlet Cooling with Thermal Energy Storage. *International Journal of Energy Research* vol 38, 2014. p. 151-161.
59. Singh, R.P., J.Y. Sze, S.C. Kaushik, D. Rakshit, and A. Romagnoli. Thermal Performance Enhancement of Eutectic PCM Laden with Functionalised Graphene Nanoplatelets for an Efficient Solar Absorption Cooling Storage System. *Journal of Energy Storage* vol 33, 2021. p. 102092.
60. Pirvaram, A., S.M. Sadrameli, and L. Abdolmaleki. Energy Management of a Household Refrigerator Using Eutectic Environmental Friendly PCMs in a Cascaded Condition. *Energy* vol 181, 2019. p. 321-330.
61. Hussain, S.I., R. Dinesh, A.A. Roseline, S. Dhivya, and S. Kalaiselvam. Enhanced Thermal Performance and Study the Influence of Sub-cooling on Activated Carbon Dispersed Eutectic PCM for Cold Storage Applications. *Energy and Buildings* vol 143, 2017. p. 17-24.
62. Kumano, H., T. Asaoka, A. Saito, and S. Okawa. Study on Latent Heat of Fusion of Ice in Aqueous Solutions. *International Journal of Refrigeration* vol 30, 2007. p. 267-273.
63. *BioPCM®*. Phase Change Solutions, 2021. Available from: <https://phasechange.com/biopcm/>
64. *NETEnergy Partnerships*. NetEnergy, November 26, 2019. Available from: <http://www.netenergytes.com/#partnerships/>
65. Narayanamurthy, R. *Thermal Energy Storage and Cooling System with Secondary Refrigerant Isolation*. Patent F25D 3/00 (20060101) held by Ice Energy Holdings, Inc. U.S. Patent and Trademark Office, 2010.
66. Phelan, P.E., R. Calhoun, S. Trimble, J.E. Baker, and J. Sherbeck. *Heat-Pump-Based Thermal Storage for Intermittent Electrical and Thermal Sources*. ASME/JSME 2011 8th Thermal Engineering Joint Conference. Honolulu, Hawaii, 2011.
67. *OpenStudio 2.9.1*. U.S. Department of Energy (DOE), 2019. Available from: <https://openstudio.net>
68. *Building Controls Virtual Test Bed 1.6.0*. Lawrence Berkley National Laboratory (LBNL), 2012. Available from: <https://simulationresearch.lbl.gov/bcvtb/>
69. *Functional Mock-up Interface*. FMI Standard, 2021. Available from: <https://fmi-standard.org/>

70. Heine, K., R. Meyer. *openstudio-load-flexibility-measures-gem*, version 0.1.2, National Renewable Energy Laboratory (NREL), 2020. Available from: <https://rubygems.org/gems/openstudio-load-flexibility-measures>
71. Heine, K., P.C. Tabares-Velasco, M. Deru, and B. Polly. *Quantifying the Value of Unitary Thermal Energy Storage Systems (UTSS): A Modelling Study*. Building Simulation 19, Rome, Italy. IBPSA, 2019. p. 8.
72. Parker, A., et al. *openstudio-standards*, version 0.2.11, National Renewable Energy Laboratory, 2020. Available from: <https://rubygems.org/gems/openstudio-standards/>
73. *Weather Data | EnergyPlus*. U.S. Department of Energy (DOE), 2020. Available from: <https://energyplus.net/weather/>
74. *ASHRAE Handbook: Fundamentals*. ASHRAE, Atlanta, GA, 2017.
75. Heine, K., P.C. Tabares-Velasco, and M. Deru. Design and Dispatch Optimization of Packaged Ice Storage Systems Within a Connected Community. *Applied Energy* vol 298, 2021. p. 117147.
76. *Rates & Pricing Choices*. Southern California Edison, 2020. Available from: <https://www.sce.com/regulatory/tariff-books/rates-pricing-choices>
77. *Business price plans*. Salt River Project, 2020. Available from: <https://www.srpnet.com/menu/electricbiz/priceplans.aspx>
78. *Electricity for West Texas and Southern New Mexico | El Paso Electric | Texas Rate Tariffs*. El Paso Electric, August 12, 2020. Available from: <https://www.epelectric.com/business/customer-service/business-rates-and-information/texas-rate-tariffs-rules-and-regulations/texas-rate-tariffs>
79. *Average Price of Electricity to Ultimate Consumers by End-Use Sector in Electric power Monthly*. U.S. Energy Information Administration, 2020. Available from: [https://www.eia.gov/electricity/monthly/epm\\_table\\_grapher.php?t=epmt\\_5\\_6\\_a](https://www.eia.gov/electricity/monthly/epm_table_grapher.php?t=epmt_5_6_a)
80. Kamal, R., F. Moloney, C. Wickramaratne, A. Narasimhan, and G.Y. Goswami. Strategic Control and Cost Optimization of Thermal Energy Storage in Buildings Using EnergyPlus. *Applied Energy* vol 246, 2019. p. 77-90.
81. Yin, R., D. Black, M. Piette, and K. Schiess. *Control of Thermal Energy Storage in Commercial Buildings for California Utility Tariffs and Demand Response*. Final Report for Contract No.500-03-026. Lawrence Berkeley National Laboratory (LBNL), 2015. p. 98.

82. Le Dréau, J. and P. Heiselberg. Energy Flexibility of Residential Buildings Using Short Term Heat Storage in the Thermal Mass. *Energy* vol 111, 2016. p. 991-1002.
83. Heine, K., P.C. Tabares-Velasco, R. Meyer, and M. Deru. *Modeling the Load Flexibility Potentials for Ice Energy Storage*. 2020 Building Performance Analysis Conference and SimBuild. Chicago, IL. ASHRAE and IBPSA-USA, 2020. p. 8.
84. *Commerical Building Energy Consumption Survey (CBECS) 2018*. U.S. Energy Information Administration (EIA), 2028. Available from: <https://www.eia.gov/consumption/commercial/>
85. Heine, K., P.C. Tabares-Velasco, and M. Deru. Design and Dispatch Optimization of Packaged Ice Storage Systems Within a Connected Community. *Applied Energy* vol 298, 2021. p. 117147.
86. Bowers, R. *Updated Renewable Portfolio Standards Will Lead to More Renewable Electricity Generation*. Today in Energy, February 27, 2019. Available from: <https://www.eia.gov/todayinenergy/detail.php?id=38492/>
87. Jingjing, L., R. Yin, M. Pritoni, A.M. Piette, and M. Neukomm. *Developing and Evaluating Metrics for Demand Flexibility in Buildings: Comparing Simulations and Field Data*. ACEEE Summer Study, 2020. p. 15. Available from: <https://buildings.lbl.gov/publications/developing-and-evaluating-metrics/>
88. Lanahan, M., S. Engert, T. Kim, and P.C. Tabares-Velasco. Rapid Visualization of the Potential Residential Cost Savings from Energy Storage Under Time-of-Use Electric Rates. *Journal of Building Performance Simulation* vol 12, 2019. p. 68-81.
89. Chen, Y., P. Xu, J. Gu, F. Schmidt, and W. Li. Measures to Improve Energy Demand Flexibility in Buildings for Demand Response (DR): A Review. *Energy and Buildings* vol 177, 2018. p. 125-39.
90. *Fact Sheet: Grid-interactive Efficient Buildings*. U.S. Department of Energy Office of Energy Efficiency and Renewable Energy (EERE), 2019. p. 2. Available from: <https://www.energy.gov/sites/default/files/2019/04/f62/bto-geb-factsheet-41119.pdf>
91. Taylor, R.D. *Development of an Integrated Building Energy Simulation with Optimal Central Plant Control*. UMI Number 9702682. PhD Thesis, University of Illinois at Urbana-Champagn. ProQuest Dissertations, 1996. p. 211.
92. Chaichana, C., W. Charters, and L. Aye. An Ice Thermal Storage Computer Model. *Applied Thermal Engineering* vol 21, 2001. p. 1769-1778.

93. Ruan, Y., Q. Liu, Z. Li, and J. Wu. Optimization and Analysis of Building Combined Cooling, Heating and Power (BCHP) Plants with Chilled Ice Thermal Storage System. *Applied Energy* vol 179, 2016. p. 738-754.
94. Monsef, H. and M. Yari. Design and Analysis of an Ice Thermal Storage System for Residential Air-Conditioning Applications. *International Journal of Exergy* vol 20, 2016. p. 122-38.
95. Van Asselt, A. *Model Predictive Control of Cool Thermal Energy Storage Under Different Electricity Rate Structures*. 2019 ASHRAE Annual Conference. Kansas City, MO. ASHRAE, 2019. p. 8.
96. Augusto, G.L., A.B. Culaba, and A.B. Maglaya. Identification of Design Criteria for District Cooling Distribution Network with Ice Thermal Energy Storage System. *Energy Procedia* vol 79, 2015.p. 233-238.
97. Mazzoni, S., et al. A Techno-Economic Assessment on the Adoption of Latent Heat Thermal Energy Storage Systems for District Cooling Optimal Dispatch & Operations. *Applied Energy* vol 289, 2021. p. 116646.
98. Massie, D.D. *Optimal Neural Network-Based Controller for Ice Storage Systems*. UMI Number 9827745. PhD Thesis, University of Colorado. ProQuest Dissertations, 1998. p. 171.
99. Al Rifaie, F. *An Integrated Approach to Optimally Design and Operate Ice Thermal Storage for Typical HVAC Systems*. ProQuest Number 10285599. PhD Thesis, North Carolina A&T State University. ProQuest Dissertations, 2017.
100. *IceBank Energy Storage Installations*. CALMAC., 2020. Available from: <http://www.calmac.com/featured-energy-storage-installations/>
101. Jones A.T. and D.P. Finn. Co-Simulation of a HVAC System-Integrated Phase Change Material Thermal Storage Unit. *Journal of Building Performance Simulation* vol 10, 2017. p. 313-325.
102. Spector, J. *Ice Energy, Thermal Storage Evangelist, Files for Bankruptcy*. Greentech Media, February 7, 2020. Available from: <https://www.greentechmedia.com/articles/read/thermal-storage-evangelist-ice-energy-files-for-bankruptcy/>
103. Heine, K., P.C. Tabares-Velasco, and M. Deru. Energy and Cost Assessment of Packaged Ice Energy Storage Implementations Using OpenStudio Measures. *Energy and Buildings* vol 248, 2021. p. 111189.

104. Barbour, E., D. Parra, Z. Awwad, and M.C. González. Community Energy Storage: A Smart Choice for the Smart Grid? *Applied Energy* vol 212, 2018. p. 489-97.
105. Jones, E.C. and B.D. Leibowicz. Co-Optimization and Community: Maximizing the Benefits of Distributed Electricity and Water Technologies. *Sustainable Cities and Society* vol 64, 2021. p. 102515.
106. Cole, W.J. *Dynamic Modeling, Optimization, and Control of Integrated Energy Systems in a Smart Grid Environment*. PhD Thesis, University of Texas. 2014. p. 194.
107. Cole, W.J., et al. Community-Scale Residential Air Conditioning Control for Effective Grid Management. *Applied Energy* vol 130, 2014. p. 428-436.
108. *REopt Capabilities*. National Renewable Energy Laboratory (NREL), December 30, 2020. Available from: <https://reopt.nrel.gov/about/capabilities.html>
109. *URBANopt SDK Documentation*. National Renewable Energy Laboratory (NREL), 2021. Available from: <https://docs.urbanopt.net/>
110. *HOMER - Hybrid Renewable and Distributed Generation System Design Software*. Homer Energy Inc, 2021. Available from: <https://www.homerenergy.com/index.html/>
111. Christians M. Email Correspondence with P.C. Tabares-Velasco, 2020. p. 2.
112. *Commercial Prototype Building Models | Building Energy Codes Program*. U.S. Department of Energy (DOE), 2020. Available from: <https://www.energycodes.gov/prototype-building-models/>
113. Goldwasser, D. and N. Long. *openstudio-common-measures-gem. 0.2.0*. National Renewable Energy Laboratory (NREL), 2020. Available from: <https://rubygems.org/gems/openstudio-common-measures/>
114. Parker, A., et al. *openstudio-standards. 0.2.14*. National Renewable Energy Laboratory (NREL), 2021. Available from: <https://rubygems.org/gems/openstudio-standards/>
115. Parsonnet, B., R. Willis, and D.L. Wiersma. System and Method for Liquid-Suction Heat Exchange Thermal Energy Storage. Patent Number 20130145780 held by Ice Energy Inc. U.S. Patent and Trademark Office, 2013.
116. Tan, P., et al. Thermal Energy Storage Using Phase Change Materials: Techno-Economic Evaluation of a Cold Storage Installation in an Office Building. *Applied Energy* vol 276, 2020. p. 115433.

117. *Database of State Incentives for Renewables & Efficiency® - DSIRE*. NC Clean Energy Technology Center, 2019. Available from: <https://www.dsireusa.org/>
118. Benders, J.F.. Partitioning Procedures for Solving Mixed-Variables Programming Problems. *Numerische Mathematik* vol 4, 1962. p. 238-52.
119. *IBM ILOG CPLEX Optimization Studio v.12.10: Benders algorithm*. IBM, 2014. Available from: [https://www.ibm.com/support/knowledgecenter/SSSA5P\\_12.10.0/ilog.odms.cplex.help/CPLEX/UsrMan/topics/dscr\\_optim/benders/introBenders.html](https://www.ibm.com/support/knowledgecenter/SSSA5P_12.10.0/ilog.odms.cplex.help/CPLEX/UsrMan/topics/dscr_optim/benders/introBenders.html)
120. Good, N., L. Zhang, A. Navarro-Espinosa, and P. Mancarella. High Resolution Modelling of Multi-Energy Domestic Demand Profiles. *Applied Energy* vol 137, 2015 p. 193-210.
121. Lu, S., et al. High-Resolution Modeling and Decentralized Dispatch of Heat and Electricity Integrated Energy System. *IEEE Transactions on Sustainable Energy* vol 11, 2020. p. 1451-1463.
122. *OpenStudio 3.2*. U.S. Department of Energy (DOE), 2021. Available from: <https://openstudio.net>
123. *AMPL | Streamlined Modeling for Real Optimization*. AMPL Optimization Inc, 2016. Available from: <https://ampl.com>
124. *How Thermal Energy Storage Works*. CALMAC, 2020. Available from: <http://www.calmac.com/how-energy-storage-works>
125. *Measure Writer's Reference Guide in OpenStudio SDK User Docs*. National Renewable Energy Laboratory (NREL), 2021. Available from: [https://nrel.github.io/OpenStudio-user-documentation/reference/measure\\_writing\\_guide/](https://nrel.github.io/OpenStudio-user-documentation/reference/measure_writing_guide/)
126. *EnergyPlus 9.5.0 Documentation: Engineering Reference*: U.S. Department of Energy (DOE), 2021. p. 1767.
127. *IBM CPLEX Optimizer – United States*. IBM, 2021. Available from: <https://www.ibm.com/products/ilog-cplex-optimization-studio>
128. *Gurobi - The fastest solver*. Gurobi Optimization LLC, 2021. Available from: <https://www.gurobi.com/>
129. Stovall, T. *CALMAC Ice Storage Test Report*. ORNL/TM-11582. Oak Ridge National Laboratory, 1991. p. 54.

130. Henze, G. and M. Krarti. *Predictive Optimal Control of Active and Passive Building Thermal Storage Inventory*. Final Report for Cooperative Agreement DE-FC26-01NT41255, University of Nebraska, 2005. p. 123. Available from: <https://www.osti.gov/biblio/894509-GH9Mqf/>
131. King, D.J. and R.A. Potter Jr.. Description of a Steady-State Cooling Plant Model Developed for Use in Evaluating Optimal Control of Ice Thermal Energy Storage Systems. *ASHRAE Transactions* vol 104, 1998. p. 12.
132. Fathollahzadeh, M.H and P.C. Tabares-Velasco. Electric Demand Minimization of Existing District Chiller Plants with Rigid or Flexible Thermal Demand. *Applied Energy* vol 289, 2021. p. 116664.
133. *Model C Tank Specs and Drawings*. CALMAC, 2020. Available from: <http://www.calmac.com/icebank-energy-storage-model-c?showSpecs/>
134. *FirstPass: Ice Bank Energy Storage Analyzer*. CALMAC, 2019. Available from: <https://www.trane.com/commercial/north-america/us/en/products-systems/design-and-analysis-tools/trane-design-tools.html/>
135. *Generator Specifications: TWD1672-1673GE*. Volvo Penta, 2017. p. 2. Available from: <https://www.volvopenta.com/en-us/industrial/power-generation/>
136. Fathollahzadeh, M. *Integrated Framework for Modeling and Optimizatoin of Commercial District Cooling Systems*. PhD Thesis, Colorado School of Mines. ProQuest Dissertations, 2021.
137. *Fuel Properties Comparison*. Clean Cities: Alternative Fuels Data Center, U.S. Department of Energy, 2021. p. 3. Available from: [https://afdc.energy.gov/files/u/publication/fuel\\_comparison\\_chart.pdf](https://afdc.energy.gov/files/u/publication/fuel_comparison_chart.pdf)
138. *Retail Prices for Diesel (On-Highway) - All Types*. U.S. Energy Information Administratoin (EIA), June 7, 2021. Available from: [https://www.eia.gov/dnav/pet/pet\\_pri\\_gnd\\_a\\_epd2d\\_pte\\_dpgal\\_a.htm/](https://www.eia.gov/dnav/pet/pet_pri_gnd_a_epd2d_pte_dpgal_a.htm/)
139. *Motor Fuel Tax*. Legislative Council Staff: Colorado General Assembly; 2021. Available from: <https://leg.colorado.gov/agencies/legislative-council-staff/motor-fuel-tax%C2%A0/>
140. *Colorado Interruptible Service Option Credit (ISOC) Information Sheet*. Xcel Energy Inc., 2020. Available from: <https://www.xcelenergy.com/staticfiles/xcel-responsive/Admin/Managed%20Documents%20&%20PDFs/CO-Business-ISOC-Information-Sheet.pdf>

141. *Rate Schedue E-32TOU L*. Arizona Public Service Company, 2017. p. 6. Available from: [https://www.aps.com/-/media/APS/APSCOM-PDFs/Utility/Regulatory-and-Legal/Regulatory-Plan-Details-Tariffs/Business/TOU-Business-NonRes-Plans/e32\\_TimeOfUseLarge.ashx?la=en](https://www.aps.com/-/media/APS/APSCOM-PDFs/Utility/Regulatory-and-Legal/Regulatory-Plan-Details-Tariffs/Business/TOU-Business-NonRes-Plans/e32_TimeOfUseLarge.ashx?la=en)
142. *Rate Rider CPP-GS*. Arizona Public Service Company; 2017. p. 2. Available from: [https://www.aps.com/-/media/APS/APSCOM-PDFs/Utility/Regulatory-and-Legal/Regulatory-Plan-Details-Tariffs/Business/Rate-Riders/cpp-gen\\_CriticalPeakPricingRateRider.ashx?la=en](https://www.aps.com/-/media/APS/APSCOM-PDFs/Utility/Regulatory-and-Legal/Regulatory-Plan-Details-Tariffs/Business/Rate-Riders/cpp-gen_CriticalPeakPricingRateRider.ashx?la=en)
143. Cole, W., S. Corcoran, N. Gates, T. Mai, and P. Das. *2020 Standard Scenarios Report: A U.S. Electricity Sector Outlook*. NREL/TP-6A20-77442. National Renewable Energy Laboratory (NREL), November, 2020.
144. *Cambium: Scenario Viewer and Data Downloader*. National Renewable Energy Laboratory (NREL), 2020. Available from: <https://cambium.nrel.gov/>
145. *ComStock Analysis Tool*. National Renewable Energy Laboratory (NREL), 2021. Available from: <https://comstock.nrel.gov/>
146. *ResStock Analysis Tool*. National Renewable Energy Laboratory (NREL), 2021. Available from: <https://resstock.nrel.gov/>

## APPENDIX A

### OPENSTUDIO MEASURES FOR PACKAGED AND CENTRAL ICE THERMAL ENERGY STORAGE SIMULATION IN ENERGYPLUS

This appendix contains the code repository references for two OpenStudio measures used to simulate ice thermal energy storage systems using the EnergyPlus building energy simulation engine. Both measures have been integrated into the OpenStudio Load Flexibility Measures gem, available for download at <https://rubygems.org/gems/openstudio-load-flexibility-measures>. Each measure is actively maintained under a National Renewable Energy Laboratory code repository found at <https://github.com/NREL/openstudio-load-flexibility-measures-gem>, where the latest unpublished code revisions and complete documentation can be found.

## APPENDIX B

### CODE FOR CTES OPTIMIZATION IN A CONNECTED COMMUNITY

This appendix contains the code required to execute the optimization program for the integrated CTES workflow using AMPL, including the model, data, and run files. These files, as well as the Python pre-processing scripts and auxiliary OpenStudio measures, are also publicly available online at the GitHub repository [https://github.com/x92499/ctes\\_opt](https://github.com/x92499/ctes_opt).

#### B.1 Model file: `integrated.mod`

```
# Central TES Optimization Formulation
# Karl Heine, Colorado School of Mines, kheine@mines.edu
# March 16, 2021
# Revised May 3, 2021
# Revised July 1, 2021

#-----
# Model File
#-----
# integrated.mod

## Parameters-----
# Set defining values
param D >= 0; # number of demand periods
param I >= 1; # number of CTES types (1=UTSS, 2=Central)
param N >= 1; # number of RTUs or plant loops
param S{1..Ns} >= 1; # number of segments in chiller curve linearization
param T >= 1; # number of timesteps
param Td_ct{1..D} >= 0; # number of ts in each demand period
param Td_v{d in 1..D, 1..Td_ct[d]} >= 0; # values which populate indexed set
Td
param TYf_ct{1..N} >= 0; # number of ts when full storage is possible
param TYf_v{n in 1..N, 1..TYf_ct[n]} >= 0; # values which populate indexed
set TYf
param TYp_ct{1..N} >= 0; # number of ts when partial-storage possible
param TYp_v{n in 1..N, 1..TYp_ct[n]} >= 0; # values which populate indexed
set TYp
param Tr_ct >= 0; # number of ts when DR events are occurring
param Tr_v{1..Tr_ct} >= 0; # values which populate indexed set Tr

# Sets
set Td{1..D} default {}; # set of ts for each demand period
set TYf{1..N} default {}; # set for full storage possible ts
set TYp{1..N} default {}; # set for partial storage possible ts
set Tr default {}; # set for demand response timesteps

# Building simulation Parameters
param l{1..N, 1..T} >= 0; # cooling load met by RTU or chiller [kWth]
param pN{1..N, 1..T} >= 0; # baseline RTU or chiller power (ts avg) [kWe]
param p{1..T} >= 0; # baseline power demand for all buildings (ts avg) [kWe]
```

```

# Thermal storage parameters
param etaI{1..N, 1..T} >= 0, default 0.9975; # timestep loss rate (5% per
day)
param epsilon{1..N} >= 0, default 0.95; # discharge effectiveness [-]
param lambdaX{1..N, 1..T}; # charging energy slopes [kWe/kWth]
param lambdaY{n in 1..N, 1..S[n], 1..T}; # partial storage discharge curve
slopes [kWe/kWth]
param lbar{n in 1..N, 1..S[n], 1..T} >= 0; # limits for each partial storage
curve segment [kWth]
param qNX{1..N, 1..T} >= 0; # max rate of charge by chiller [kWth]
param qIX{1..I} >= 0; # max rate of charging for CTES [kWth]
param qIY{1..N, 1..T} >= 0; # max rate of discharging for CTES [kWth]
param qbar{1..I} >= 0; # nominal (usable) capacity of the CTES [kWth]

# Cost parameters
param c_d{1..D}; # cost of electric power in demand period [$/kW(max)]
param c_e{1..T}; # cost of electric energy at each timestep [$/kWh]
param c_r{Tr}; # cost of electric energy during demand response timesteps
param k{1..I} >= 0; # capacity cost of storage by type and plant [$/kWh_t]

# Miscellaneous parameters
param delta > 0, <= 1; # timestep [hr]
param yrs{1..I} >= 0, default 20; # expected lifespan of TES [years]
param zbar{1..I, 1..N} >= 0, integer; # maximum number of CTES I at plant N

## Variables-----
# Integer variables
var alpha{n in 1..N, t in TYf[n]} binary; # 1 iff. full storage mode
var Z{i in 1..I, n in 1..N} >= 0, <= zbar[i,n], integer; # Number of CTES

# Continuous variables
var LX{1..N, 1..T} >= 0; # charging load added [kW_th]
var LYf{n in 1..N, TYf[n]} >= 0; # discharging load reduced via full storage
[kW_th]
var LYp{n in 1..N, 1..S[n], TYp[n]} >= 0; # discharging load reduced via
partial storage [kW_th]
var Pd{1..D} >= 0; # max power demand [kW_e (max)]
var P{1..T} >= 0; # power demand (all buildings) [kW_e]
var PX{1..N, 1..T} >= 0; # power increase from charging [kW_e]
var PYf{n in 1..N, TYf[n]} >= 0; # power decrease from partial storage
[kW_e]
var PYp{n in 1..N, TYp[n]} >= 0; # power decrease from full storage [kW_e]
var Q{1..N, 1..T} >= 0; # TES energy inventory [kWh_th]

## Objective-----
minimize annual_cost: (sum{t in 1..T} 1.31 * c_e[t] * delta * P[t]) + (sum{d
in 1..D} c_d[d] * Pd[d]) + (sum{i in 1..I} (k[i] * qbar[i] / yrs[i] * sum{n
in 1..N} Z[i,n]));

## Constraints-----
# charging
s.t. charge_limit_ctes {n in 1..N, t in 1..T}: LX[n,t] <= sum{i in 1..I}
qIX[i] * Z[i,n];
s.t. charge_limit_plant {n in 1..N, t in 1..T}: LX[n,t] <= qNX[n,t];

# discharging - full storage

```

```

s.t. discharge_full_load {n in 1..N, t in TYf[n]}: LYf[n,t] = l[n,t] *
alpha[n,t];
s.t. discharge_full_rate {n in 1..N, t in TYf[n]}: LYf[n,t] <= sum{i in 1..I}
qIY[n,t] * Z[i,n];

# discharging - partial storage
s.t. discharge_part_load {n in 1..N, s in 1..S[n], t in TYp[n]}: LYp[n,s,t]
<= (if t in TYf[n] then ((1-alpha[n,t]) * lbar[n,s,t]) else lbar[n,s,t]);
s.t. discharge_part_rate {n in 1..N, t in TYp[n]}: sum{s in 1..S[n]}
LYp[n,s,t] <= sum{i in 1..I} qIY[n,t] * Z[i,n];

# inventory (kWth avail at end of timestep)
s.t. tank_inventory{n in 1..N, t in 1..T: t>1}: Q[n,t] = etaI[n,t] * Q[n,t-1]
+ delta * (LX[n,t] - (if t in TYp[n] then (sum{s in 1..S[n]} LYp[n,s,t] - (if
t in TYf[n] then LYf[n,t] else 0)) else 0));
s.t. max_soc {n in 1..N, t in 1..T}: Q[n,t] <= sum{i in 1..I} qbar[i] *
Z[i,n];
s.t. soc_full {n in 1..N, t in TYf[n]: t>1}: delta * LYf[n,t] <= etaI[n,t] *
Q[n,t-1];
s.t. soc_part {n in 1..N, t in TYp[n]: t>1}: delta * sum{s in 1..S[n]}
LYp[n,s,t] <= etaI[n,t] * Q[n,t-1];
s.t. init_soc {n in 1..N}: Q[n,1] = 0;

# energy conversion
s.t. pwr_part {n in 1..N, t in TYp[n]}: PYp[n,t] <= epsilon[n] * (sum{s in
1..S[n]} lambdaY[n,s,t] * LYp[n,s,t]);
s.t. pwr_full {n in 1..N, t in TYf[n]}: PYf[n,t] <= epsilon[n] * pN[n,t] *
alpha[n,t];
s.t. pwr_charge {n in 1..N, t in 1..T}: PX[n,t] >= lambdaX[n,t] * LX[n,t];
s.t. profile {t in 1..T}: P[t] >= p[t] + sum{n in 1..N} (PX[n,t] - (if t in
TYp[n] then (PYp[n,t] - (if t in TYf[n] then PYf[n,t] else 0)) else 0));
s.t. peak_demand {d in 1..D, t in Td[d]}: Pd[d] >= P[t];

# prevent full storage operation except during DR events - used for testing
to arbitrarily eliminate binary options
# s.t. no_full {n in 1..N, t in TYf[n]: t not in Tr}: alpha[n,t] <= 0;

# enforce 200kW reduction for CPP events
# s.t. cpp {t in Tr}: P[t] <= p[t] - 200;

```

## B.2 Data file: integrated.dat

```

# Integrated Optimization Formulation Data Read-in
# Karl Heine, Colorado School of Mines, kheine@mines.edu
# March 16, 2021
# Revised June, 2021

#-----
# Data File
#-----
# integrated.dat

# Set fixed parameter data

```

```

read D, I, N, T, {d in 1..D} Td_ct[d], {n in 1..N} TYf_ct[n], {n in 1..N}
TYp_ct[n], Tr_ct, delta, {i in 1..I} yrs[i], {n in UTSS} zbar[1,n], {d in
1..D} c_d[d] < fixed_params.dat;

# Set thermal storage parameters
let {n in 1..N, t in 1..T} etaI[n,t]:= 2.718281828459^(-0.5129 / 24 * delta);
# timestep loss rate (5% per day)
let {n in UTSS} epsilon[n]:= 0.93;
let {n in Central} epsilon[n]:= 0.95;

# Set S and zbar values
let {n in UTSS} S[n]:= 1;
let {n in Central} S[n]:= 3;
let {n in Central} zbar[1,n]:= 0;
let {n in UTSS} zbar[2,n]:= 0;
let {n in Central} zbar[2,n]:= 10;

# Set CTES cost parameters
let k[1]:= 75.19; # $/kWh_t for UTSS
let k[2]:= 39.81; # $/kWh_t for Central

# Set CTES capacities
let qbar[1]:= 133;
let qbar[2]:= 570;

param filename symbolic;
## Read parameter sets for each chiller:
for {n in 1..N} {
# read baseline cooling load profiles for each cooler
let filename:="l" & n & ".dat";
read {t in 1..T} l[n,t] < (filename);
# read baseline cooler electric demand profiles
let filename:="pN" & n & ".dat";
read {t in 1..T} pN[n,t] < (filename);
# read slopes for charging
let filename:="lambdaX" & n & ".dat";
read {t in 1..T} lambdaX[n,t] < (filename);
# read slopes for partial storage cooler discharge curves
let filename:="lambdaY" & n & ".dat";
read {t in 1..T, s in 1..S[n]} lambdaY[n,s,t] < (filename);
# read limits for partial storage discharge curve segments
let filename:="lbar" & n & ".dat";
read {t in 1..T, s in 1..S[n]} lbar[n,s,t] < (filename);
# read max rate of cooler charging
let filename:="qNX" & n & ".dat";
read {t in 1..T} qNX[n,t] < (filename);
# read max discharging rates for each CTES
let filename:="qIY" & n & ".dat";
read {t in 1..T} qIY[n,t] < (filename);

# read indexed set values
let filename:="Tsets" & n & ".dat";
read {t in 1..TYf_ct[n]} TYf_v[n,t], {t in 1..TYp_ct[n]} TYp_v[n,t] <
(filename);
}

```

```

# Set the qIX limit for each CTES system
let qIX[1]:= 20; # Arbitrary limit ~ 6 tons
let qIX[2]:= 71;# This is ~20 tons per tank charging rate (CALMAC data point)

# Read Electricity Rate Data
read {d in 1..D, t in 1..Td_ct[d]} Td_v[d,t] < Td.dat;
read {t in 1..T} c_e[t] < cost_elecCambium.dat;

# Read Baseline Power Profile
read {t in 1..T} p[t] < p.dat;

# Read Demand Response Timesteps Data
read {t in 1..Tr_ct} Tr_v[t] < TrCambium.dat;

# Populate Sets
let Tr:= setof {t in 1..Tr_ct} Tr_v[t];
for {n in 1..N} {
let TYf[n]:= setof {t in 1..TYf_ct[n]} TYf_v[n,t];
let TYp[n]:= setof {t in 1..TYp_ct[n]} TYp_v[n,t];
}
for {d in 1..D} {
let Td[d]:= setof {t in 1..Td_ct[d]} Td_v[d,t];
}

```

### B.3 Run file: integrated.run

```

# CTES Optimization Formulation
# Karl Heine, Colorado School of Mines
# March 18, 2021
# Revised July 1, 2021

#-----
# Run File
#-----
# ctes.run

# Set applicable storage types
set UTSS = 3..25;
set Central = 1..2;

model integrated.mod;
data integrated.dat;

# Begin Run Logging
option log_file 'runlog.out';

# Set Options
option solver gurobi;
option gurobi_options 'mipgapabs=100 logfile=runlog.out';

option display_round 0;

param e_bill >= 0;
param d_bill >= 0;
param capex >= 0;

```

```

# Solve
solve;

let e_bill:= ( sum{t in 1..T} c_e[t] * delta * P[t] );
let d_bill:= ( sum{d in 1..D} c_d[d] * Pd[d] );
let capex:= ( sum{i in 1..I} (k[i] * qbar[i] / yrs[i] * sum{n in 1..N}
Z[i,n]) );

option print_round 2;
display annual_cost, Z, sum{i in 1..I, n in 1..N} Z[i,n], e_bill, d_bill,
capex > soln.out;
print{t in 1..T}: P[t] > P.out;
print{d in 1..D}: Pd[d] > P_hat.out;
print{t in 1..T}: {n in 1..N} Q[n,t] > Q.out;

option print_round 0;
display annual_cost, Z;

option log_file;
exit;

```

APPENDIX C  
PERMISSION FROM PUBLISHERS

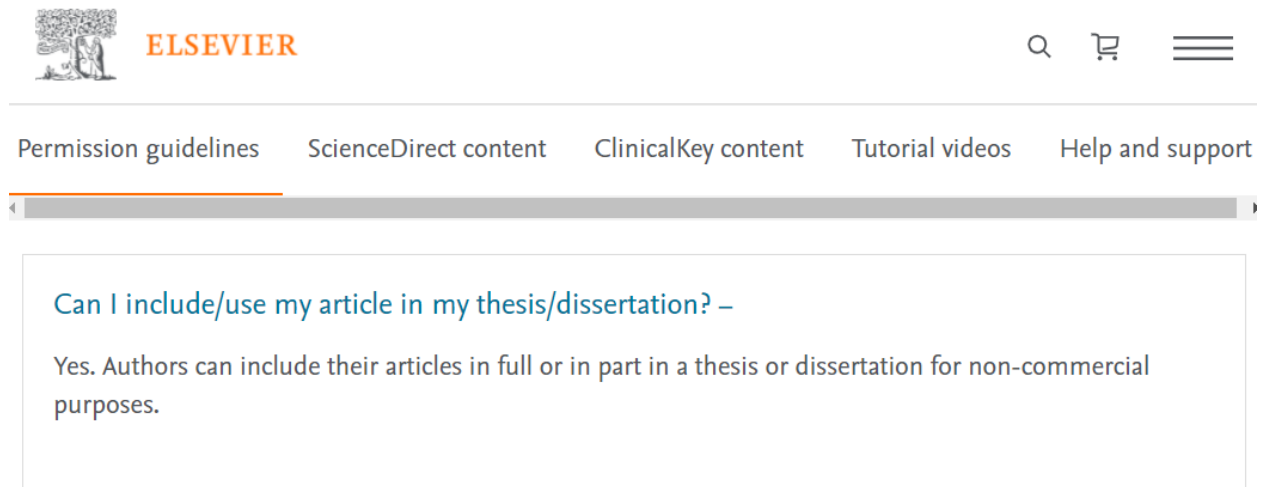


Figure C-1: Elsevier permission to re-use published content in a thesis

ASHRAE retains **exclusive copyright** of papers published as part of the ASHRAE Winter or Annual Conference Papers via the [ASHRAE Technology Portal](#) and in *ASHRAE Transactions*. Works published by ASHRAE are final and complete works.

Under ASHRAE copyright policies, authors retain the right for certain **specific uses** of their paper without requesting ASHRAE's permission. Only the "as published" version of the paper may be used by the author. These uses are as follows:

- to make copies of the paper for their own **personal use**;
- to **make copies and distribute copies** of the paper to researchers or customers of the author's employer for the personal use by such researchers or customers;
- to post the paper as published by ASHRAE on the author's personal, institutional, or corporate website or server with a link to [ASHRAE's website](#);
- to present the paper (after ASHRAE publication) at a meeting or conference and to distribute copies of such paper to the delegates attending the meeting with written permission from ASHRAE;
- to allow use of the paper by the author's employer for posting on the employer's website, for use by the employer in training or educational courses offered by the employer, for internal research work that is conducted by the employer, and for internal publications published by the employer;
- to include the paper in full or in part in a thesis or dissertation;
- to include the paper in a printed compilation of works of the author, such as collected writings or lecture notes; and
- to prepare other derivative works, such as extending the paper into book-length form, or to otherwise re-use portions or excerpts in other works, providing there is acknowledgement of its publication by ASHRAE.

Other uses must be authorized by ASHRAE. Authors should contact [ASHRAE](#) explaining their specific need and identifying the paper and ASHRAE publication in which the paper appeared.

Others wishing to use ASHRAE copyrighted content should visit [ASHRAE's website](#) for more information and to make their request.

Figure C-2: ASHRAE permission to re-use published content in a thesis

**Karl Heine**

---

**From:** Meyer, Ryan <Ryan.Meyer@nrel.gov>  
**Sent:** Tuesday, July 6, 2021 6:07 AM  
**To:** Karl Heine  
**Subject:** Re: Request permission to use 2020 BPACS paper content as part of my thesis

Yes!

Ryan Meyer, PhD

---

**From:** Karl Heine <kheine@mymail.mines.edu>  
**Date:** Friday, July 2, 2021 at 11:23 AM  
**To:** "Meyer, Ryan" <Ryan.Meyer@nrel.gov>  
**Subject:** Request permission to use 2020 BPACS paper content as part of my thesis

**CAUTION:** This email originated from outside of NREL. Do not click links or open attachments unless you recognize the sender and know the content is safe.

Ryan,

I hope all is going well with you these days. I am putting the final touches on my thesis and realized that I need co-author permission to re-use previously published content. I would like to add our BPACS paper as a chapter in the thesis to round-out the discussion on thermal storage modeling. ASHRAE authorizes re-use of the paper for thesis purposes, but I still need co-author agreement.

May I have your permission to re-use our 2020 BPACS paper on ice thermal storage modeling as a chapter within my thesis?

Thanks,  
Karl

Figure C-3: Co-author permission to re-use published content as part of the thesis.